Earth-Science Reviews 142 (2015) 79–119

Contents lists available at ScienceDirect

Earth-Science Reviews

journal homepage: www.elsevier.com/locate/earscirev

Quantitative characterisation of deltaic and subaqueous clinoforms

Stefano Patruno *, Gary J. Hampson, Christopher A-L. Jackson

Department of Earth Science & Engineering, Imperial College, London SW7 2BP, UK

ARTICLE INFO

Article history:
Received 9 November 2013
Accepted 11 January 2015
Available online 27 January 2015

Keywords:
Clinoform
Subaerial delta
Subaqueous delta
Compound clinoform

ABSTRACT

Clinoforms are ubiquitous deltaic, shallow-marine and continental-margin depositional morphologies, occurring over a range of spatial scales (1–10^4 m in height). Up to four types of progressively larger-scale clinoforms may prograde synchronously along shoreline-to-abyssal plain transects, albeit at very different rates. Paired subaerial and subaqueous delta clinoforms (or 'delta-scale compound clinoforms'), in particular, constitute a hitherto overlooked depositional model for ancient shallow-marine sandbodies. The topset-to-foreset rollovers of subaqueous deltas are developed at up to 60 m water depths, such that ancient delta-scale clinoforms should not be assumed to record the position of ancient shorelines, even if they are sandstone-rich.

This study analyses a large dataset of modern and ancient delta-scale, shelf-prism- and continental-margin-scale clinoforms, in order to characterise diagnostic features of different clinoform systems, and particularly of delta-scale subaqueous clinoforms. Such diagnostic criteria allow different clinoform types and their dominant grain-size characteristics to be interpreted in seismic reflection and/or sedimentological data, and prove that all clinoforms are subject to similar physical laws.

The examined dataset demonstrates that progressively larger scale clinoforms are deposited in increasingly deeper waters, over progressively larger time spans. Consequently, depositional flux, sedimentation and progradation rates of continental-margin clinoforms are up to 4–6 orders of magnitude lower than those of deltas. For all clinoform types, due to strong statistical correlations between these parameters, it is now possible to calculate clinoform paleobathymetries once clinoform heights, age spans or progradation rates have been constrained.

Muddy and sandy delta-scale subaqueous clinoforms show many different features, but all share four characteristics. (1) They are formed during relative sea-level stillstands (e.g., Late Holocene); (2) their stratigraphic architecture and facies character are dominated by basinal processes, and are quite uniform; (3) their plan-view morphology is shore-parallel and laterally extensive; (4) their sigmoidal cross-sectional geometry contrasts with the oblique profiles of most subaerial deltas. Holocene-age, delta-scale, sand-prone subaqueous clinoforms occur on steep (≥0.26°) and narrow (5–32 km) shelves, at typical distances of 0.6–7.2 km from the shoreline break. That contrasts with mud-prone subaqueous deltas, which form clinoforms on gently-sloping (0.01–0.38°), wide (23–376 km) shelves, at usual distances of 7.5–125 km from the shoreline. Delta-scale sand-prone subaqueous clinoforms have diagnostically steep foresets (0.7–23°). Similarly steep gradients were observed in much larger shelf-prism- and continental-margin-scale clinoforms. Gentler foreset gradients are shown by sand-prone subaerial deltas (0.1–2.7°), and mud-prone subaqueous and subaerial deltas (0.03–1.50°). Due to the lack of connections with river mouths, Holocene delta-scale sand-prone subaqueous clinoform deposits have progradation rates (1–5 × 10^2 km/Myr) and unit-width depositional flux (1–15 km^2/Myr) that are up to 3–4 and 2–3 orders of magnitude lower, respectively, than age-equivalent input-dominated subaerial deltas and muddy subaqueous deltas. Lower progradation/aggradation ratios are reflected in a larger spread of clinoform trajectory angles (from −0.4° to +3.5°) than the very low values displayed by age-equivalent subaerial and muddy subaqueous deltas.

As slowly prograding, steep, sigmoidal clinoforms are strongly suggestive of sand-prone subaqueous deltas, the Sognefjord Formation and Bridport Sand are likely Jurassic examples of this clinoform type, and host hydrocarbon reservoirs. In contrast, the Campanian Blackhawk Formation is an outcrop example of delta-scale compound clinoforms with a muddy subaqueous component.

* Corresponding author.
E-mail address: stefano.patruno@gmail.com (S. Patruno).

http://dx.doi.org/10.1016/j.earscirev.2015.01.004

Contents

1. Introduction

1.1. Deltaic, shallow-marine and continental-margin compound clinoforms

Clinoforms are basinward-dipping, chronostratigraphic stratal surfaces that constitute the dominant architectural component of most deltaic-to-continental-slope successions (e.g., Gilbert, 1885; Rich, 1951; Bates, 1953; Asquith, 1970; Mitchum et al., 1977; Pirmez et al., 1998; Adams and Schlager, 2000; Bhattacharya, 2006; Patruno et al., 2015). They usually comprise a central seaward-dipping portion (foreset) and two gently dipping parts, respectively updip (topset) and downdip (bottomset) of the foreset (Steel and Olsen, 2002), even though the complete visualization of a 'full' clinoform in seismic data is heavily reliant on seismic resolution and the acoustic impedance contrast across it. Clinoform cross-sectional profiles vary from planar to sigmoidal to concave-upward (or 'oblique') (Sangree and Widmier, 1977), in response to environmental forcing, basin physiography and average sediment grain-size (e.g., Pirmez et al., 1998; Driscoll and Karner, 1999; Adams and Schlager, 2000). The cross-sectional geometry of clinoforms has therefore been used to characterise ancient environmental conditions.

Clinoforms and inclined, clinoform-bounded stratal packages (clinothems sensu Rich, 1951) occur over a range of vertical scales (tens to thousands of metres). In certain cases, up to four types of progressively larger-scale clinoforms prograde synchronously along shoreline-to-abyssal plain transects, albeit at very different rates (Fig. 1A). These 'compound clinoforms' are genetically and morphologically linked, such that the bottomset of one clinoform in an up-dip location corresponds to the topset of a larger-scale clinoform in a down-dip location (Swenson et al., 2005; Helland-Hansen and Hampson, 2009; Henriksen et al., 2009; Helland-Hansen and Gjelberg, 2012; Fig. 2). As previously argued by Helland-Hansen and Gjelberg (2012), from the most proximal to the most distal, these clinoforms are: (1) subaerial deltas (or shorelines); (2) subaqueous deltas; (3) shelf prisms and (4) continental margins (Figs. 1–2).

It's important to point out that the simultaneous occurrence of these four different types of clinoforms in the same basin is a relatively rare event. For example, a well-defined shelf-margin break and a distinct contrast between delta, shelf, slope and deep basin are sometimes absent (e.g., Olariu and Steel, 2009). In other cases, deltas have prograded to the shelf edge, and therefore there is only one delta to shelf-prism foreset ('shelf-edge delta' sensu Porębski and Steel, 2003; Burgess and Steel, 2008), and often this also coincides with the continental-margin clinoform. In the latter case only one clinoform is present along the entire shoreline to basin floor transect. More generally, depth profiles are variable, particularly in basins associated with active tectonics (e.g., foreland and forearc basins).

Both subaerial and subaqueous delta-scale clinoforms are characterised by vertical relief of tens of metres, and typically occur

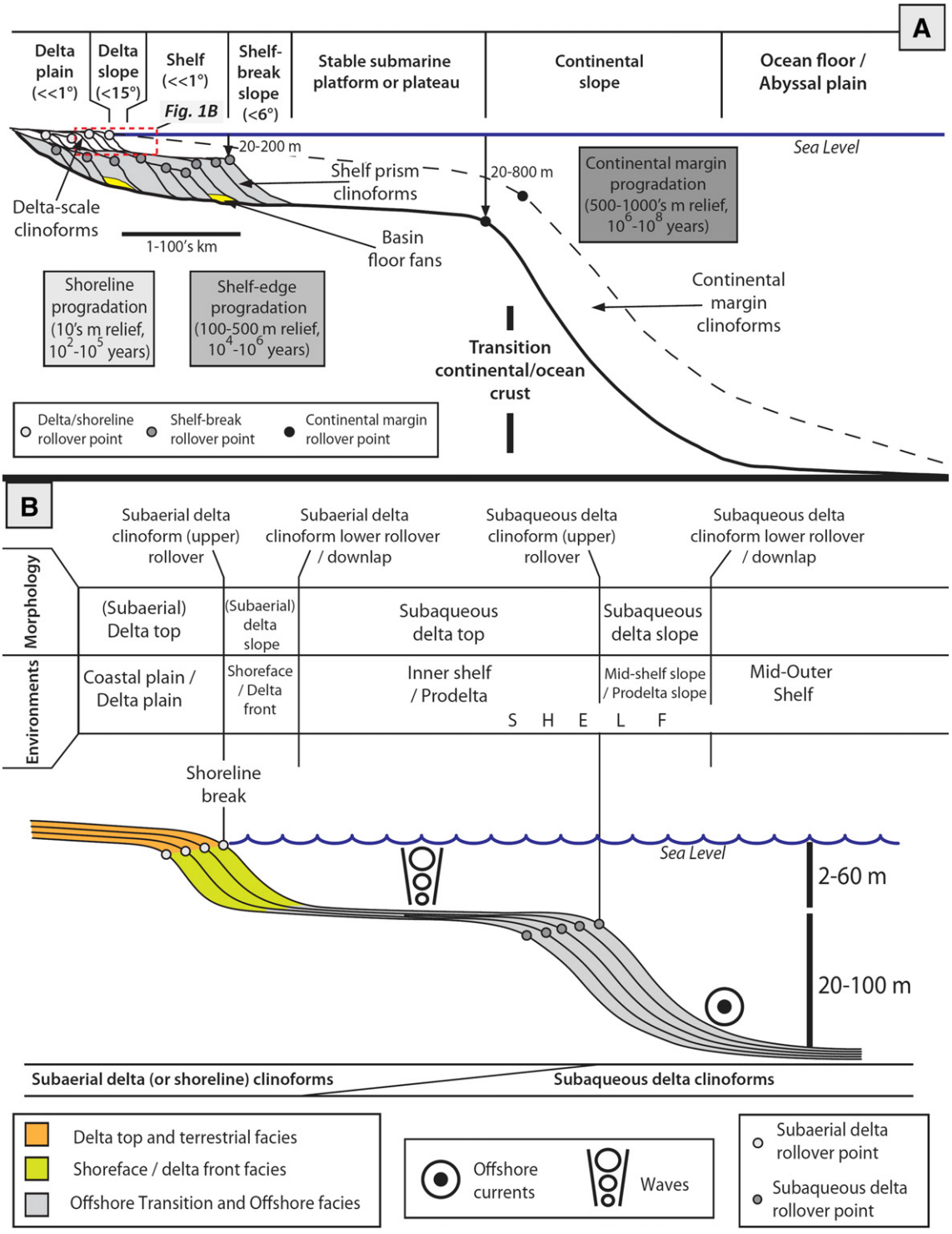

Fig. 1. Compound clinoform systems at different scales. (A) Idealized regional cross-section parallel to regional depositional dip, showing three actively growing clinoforms systems: delta, shelf-prism and continental-margin clinoforms (modified after Henriksen et al. (2009)). (B) Cross-sectional profile parallel to depositional dip showing a typical delta-scale compound clinoform system (located in Fig. 1A), comprising subaerial delta and subaqueous delta clinoforms (modified after Helland-Hansen and Hampson (2009)).

within progradational–retrogradational cycles of 10^2–10^5 years duration (e.g., Burgess and Hovius, 1998; Hampson and Storms, 2003). These clinoforms have their rollovers either in the immediate vicinity of the shoreline break (subaerial deltas or shoreline clinoforms) or at water depths of up to 60 m on the shelf (subaqueous delta clinoforms) (Fig. 1B). They show highly variable geometries, whereas subaqueous clinoforms have rollovers at water depths of up to 40–60 m and are characterised by more regular geometries (Cattaneo et al., 2003, 2007; Helland-Hansen and Gjelberg, 2012; Mitchell et al., 2012; Patruno et al., 2015). The height of shelf-prism clinoforms is ca. 100–500 m, and they generally occur in sedimentary units that represent 10^4–10^6 years (e.g., Vanney and Stanley, 1983;

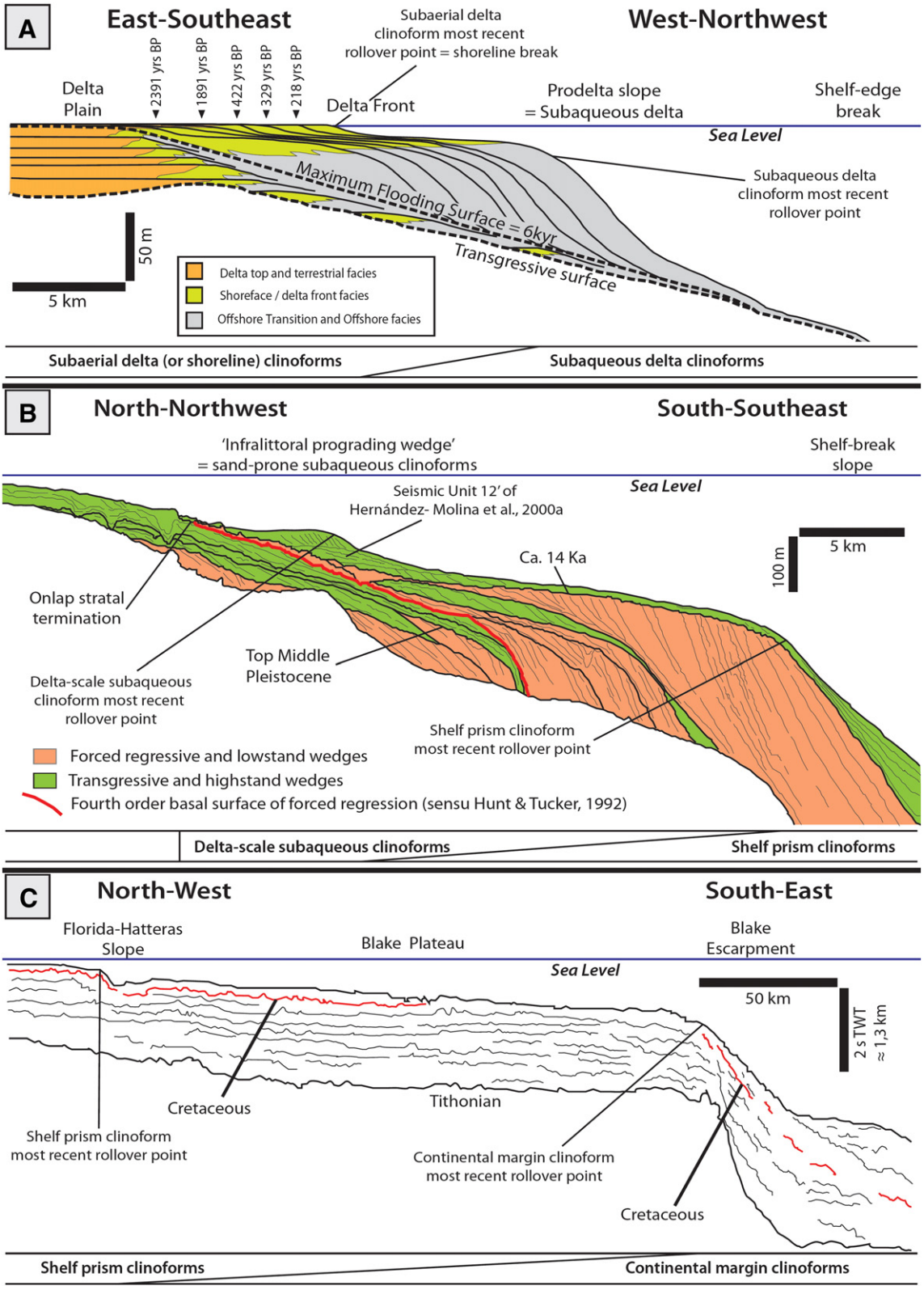

Fig. 2. Examples of compound clinoform systems at different scales. (A) Upper Holocene delta-scale compound clinoforms at the mouth of the present-day Tiber River (modified after Amorosi and Milli (2001)); (B) cross-section oriented perpendicular to the southern Portugal shelf, showing the transition between an isolated Quaternary delta-scale sand-prone subaqueous clinoform and its associated, time-equivalent shelf-prism clinoform. The uppermost unit ('Seismic Unit 12' of Hernández-Molina et al. (2000a)) is interpreted to have been formed during the overall latest-Pleistocene-to-earliest-Holocene transgression, with the regressive delta-scale compound clinoform body deposited during the 'Younger Dryas' relative sea level stillstand (modified after Line 1-Fig. 2 of Hernández-Molina et al. (2000b)); (C) regional cross section showing a continental shelf-slope profile, including Tertiary shelf-prism clinoforms (Florida–Hatteras Slope) and their associated, time-equivalent continental-margin clinoforms (Blake Escarpment) (modified after Schlee et al. (1979), their reflection profile FCB).

Steel and Olsen, 2002; Helland-Hansen and Hampson, 2009). After major flooding events, clinoforms of this type are separated from the shoreline clinoforms, but the two clinoforms coincide when the shoreline/delta transits across the shelf, giving rise to 'shelf-edge deltas' (Porębski and Steel, 2003; Burgess and Steel, 2008; Helland-Hansen and Gjelberg, 2012). Clinoforms that approach several thousands of metres in relief usually are those that construct continental margins, and their progradational–retrogradational cycles typically occur over 10^6–10^8 years (Henriksen et al., 2009; Helland-Hansen and Gjelberg, 2012). The results of our analysis demonstrate that these different scales of clinoforms indeed represent depositional cycles of remarkably different durations consistent with those mentioned above.

Both autogenic controls and high-frequency allogenic controls exert progressively less influence on the architecture of clinoforms developed at increasingly larger spatial and temporal scales. As a result, larger-scale clinoforms are characterised by increasingly simpler clinoform trajectories. In particular, only delta-scale clinoforms occur in units that translate both seawards (i.e., progradation) and landwards (i.e., retrogradation). In contrast, shelf-prism and continental-margin clinoforms only accrete basinwards or remain fixed through time (Helland-Hansen and Hampson, 2009). Nonetheless, fundamental aspects of the style and dynamics of clinoform outbuilding are scale-invariant, despite their markedly different magnitudes (c.f., Thorne, 1995). For example, both delta-scale clinoforms (Kuehl et al., 1986; Michels et al., 1998; Friedrichs and Wright, 2004; Walsh et al., 2004; Cattaneo et al., 2007) and shelf-prism clinoforms (e.g., Pratson et al., 1994) record maximum sedimentation rates in the upper part of their foresets (Nittrouer and Wright, 1994; Pirmez et al., 1998). An abrupt increase of depositional rates seaward of the topset-to-foreset rollover serves to maintain the clinoform shape over time, and suggests that topset-to-foreset rollovers mirror critical, time-averaged bed shear stress conditions (Walsh et al., 2004; Mitchell et al., 2012). Laterally extensive, alongshore clinoform geometries, with little along-strike variability and only minor protuberances that correspond to the position(s) of feeder rivers, are characteristic of subaqueous delta-scale clinoforms (Cattaneo et al., 2003, 2007; Mitchell et al., 2012; Patruno et al., 2015) and are also common in both shoreline clinoforms and shelf-prism clinoforms that accumulated during times of ascending clinoform trajectories and/or in locations lacking focused fluvial input(s) and dominated by basinal processes (e.g., Suter and Berryhill, 1985; Johannessen and Steel, 2005; Olariu and Steel, 2009). Furthermore, the range of progradational clinoform trajectory angles of both delta-scale and shelf-prism clinoforms is similar within a single progradational clinoform set, typically between $-2°$ and $+2°$ (e.g., Bullimore et al., 2005; Johannessen and Steel, 2005; Carvajal and Steel, 2006; Løseth et al., 2006).

Overall aggradation of shelfal strata is therefore generated by vertical stacking of successive deltaic and shoreline clinothem sets (Bullimore et al., 2008; Helland-Hansen and Hampson, 2009). The repeated, regressive–transgressive transit of deltas and shorelines across the shelf is the process responsible for the outbuilding of continental-shelf successions (Johannessen and Steel, 2005), and can, through time, contribute to the basinward accretion and morphological evolution of the larger-scale, shelf-prism and continental-margin clinoforms (e.g., via the establishment of shelf-edge deltas; Burgess and Hovius, 1998; Olariu and Steel, 2009; Helland-Hansen and Hampson, 2009).

1.2. Controls on the evolution of delta-scale subaqueous clinoforms

Two types of delta-scale clinoforms exist (Figs. 1B, 2A–B). In subaerial deltas (or shorelines), the clinoform topset is composed of subaerial delta top or coastal plain deposits, the topset-to-foreset rollover approximates the shoreline-break position, the foreset corresponds to the shoreface or delta front, and the bottomset is contiguous with the inner shelf or prodelta. In contrast, subaqueous delta clinoforms occur within regressive wedges, largely deposited below fairweather wave base. They are characterised by a subaqueous topset dominated by sediment bypass across the inner shelf, a shoreline-detached, topset-to-foreset rollover situated in water-depths approximating fairweather-wave base, a subaqueous delta slope (or prodelta slope), and a bottomset that is contiguous with the mid-to-outer shelf (Kuehl et al., 1986; Alexander et al., 1991; Pirmez et al., 1998; Driscoll and Karner, 1999; Hernández-Molina et al., 2000a; Cattaneo et al., 2003, 2007; Swenson et al., 2005; Helland-Hansen and Hampson, 2009; Mitchell et al., 2012; Patruno et al., 2015). Subaqueous deltas have been so far recognized mostly on present-day shelves. Only a few ancient delta-scale subaqueous clinoform systems have been identified, based on detailed sedimentological and geomorphological characterisation (e.g., Jackson, 1964; Asquith, 1970; Hampson, 2010; Hampson et al., in press; Patruno et al., 2015).

Recent delta-scale subaerial and subaqueous clinoforms either occur in isolation or are dynamically linked to each other along-strike or down-depositional dip, thus forming compound clinoform systems (Figs. 2A, 3). Sediment bodies containing delta-scale subaqueous clinoforms tend to be deposited during relative stillstands or highstands of sea level on near-shore areas between fairweather and storm wave bases (e.g., Hernández-Molina et al., 2000a, 2000b; Cattaneo et al., 2003), and often exhibit along-shore-elongated to convex-seawards plan-view morphologies (Field and Roy, 1984; Driscoll and Karner, 1999; Hernández-Molina et al., 2000a; Cattaneo et al., 2003; Lobo et al., 2005; Mitchell et al., 2012; Patruno et al., 2015). Delta-scale subaqueous clinoforms can be either mud-rich or sand-prone (e.g., in the 'infra-littoral prograding wedges' of Hernández-Molina et al., 2000a). Recent delta-scale sand-prone subaqueous clinoform bodies are usually composed of fine-grained sands, but their average grain-size may range from very fine-grained (e.g., New Zealand) to medium-grained (e.g., southern Iberia, south-east Australia, Monterey Bay) (Mitchell et al., 2012). In previous case studies, mud- and sand-rich subaqueous clinoforms have been treated in isolation (e.g., Hernández-Molina et al., 2000a; Cattaneo et al., 2003), even though their morphological and environmental similarities outnumber their differences. Herein, all delta-scale subaqueous clinoforms are systematically compared, irrespective of their grain size.

Subaerial deltas are actively affected by river input, whereas subaqueous clinoforms are formed in shallow marine environments where sediment advection driven by basin dynamics (e.g., waves, tides and currents), rather than river discharge, is the principal mechanism by which sediment dispersal and deposition occur (e.g., Pirmez et al., 1998; Driscoll and Karner, 1999; Adams and Schlager, 2000; Hernández-Molina et al., 2000a; Cattaneo et al., 2003, 2007; Swenson et al., 2005; Mitchell, 2012; Mitchell et al., 2012). As a consequence, subaerial clinoforms are oriented normal or radial to the sediment input direction at a river-mouth point source (Barrell, 1912; Bates, 1953; Bhattacharya, 2006). In contrast, the elongated plan-view geometries typical of delta-scale subaqueous clinoforms strike parallel to the alongshore advective transport belt that feeds and sculpts them (Fig. 4; Field and Roy, 1984; Driscoll and Karner, 1999; Hernández-Molina et al., 2000a; Cattaneo et al., 2003, 2007; Liu et al., 2007; Fernández-Salas et al., 2009; Mitchell et al., 2012; Patruno et al., 2015). As shown schematically in Fig. 4, significant near-bed shear stresses in shallow-marine areas marked by high-energy waves, tides and/or currents often prevent deposition along subaqueous clinoform topsets, causing topographic flattening and bypass of these areas through lateral advection and resuspension of sediment (Pirmez et al., 1998; Driscoll and Karner, 1999; Swenson et al., 2005; Cattaneo et al., 2007). Time-averaged deposition occurs preferentially just seaward of the topset-to-foreset rollover point, where wave- and current-induced, near-bed agitation declines below the threshold of sediment motion (Mitchell, 2012; Mitchell et al., 2012), causing maximum sediment accumulation rates in the upper foreset region of most clinoforms. The

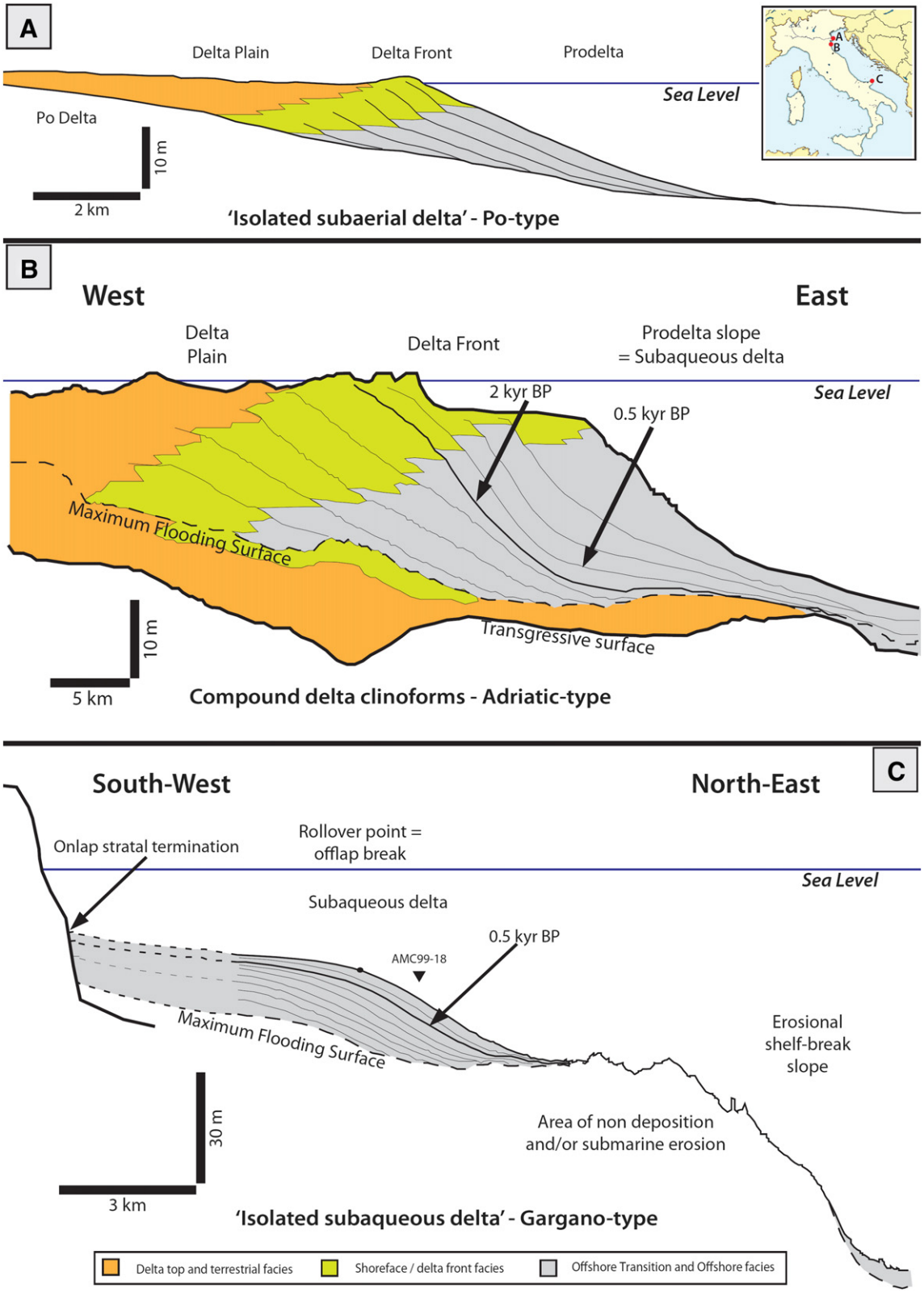

Fig. 3. The three main types of delta-scale clinoform configurations, with reference to their characteristic depositional profiles on the western Adriatic shelf (Cattaneo et al., 2003, 2007; Correggiari et al., 2005). (A) Isolated subaerial delta clinoforms, such as at the mouth of the present-day Po River; (B) delta-scale compound clinoforms, comprising a shoreline or subaerial delta clinoform and a time-equivalent subaqueous delta clinoform, formed along the western Adriatic shelf to the south of the Po River mouth; (C) isolated subaqueous delta clinoform offshore of the Gargano peninsula on the south-western Adriatic shelf, onlapping onto a pre-existing erosional substrate.

along-strike uniformity of subaqueous deltas is due to the energetic hydrodynamic forces active on the shelf, whereas in their subaerial counterparts, high-frequency allogenic forcing and autogenic behaviours result in very rapid episodes of local progradation that alternate with periods of abandonment, erosion and retreat (Cattaneo et al., 2003; Correggiari et al., 2005).

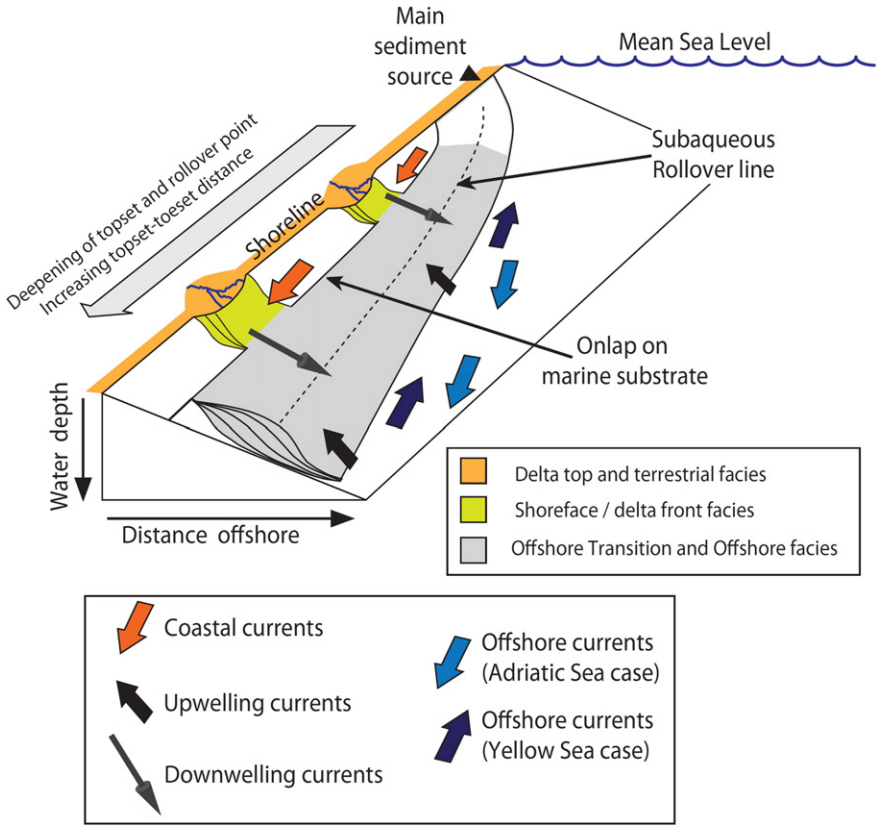

Fig. 4. Three-dimensional scheme portraying the main architectural features and the typical oceanographic environment of present-day delta-scale compound clinoforms, such as the western Adriatic shelf (Cattaneo et al., 2003, 2007) and the western Yellow Sea (Liu et al., 2006, 2007). Shore-parallel coastal currents contribute to the uniform growth of the subaqueous clinoform, by along-shelf redistribution of sediments fed by fluvial input points. Offshore currents influence the overall shore-parallel strike-direction of the subaqueous clinoforms. Downwelling currents transport shoreface sediments offshore, thereby sustaining the overall growth and progradation of the subaqueous clinoform perpendicular to the alongshore currents that feed it. In well-documented modern examples, the position of subaqueous clinoform bottomsets is controlled by seafloor-hugging offshore currents flowing parallel to the clinoform strike and/or by upwelling processes, which force sediment transport along clinoform strike rather than offshore (e.g., Cattaneo et al., 2003, 2007; Liu et al., 2006, 2007).

1.3. Aims

A systematic, quantitative review of clinoforms and clinoform geometries has never been published in the scientific literature. This makes pin-pointing the differences between different scales of clinoforms difficult and often subjective. In addition, the model of delta-scale sand-prone subaqueous clinoforms proposed by Hernández-Molina et al. (2000a), Mitchell et al. (2012) and Patruno et al. (2015, in press) provides an interpretative template that may be applicable to other ancient shallow-marine strata. Their very existence indicates that delta-scale clinoforms in the rock record or in seismic reflection data should not be automatically linked to ancient shoreline positions, even if they are sand-rich, as their toeset-to-foreset rollovers may have been formed at up to 60 m water depth (Mitchell et al., 2012). However, in the absence of sedimentological characterisation, it is at present impossible to distinguish whether an ancient delta-scale clinoform was formed at the shoreline or in a subaqueous setting.

In order to improve our understanding of these different clinoform types, this study analyses a large architectural and chronological dataset of modern and ancient delta-scale, shelf-prism and continental-margin clinoforms in order to: (1) test the existence of geomorphological proxies to constrain the depositional water depth of clinoforms; (2) characterise diagnostic architectural, sedimentological and stratigraphic features of compound clinoform systems, and particularly of delta-scale subaqueous clinoforms; (3) construct a data-driven interpretation methodology that allows delta-scale subaqueous clinoforms to be interpreted in seismic reflection, sedimentological and/or stratigraphical data; and (4) elucidate the impact of this hitherto underappreciated depositional system on existing sequence stratigraphic models.

2. Definition of terms and parameters

The term 'shelf' is here utilized to refer to the 'subaqueous marine shelf' (sensu Burgess and Steel, 2008; Olariu and Steel, 2009), which has a low overall gradient (typically 0.01–0.02°, but as steep as 0.7°; Asquith, 1970; Olariu and Steel, 2009) and is located between the shoreline break and shelf-edge break. Using this definition, the whole of a subaqueous delta clinoform forms part of the shelf. The shelf-edge break is identified at the first change in bathymetric gradient occurring at water depths of 50–300 m (Shepard, 1959; Wear et al., 1974; Southard and Stanley, 1976; Olariu and Steel, 2009) and with a minimum total bathymetric relief of 100 m (Henriksen et al., 2009; Helland-Hansen and Hampson, 2009; Helland-Hansen et al., 2012; Fig. 1A–B). This definition implies that non-erosional shelves correspond to the topset component of shelf-prism clinoforms and to the bottomset of subaerial delta and shoreline clinoforms (Burgess and Steel, 2008), and that shelf-prism trajectories approximately demarcate neritic and bathyal subaqueous environments (Henriksen et al., 2009).

Shelf-prism clinoforms and continental-margin clinoforms (Figs. 1A; 2C) are here differentiated because, in certain cases, the seaward termination of a shelf-break slope is not situated on the oceanic crust, but lies above another sub-horizontal, bathyal platform over the continental crust (e.g., Florida Hatteras Slope to Blake Escarpment system, Fig. 2C, Schlee et al., 1979; submarine shelf offshore California, Fig. 7C–OC). In these cases, the continental margin is situated seaward of this submarine plateau or platform, and may be marked by a further clinoform whose position is primarily controlled by the transition between continental and oceanic crust. However, in most present-day shelves, shelf-break and continental-margin clinoforms are coincident.

Table 1
Clinoforms and clinoform sets analysed using direct measurements from published cross sections, thickness and facies maps. Abbreviations are used in Figs. 6–11. The classification of subaerial deltas by Orton and Reading (1993) comprises both information about the dominant grain size (MS = mud-silt; FS = fine sand; GR = gravel) and the dominant depositional processes (I = input; w = waves; t = tides). In brackets we have added the estimated dominant grain-size at the river mouth.

Type	Location	Subaerial delta classification Orton and Reading (1993)	Tectonic context	Age	Average clinoform trajectory	Abbrev.	Reference
Continental-margin clinoforms	Western Florida escarpment + continental margin (Blake escarpment)	–	Passive margin	Units I/II = Miocene-Recent; from Top Tithonian (Blake Escarpment)	+1.7° to +7.8°	FL	Mullins et al. (1988), Profile 40–42; Schlee et al. (1979), Fig. 13, Profile FC8
	Antarctic pacific margin	–	Passive margin	Cenozoic and Pliocene	+51.1°	AN	Adams and Schlager (2000), Figs. 4A, 8A
	Western Great Bahama Bank	–	Passive margin	Cenozoic	+6.8°	GBH	Adams and Schlager (2000), Fig. 6C
	Prydz Bay, Antarctica	–	Passive margin	Unit PS1 = Post–Middle Miocene	+10.1°	PB	Adams and Schlager (2000), Fig. 6B
	SW Africa	–	Passive margin	Post-surface D (Upper Paleocene)	+0.8°	AF	Adams and Schlager (2000), Fig. 7C
	Baffin Bay, West Greenland	–	Passive margin	Cenozoic	+5.2°	BAF	Adams and Schlager (2000), Fig. 7B
	Georges Bank Basin, U.S.A.	–	Passive margin	Cenozoic	+1.1°	GBB	Adams and Schlager (2000), Fig. 7A
	Scotian Slope, Canada	–	Passive margin	Cenozoic	+47.7°	SC	Adams and Schlager (2000), Fig. 4B
Shelf-prism clinoforms	Backstripped New Jersey	–	Passive margin	Oligocene–Miocene	0° to +2.0°	NJ	Steckler et al. (1999), 7 clinoforms labelled: m2.3, m 2.5, m3, m4, m5, m5.4, m6
	Shelf edge off Guadiana River	–	Active margin	Pleistocene	Regressive descending	GS	Hernández-Molina et al. (2000b), Fig. 2
	SE south island, New Zealand	–	Active margin	Cenozoic, Post-'reflector 4'	+1.5°	NZ	Adams and Schlager (2000), Fig. 6A
	Florida Hatteras slope	–	Passive margin	Post-Top Tithonian	+1.3°	HT	Schlee et al. (1979), Profile FC8, Fig. 13
	Carbonate shelf edge Australia	–	Passive margin	Upper Miocene arrow reflection	+0.8° to +2.5°	AUS	Adams and Schlager (2000), Fig. 8B, Line-45
Mud-rich subaqueous delta clinoforms	Amazon Delta	MSti (0.030 mm, silt)	Passive margin	Holocene–Recent	+0.24° to +0.47°	AMs	Nittrouer et al. (1986), Figs. 9, 13, Profiles F. G, M; Nittrouer et al. (1996), Figs. 9a, 9b
	Ganges–Brahmaputra	FS t (0.160 mm, FS)	Active margin	Holocene–Recent	+0.02° to +0.25°	GBs	Michels et al. (1998), Fig. 4, Profiles 1, 2, 3; Palamenghi et al. (2011), Figs. 4–5
	Yangtze Delta	MS it (silt)	Intracratonic seaway	Holocene–Recent	−0.04° to +0.57°	YGs	Liu et al. (2007), Profiles 1–2, 4–6
	Adriatic and Gargano clinoforms	PO delta: FS i (0.520 mm, 23% sand, MS-CS)	Active margin	Holocene–Recent; post 1500 AD; from 1886 to 1959	0° to +0.45°	AD and GA	Cattaneo et al. (2003, 2004), Figs. 6, 8, Profiles A–C, YD5-8, AMC167-175; Cattaneo et al. (2007), Fig. 2, Profiles A–F; Friedrichs and Scully (2007), Fig. 8a
	Gulf of Papua, New Guinea	–	Active margin	Holocene–Recent	Ca. +0.20°	FLYs	Walsh et al. (2004), Profile I, G, F, D
	Atchafalaya subaqueous delta	–	Passive margin	Holocene–Recent	+0.02° to +0.07°	AT	Neill and Allison (2005), lines A, B, C, D
	Yellow River Subaqueous Delta (known as Shandong Delta)	MS i (0.020–0.060 mm, silt)	Intracratonic seaway	Holocene–Recent	–0.08° to +0.16°	HHs	Liu et al. (2004), Figs. 8, 9, 10, 11, 13; Yang and Liu (2007), Fig. 2A, 2B, 2D
	Tiber subaqueous delta	FS w (silty sand)	Rift basin	Holocene–Recent; Post 422 BP	+0.06° to +0.57°	TBs	Amorosi and Milli (2001) (subaqueous delta), Fig. 3
	Rhone	FS wi (0.080–0.500 mm, VS-CS)	Active margin/rift basin	Pleistocene–Holocene	−0.10° to 0°	RHs	Tesson et al. (2000), clinoforms around IUc', RPUd, dIUc' surfaces in Figs. 13, 15; clinoforms in unit from 5″ to 6 in Fig. 10; post-glacial inner clinoforms in Profile F of Fig. 5

Sand-prone subaqueous delta clinoforms	Almeria prograding clastic wedge	–	Active margin	Holocene–Recent	+1.2° to +1.4°	AL	Hernández-Molina et al. (2000a), Fig. 3; Mitchell et al. (2012), Fig. 3 + Table 1
	Manawatu, New Zealand	–	Active margin	Holocene–Recent	+0.27°	MN	Dunbar and Barrett (2005), Fig. 2, Lines 27–29; Mitchell et al. (2012), Fig. 3 + Table 1
	Port Jackson (Sidney) subaqueous sandbodies, SE Australia	–	Intracratonic seaway	Late Holocene–Recent	?	PJ	Field and Roy (1984), Fig. 1, Profiles 11, 18, 23, 29
	Bate Bay-Malabar subaqueous sandbodies, SE Australia	–	Intracratonic seaway	Late Holocene–Recent	0° to +4.9°	BB	Field and Roy (1984), Fig. 2, Profiles D, K, N, R
	Faro and Tavira depocentre	–	Active margin	Late Holocene–Recent	−0.5° to −0.2°	FA	Lobo et al (2005), Figs. 5, 8; Hernández-Molina et al. (2000a), Fig. 4; Mitchell et al. (2012), Fig. 3 + Table 1 (10 ms = 7.5 m)
	Monterey Bay, La Jolla, California (active margin)	–	Active margin	Holocene	0	MB	Le Dantec et al. (2010); Chin et al. (1988); Fig. 10
	Oceanside, San Diego, California (active margin)	–	Active margin	Holocene–Recent	1.4° to +2.6°	OC	Mitchell et al. (2012), Fig. 3 + Table 1
	Ascension Island (mid-Atlantic ridge)	–	Mid Atlantic ridge	Holocene?	?	AS	Mitchell et al. (2012), Fig. 3
	Menorca (Spain) carbonatic clinoforms (active margin)	–	Active margin	Tortonian-age outcrops	Low angle	MN	Pomar et al. (2002)
	Matera, southern Italy (active margin)	–	Active margin	Plio-Pleistocene-age outcrops	Ascending to descending regressive	MT	Pomar and Tropeano (2001)
Subaerial delta/shoreline clinoforms	Mississippi subaerial and shelf-edge delta (passive margin)	MS i (0.014 mm, silt)	Passive margin	Post-1550 profiles of years 1838, 1874, 1921, 1947	0°	MI	Kenyon and Turcotte (1985)
	Amazon subaerial delta	MSti (0.030 mm, silt)	Passive margin	Holocene–Recent	+0.01°	AM	Nittrouer et a 96, subaerial delta = Rio Fleshal sandflat (Fig. 4)
	Yangtze subaerial delta	MS it (silt)	Intracratonic seaway	Late Holocene (3.31 Ka)–Recent	0°	YG	Hori et al. (2001), present (subaerial delta)
	Po Delta	FS i (0.520 mm, 23% sand, MS-CS)	Active margin	Post-1500 AD profiles, until year 2002	0°	PO	Correggiari et al. (2005), Figs. 3, 4, 5, 8, profiles A–B, C–D–E; Cattaneo et al. (2003), Fig. 6, profile A–C; Friedrichs and Scully (2007), Fig. 8a, b
	Mekong Subaerial Delta	FS m (VFS)	Intracratonic seaway	Post 5 Ka BP to Recent	+0.01°	ME	Ta et al. (2002), Fig. 2, profiles X–Y, A–B
	Tiber subaerial delta	FS w (silty sand)	Rift basin	Holocene–Recent; Post 422 BP	+0.01°	TB	Amorosi and Milli (2001) (subaerial delta), Fig. 3
	Long beach and Willapa Bay spit	–	Active margin	Recent (80 years)	0°	LB	Jol et al. (2002), Fig. 5C
Ancient subaqueous clinoforms	Blackhawk Fm.–Mancos shale, K4 shoreface and X–Y associated subaqueous clinoforms	FS wi (FS-MS)	Rift basin	F100 to F150 surfaces – Lower Campanian-age	+0.04°	BH	Hampson (2010), Fig. 13
	Sognefjord Formation	FS wti (FS-MS)	Rift basin	Upper Callovian to Oxfordian	0° to +0.6°	SG	Patruno et al. (2013a), Figs. 1–3
	Bridport Sand (subaerial clinoform?) and Down Cliff Clay (subaqueous clinoform)	FS wi (FS)	Rift basin	Toarcian-?Aalenian-age	+3.5°	BRD	Morris et al. (2006), Fig. 14

Table 2
Clinoforms and clinoform sets analysed using measurements taken from published literature compilations (i.e. not directly measured by the authors). Abbreviations are used in Figs. 6–11. Clinoform topset and foreset slope gradients are assumed to equate to the parameters 'average delta plain gradient' and 'average upper delta slope gradient' of Orton and Reading (1993). Delta bottomset slopes are assumed to equate to average shelf gradient (e.g., Olariu and Steel, 2009). Classification of subaerial delta type is after Orton and Reading (1993), and is based on both dominant grain size (GR = m gravelly sand; FS = fine-grained sand; MS = mud-silt) and dominant depositional processes (i = input; w = wave; t = tide). References are cited as follows: (a) Orton and Reading (1993); (b) Burgess and Hovius (1998); (c) Olariu and Steel (2009); (d) Howell et al. (2008); (e) Bristow and Pucillo (2006).

Type	Location	Age	Abbrev.	Average quantitative parameters												
				Subaerial delta type	Shelf-edge *wd* (m)	Shelf-edge *Fs* (°)	shelf-edge *Ts* (°)	%Sand in delta front	Subaerial delta *Fh*(m)	Subaerial delta *Ts* (°)	Subaerial delta *Fs* (°)	Duration (Myr)	*Sv* (m/Myr)	*P* (km/Myr)	*F* (km2/Myr)	*R* (adim.)	Shoreline *CT* (°)
				a	Mean *b* + *c*	*c*	*c*	*b*; *d*	After *d*	*a*	*a*; *e*; *d*	After *b*; *d*	After *b*; *c*; *d*	After *b*; *d*; *e*	After *b*; *d*	After *d*	*d*
Present-day shelf-prism clinoforms	Limpopo	Holocene	LM		87	1.04	0.27										
	Magdalena	Holocene	MG		99.6	1.89	0.36										
	Parana	Holocene	PA		98.3	2.75	0.07										
	Pearl (Zhujiang)	Holocene	ZH		189	0.59	0.03										
	Santa	Holocene	SN		173	1.05	0.18										
	Yangtze	Holocene	YG	MS it	180	0.78	0.01										
	Zambese	Holocene	ZA		92.3	1.55	0.10										
Present-day subaerial delta/shoreline clinoforms and associated shelf margin clinoforms	Amazon	Recent	AM	Msti	94	2.63	0.02	16		0.001	0.315	$1.16\ 10^{-2}$	$8.13{\cdot}10^{3}$	$2.77\ 10^{4}$	$1.19\ 10^{3}$	$3.07\ 10^{-4}$	
	Copper	Recent	CP	FS wt	193	2.58	0.13	98		0.034	0.401	$8.52°10^{-3}$	$2.27°10^{4}$	$9.98°10^{3}$	4.99E + 02	$4.54°10^{-3}$	
	Danube	Recent	DN		107	2.30	0.16					$1.08\ 10^{-2}$	$9.94\ 10^{3}$	$1.04\ 10^{4}$	$1.56\ 10^{2}$	$1.91\ 10^{-3}$	
	Ganges–Brahmaputra	Recent	GB	FS t	150	1.42	0.09	45		0.006	0.010	$4\ 10^{-2}$	$4.\cdot 10^{3}$	$4.64\ 10^{3}$	$4.20\ 10^{2}$	$1.05\ 10^{-3}$	
	Indus	Recent	IN		126	2.156	0.07	2				$1.55\ 10^{-2}$	$8.20\ 10^{3}$	$7.44\ 10^{3}$	$2.97\ 10^{2}$	$1.38\ 10^{-3}$	
	Irrawady (and Salween)	Recent	IW	MS m	146	1.21	0.32			0.003	0.034	$3.11°10^{-2}$	$4.70°10^{3}$	$5.94°10^{3}$	$2.88°10^{2}$	$9.79°10^{-4}$	
	Krishna (and Godavari)	Recent	KR		95.7	3.79	0.22	42				$8.70\ 10^{-3}$	$1.10\ 10^{4}$	$5.52\ 10^{3}$	$1.10\ 10^{2}$	$3.99\ 10^{-3}$	
	Mackenzie* (McKenzie)	Recent	MK	FS i	112	1.02	0.03	5		0.003	0.017	$1.16\ 10^{-1}$	$9.64\ 10^{2}$	$1.72\ 10^{3}$	$1.03\ 10^{2}$	$9.35\ 10^{-4}$	
	Mississippi	Recent	MI	MS i	127	0.75	0.05	2		0.001	0.516	$1.31\ 10^{-2}$	$9.73\ 10^{3}$	$8.79\ 10^{3}$	$5.00\ 10^{2}$	$1.26\ 10^{-3}$	
	Niger	Recent	NG	FS m	95.5	1.44	0.11				0.115						
	Nile	Recent	NL	FS wi	152	1.97	0.34	20		0.005	0.015	$2.80\ 10^{-2}$	$5.44\ 10^{3}$	$1.79\ 10^{3}$	$1.34\ 10^{2}$	$5.08\ 10^{-3}$	
	Orange	Recent	OR		174	0.41	0.17					$3.35\ 10^{-2}$	$5.19\ 10^{3}$	$5.37\ 10^{3}$	$2.95\ 10^{2}$	$1.93\ 10^{-3}$	
	Orinoco*	Recent	ON	MS m	83.6	1.48	0.04	7		0.004	0.026	$2.33\ 10^{-2}$	$3.59\ 10^{3}$	$4.50\ 10^{3}$	$1.35\ 10^{2}$	$1.20\ 10^{-3}$	
	Rhone	Recent	RH	FS wi	142	3.18	0.43				0.195	$1.02\ 10^{-2}$	$1.40\ 10^{4}$	$4.72\ 10^{3}$	$1.53\ 10^{2}$	$5.93\ 10^{-3}$	
	Zaire (Congo)*	Recent	CO		140	1.14	0.10	2				$4.18\ 10^{-2}$	$3.35\ 10^{3}$	$1.67\ 10^{3}$	8.37E + 01	4.00E-03	
Present-day subaerial delta/shoreline clinoforms	Alta	Recent	AA	GS i						0.086	20.06						
	Bella Coola	Recent	BC	GS iw						0.127	9.589						
	Brazos	Recent	BR		100			10				$3.16{\cdot}10^{-2}$	$3.16.10^{3}$	$4.43.10^{3}$	$1.11.10^{2}$	$1.43.10^{-3}$	
	Burdekin	Recent	BU	FS/GS m													
	Chachaguala	Recent	CG	GR w						0.057	2.291						

	Colorado	Recent	CL		200	15				$1.13\ 10^{-1}$	$1.77\ 10^{3}$	$9.29\ 10^{2}$	4.64E +01	$3.81\ 10^{-3}$	
	Columbia	Recent	COL		165					$7.77\ 10^{-2}$	$2.12\ 10^{3}$	$1.08\ 10^{3}$	4.46E +01	$3.93\ 10^{-3}$	
	Colville	Recent	CV	GS											
	Ebro	Recent	EB	FS iw	125			0.022	0.498	$2.04\ 10^{-2}$	$6.13\ 10^{3}$	$3.43\ 10^{3}$	$1.07\ 10^{2}$	$3.57\ 10^{-3}$	
	Fly	Recent	FLY		65					$1.32\ 10^{-2}$	$4.92\ 10^{3}$	$1.1 \cdot 10^{4}$	$1.79 \cdot 10^{2}$	$8.97 \cdot 10^{-4}$	
	Fraser	Recent	FR	FS it					1.432						
	Guichen Bay	Recent	*GU*						5.20			$7.80\ 10^{3}$			
	Homathko	Recent	HM	GS it				0.063	3.712						
	Huanghe (Yellow River)	Recent	HH	MS i				0.001	0.344						
	Kizil Irmak	Recent	KI		100					$2.78\ 10^{-2}$	$3.60\ 10^{3}$	$1.26\ 10^{3}$	$3.15\ 10^{1}$	$5.71\ 10^{-3}$	
	Klang	Recent	KG	FS t				0.003							
	Klinaklini	Recent	KK	GS i				0.083	2.860						
	Mahakam*	Recent	MA	FS it	130	30			0.372	$5.46\ 10^{-2}$	$2.38\ 10^{3}$	$7.33\ 10^{2}$	$2.38\ 10^{1}$	$6.50\ 10^{-3}$	
	Mekong	Recent	ME	FS m				0.001	0.029						
	Noeick	Recent	NO	GS i					5.426						
	Po	Recent	PO	FS i	120	23		0.003	0.189	$1.12\ 10^{-1}$	$1.07\ 10^{3}$	$2.14\ 10^{3}$	6.43E + 01	$1.00\ 10^{-3}$	
	Punta Gorda	Recent	PG	GR w				0.802	2.291						
	Rio Grande	Recent	RG		200	4				$3.73\ 10^{-2}$	$5.36\ 10^{3}$	$2.14\ 10^{3}$	$1.07\ 10^{2}$	$5.00\ 10^{-3}$	
	Sao Francisco	Recent	SF	FS w					0.246						
	Senegal	Recent	SN	FS w					0.401						
	Shoalhaven	Recent	SH	FS m					0.802						
	Skeidararsandur	Recent	SS	GS w				0.115	0.917						
	Tiber	Recent	TB	FS w					0.687						
	Tunsberg Dalbre	Recent	TU	GR i				1.489	5.711						
	Volta	Recent	VL		200					$2.36\ 10^{-2}$	$8.49\ 10^{3}$	$1.70\ 10^{3}$	$8.48\ 10^{1}$	$1.00\ 10^{-2}$	
	Yallahs	Recent	YL	GR wi				0.859	10.2						
Ancient subaerial delta/shoreline clinoforms (Howell et al., 2008)	Panther Tongue	Campanian	BK (Book Cliffs, U.S.)	FS i		41	30		2.1	0.5	10	$3.17\ 10^{4}$	0.16	$3.15\ 10^{-4}$	0.07
	Spring Canyon Mb.	Campanian		FS w		16	19		0.27	0.5	20	$9.26\ 10^{3}$	0.09	$2.16\ 10^{-3}$	0.21
	Kenilworth Mb.	Campanian		FS w		12	21		0.04	0.5	20	$3.76\ 10^{4}$	0.38	$5.32\ 10^{-4}$	0.04
	Sunnyside Mb.	Campanian		FS w		31	22		0.22	0.5	20	$2.46\ 10^{4}$	0.25	$8.14\ 10^{-4}$	0.10
	Grassy Mb.	Campanian		FS w		24	25		0.06	0.5	20	$2.55\ 10^{4}$	0.26	$7.83\ 10^{-4}$	0.13
	Ferron Sst., USA (1)	Turonian	FER	FS i		22	26		5.2	0.8	35	$1.31\ 10^{4}$	0.37	$2.67\ 10^{-3}$	1.90
	Ferron Sst., USA (2)	Turonian		FS i		16	26		6.4	0.8	35	$1.53\ 10^{4}$	0.43	$2.30\ 10^{-3}$	1.10
	John Henry Mb., USA	Santonian	JH	FS w		23	70			1	30				
	Judith River Fm., USA	Upper Cretaceous	JR	FS w		23	16			4	30				
	Mesaverde, USA	Upper Cretaceous	MV	FS wti			16			6.5	35				
	Clyde Field, North Sea	Upper Jurassic	CLY	FS w			21			1	120				
	Cormorant Field, Shetland Basin	Middle Jurassic	COR	FS w			22			1.5	5				
	Thistle Field, Viking Graben	Middle Jurassic	TH	FS w			26			3	5				
	Hutton Field, Shetland Basin	Middle Jurassic	HUT	FS wti			14			3	5				
	Tern Field, Shetland Basin	Middle Jurassic	TRN	FS w			4			3	5				

More generally, the clinoform nomenclature used throughout this article stresses the idea of different scales of clinoforms, following a recognisable trend in recent literature (e.g., Henriksen et al., 2009; Helland-Hansen and Gjelberg, 2012). As a consequence, the difference between continental-margin and shelf-prism clinoforms is here based primarily on their respective heights. Shelf-margin clinoforms located at the boundary between continental and oceanic crust (as is normally the case), but characterised by an overall height of 100–1000 m, are here still classified as 'shelf-prism'-scale clinoforms. Conversely, clinoforms showing a total relief greater than 1000 m are here classified as 'continental-margin'-scale clinoforms, even if they occur at a significant distance from the continental–oceanic crust boundary. The results of this work prove that such a distinction is indeed meaningful, because 'continental-margin' and 'shelf-prism' clinoforms are characterised by conspicuously different morphologies, clinoform trajectories and rates of aggradation, progradation and sediment flux.

In this work, several clinoform architectural and geochronological parameters have been measured from published cross-sections, maps and other data (Fig. 6, Tables 1 and 2). Below, and in Fig. 5, these parameters are briefly defined. On the cross-sectional profile of a clinoform surface, two points of maximum curvature ('rollover points') are usually located landward and basinward of the point of maximum slope gradient ('inflection point'; Fig. 5). Upper and lower rollover points are centred respectively on the upward-convex topset-to-foreset transition of a clinoform surface (e.g., Fig. 1A–B) and on the upward-concave foreset-to-bottomset transition of a clinoform surface. The positions of these two prominent breaks-in-slope subdivide the clinoform surface into a steeper central area ('foreset') and two gently-sloping areas, respectively landward ('topset') and basinward ('bottomset' or 'toeset') of the rollover points (Barrell, 1912; Mitchum et al., 1977; Pirmez et al., 1998; Fig. 5). Bottomsets and topsets are here subdivided into inner and outer parts, based on the positions of the points where bottomset and topset become horizontal or conformable with the underlying surface (clinoform 'toe point' and 'head point', respectively; Pirmez et al., 1998; Fig. 5). The height and dip extent of a foreset (*Fh*, *Fd*), outer topset (*Th*,*Td*) and inner bottomset (*Bh*, *Bd*) are determined by the vertical and horizontal distances between the toe point, the two rollover points and the head point of the clinoform (Fig. 5). The elevation of the inflection point (*Ih*) is measured from the toe point, whereas the 'total clinoform relief' (*Hh*) corresponds to the vertical distance from the toe point to the head point of a horizontal topset or to the shallowest point at the mouth of the river in the case of a sloping topset (Pirmez et al., 1998; Fig. 5). A parameter named 'shape ratio' (c.f., Fig. 5) or 'normalized elevation of the inflection point' (*h*/*H*) was defined by Pirmez et al. (1998) as the height of the inflection point (*Ih*) divided by the clinoform total relief (*Hh*). This parameter was proposed to quantitatively distinguish symmetrical, sigmoidal clinoforms ($h/H < 0.4$) from asymmetrical, oblique clinoforms ($h/H \geq 0.4$).

Vertical sediment accumulation rate is considered to be the maximum vertical thickness of a clinothem divided by the age difference between the basal and top clinoform surface, which usually corresponds to flooding surfaces. Progradation rate in recent clinoforms is measured as the horizontal distance between the inflection point positions of two dated clinoforms divided by their age difference. Wherever possible for ancient clinoform successions, progradation rate was measured by following the method proposed by Patruno et al. (in press). Progradation resistance ratio is a dimensionless number corresponding to the ratio between mean vertical sediment accumulation rate and progradation rate calculated along a cross section parallel to the clinoform dip (cf., Patruno et al., in press). This ratio reflects the

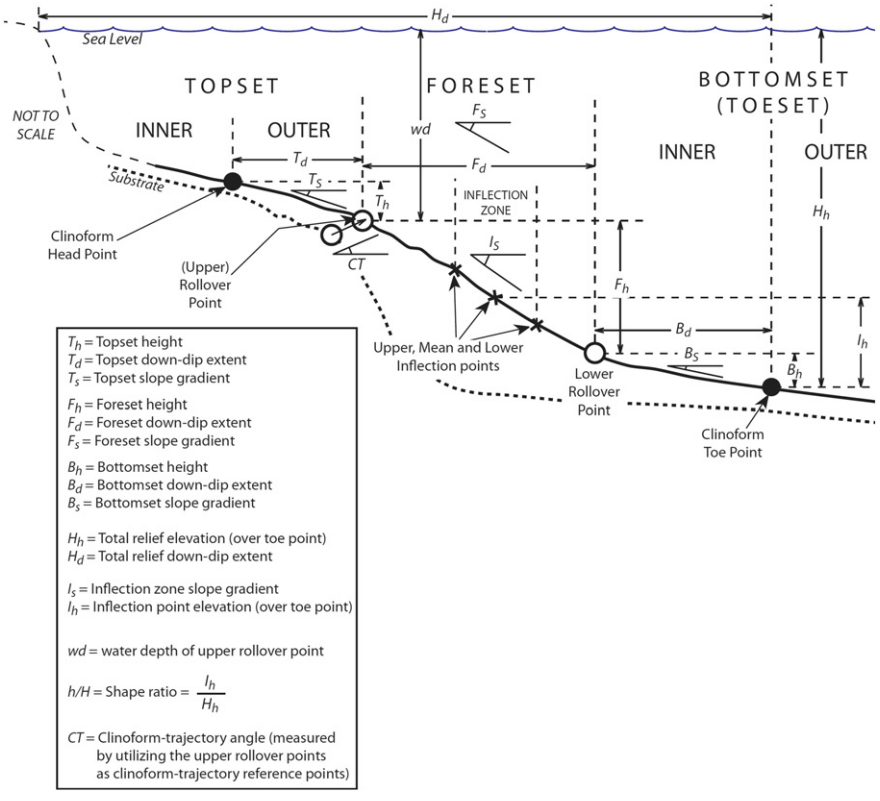

Fig. 5. Summary of clinoform nomenclature, illustrated for a delta-scale subaqueous clinoform (Fig. 1B). The clinoform inflection point is the point where the gradient reaches maximum values. The inflection zone is defined as a relatively small area around the inflection point, and it is often a more readily observable parameter. The rollover points are the two points of maximum curvature located landward and seaward of the inflection point. The rollover points separate a foreset of steeper gradient from the landward-lying topset and seaward-lying bottomset, which both have gentler gradients. The toe of the clinoform occurs in the bottomset, where the clinoform becomes conformable with the underlying substrate. The clinoform height (H_h) is the difference in elevation between the clinoform toe point and the clinoform head point, where the topset becomes conformable with the underlying substrate. Additional parameters are described in the text.

amount of sediment that needs to accumulate vertically in order for the clinothem foreset to prograde for a single unit of distance. Akin to the electrical resistance, this parameter represents the measure of the cumulative 'environmental' opposition to clinoform progradation (e.g. factors like initial water depth, current distribution and strength, local tectonics). The cross-sectional net sediment flux is the product of progradation rate and mean thickness of a clinothem, both measured along a cross section parallel to the depositional dip. This parameter was defined by Burgess and Hovius (1998) and Patruno et al. (in press), and is equal to the initial river-fed sediment input rate, minus the sum of the rates of sediment addition by deposition and removal by erosion down depositional dip (e.g., by gravity flows) and the rate of sediment addition or removal by out-of-plane transport (e.g., by alongshore currents).

3. Recent delta-scale compound clinoforms

Plan views and cross sections oriented parallel to the depositional dip of twenty recent delta-scale compound clinoforms are located in Fig. 6 and presented in Figs. 7–10 and in Table 3. These systems are either formed by deltaic systems (e.g., off the mouth of the Yangtze, Yellow-Shandong, Ganges–Brahmaputra, Amazon, Fly, Orinoco, Shoalhaven, Atchafalaya, Salinas, San Diego, Manawatu, Rhone, Tiber, Arno-Cecina and Italian Adriatic rivers), or are not directly related to river mouths (e.g., mid-shelf clinoforms off the coast of southern Spain, southern Portugal, south-eastern Australia, western Ascension Island). Detailed cross sections of modern delta-scale subaqueous clinoforms, based on interpretations of seismic reflection profiles, are shown in Fig. 10.

A wealth of publications exists for many recent delta-scale subaqueous clinoforms and associated compound clinoforms. The reader is referred to Hori et al. (2001) and Liu et al. (2006, 2007) (Yangtze River delta); Bornhold et al. (1986), Alexander et al. (1991), Liu et al. (2004) and Yang and Liu (2007) (Yellow River delta and subaqueous Shandong delta); Kuehl et al. (1997, 2005), Michels et al. (1998), and Palamenghi et al. (2011) (Ganges–Brahmaputra River subaqueous delta); Kuehl et al. (1986), Nittrouer et al. (1986, 1996) and Methling et al. (1996) (Amazon River delta); Walsh et al. (2004) (Fly River delta); Warne et al. (2002) (Orinoco River delta); Neill and Allison (2005) (Atchafalaya delta); Amorosi and Milli (2001) and Correggiari et al. (2005) (Tiber and Po River deltas); Cattaneo et al. (2003, 2004, 2007) (Adriatic subaqueous clinoforms); Dunbar and Barrett (2005) (Manawatu coastlines, New Zealand); Field and Roy (1984) (south-eastern Australia coastlines); Hernández-Molina et al. (2000a,b) and Lobo et al. (2005) (southern Spanish and Portuguese coastlines); and Chin et al. (1988) (Monterey Bay coastlines). Mitchell et al. (2012) provided a synthesis of delta-scale sand-prone subaqueous clinoforms (e.g., offshore of Manawatu, southern Spanish and Portuguese, and south-eastern Australia coastlines), as well as describing similar clinoforms off the coasts of western Ascension Island and Oceanside, USA. Some of the systems shown in Figs. 7–10 have not been previously investigated, but they contain

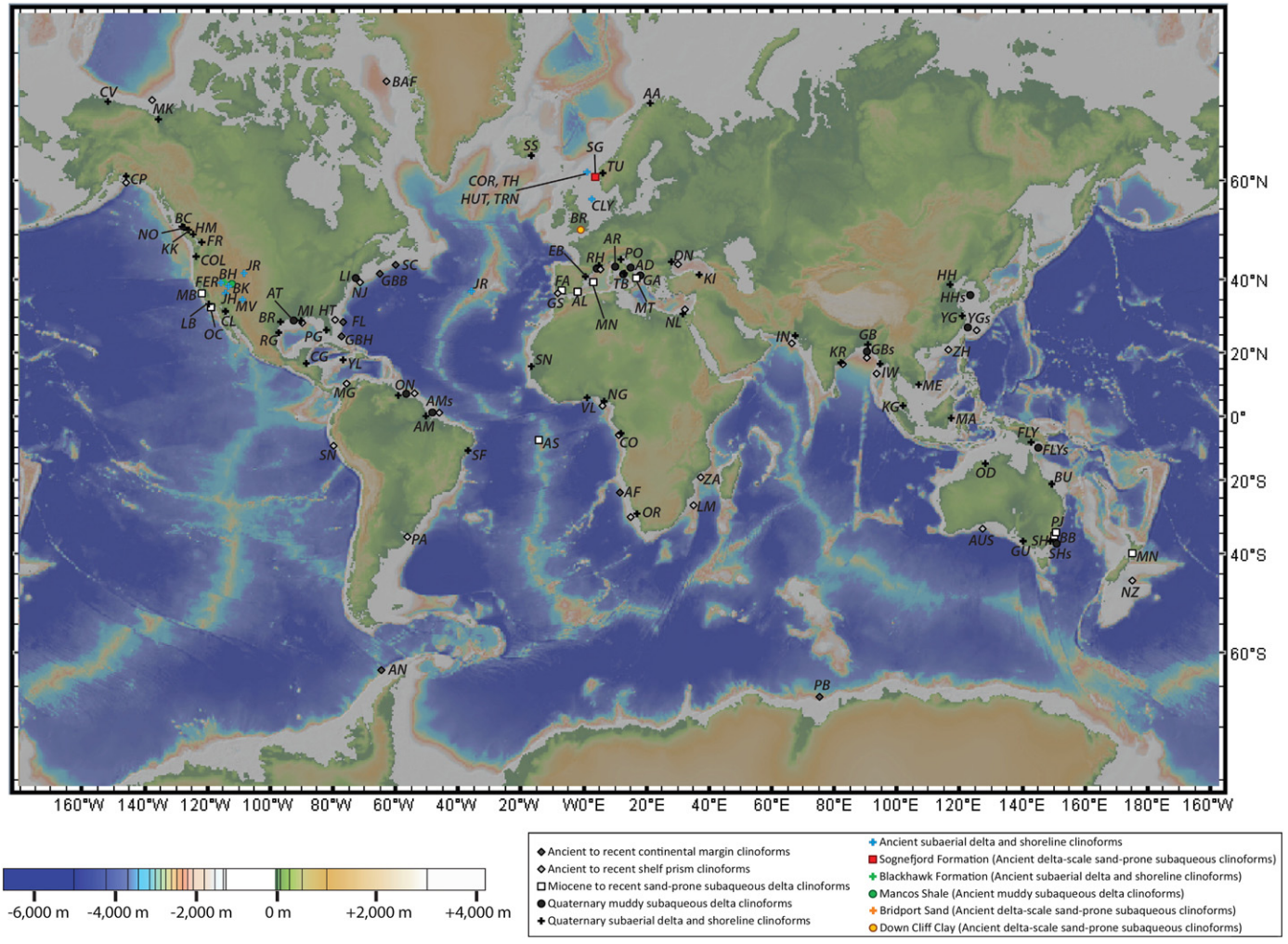

Fig. 6. Location of recent and ancient clinoforms and clinoform sets analysed in this study. Bathymetry and topography are derived from the Global Multi-Resolution Topography dataset of Ryan et al. (2009), and are plotted using GeoMapApp freeware. Abbreviations for clinoforms and clinoform sets are given in Tables 1 and 2.

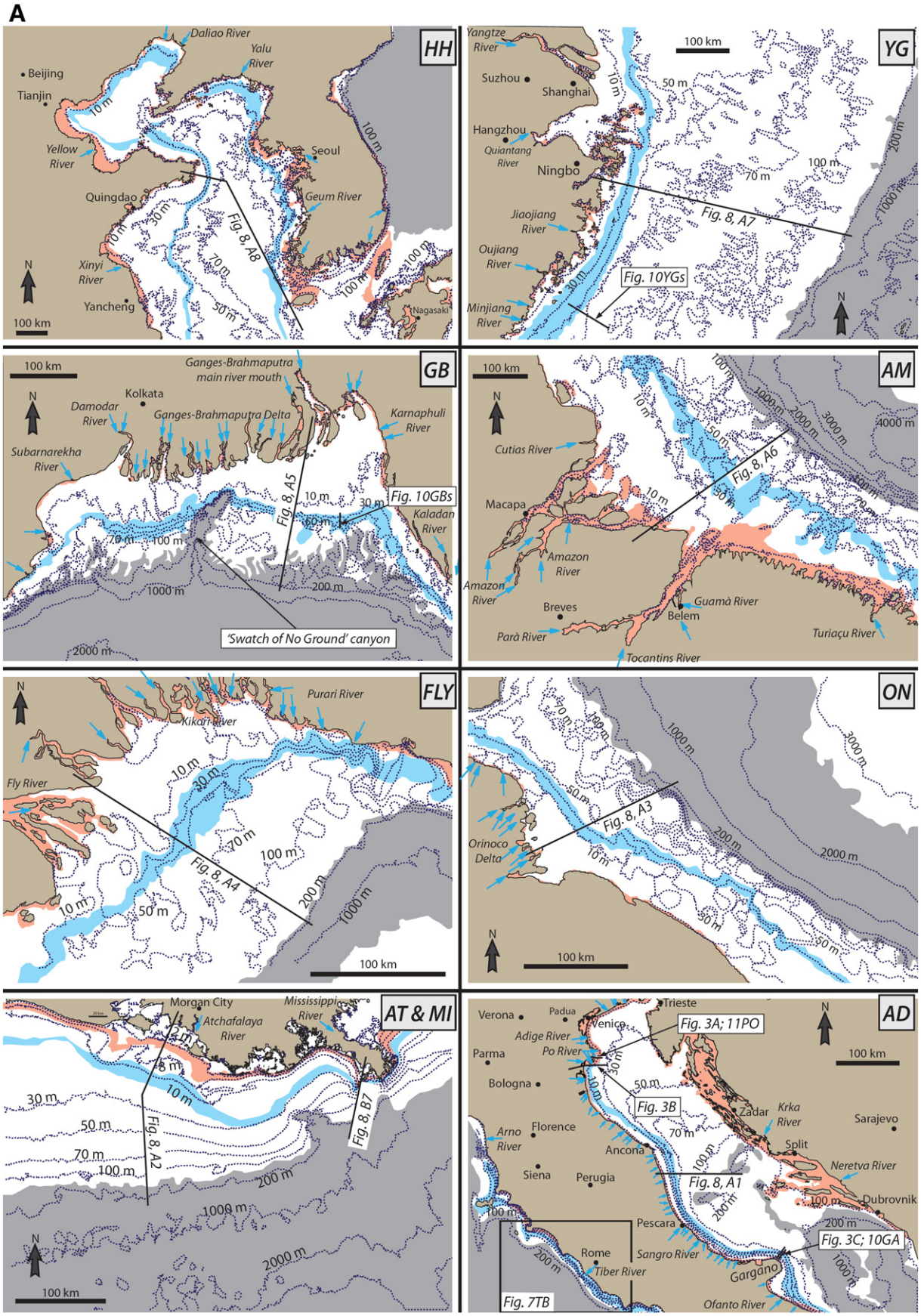
A
HH
Daliao River
Yalu River
Beijing
Tianjin
Yellow River
Seoul
Quingdao
Geum River
Xinyi River
Yancheng
Nagasaki
Fig. 8, A8
10 m
30 m
50 m
70 m
100 m
100 km
YG
Yangtze River
Suzhou
Shanghai
Hangzhou
Quiantang River
Ningbo
Jiaojiang River
Oujiang River
Minjiang River
Fig. 8, A7
Fig. 10YGs
10 m
50 m
70 m
100 m
200 m
1000 m
100 km
GB
Ganges-Brahmaputra main river mouth
Kolkata
Damodar River
Ganges-Brahmaputra Delta
Karnaphuli River
Subarnarekha River
Kaladan River
Fig. 8, A5
Fig. 10GBs
'Swatch of No Ground' canyon
10 m
30 m
60 m
70 m
100 m
200 m
1000 m
2000 m
100 km
AM
Cutias River
Macapa
Amazon River
Amazon River
Breves
Guamà River
Belem
Parà River
Turiaçu River
Tocantins River
Fig. 8, A6
10 m
50 m
70 m
100 m
1000 m
2000 m
3000 m
4000 m
100 km
FLY
Purari River
Kikori River
Fly River
Fig. 8, A4
10 m
30 m
50 m
70 m
100 m
200 m
1000 m
100 km
ON
Orinoco Delta
Fig. 8, A3
10 m
30 m
50 m
100 m
200 m
1000 m
2000 m
3000 m
100 km
AT & MI
Morgan City
Atchafalaya River
Mississippi River
Fig. 8, A2
Fig. 8, B7
8 m
10 m
30 m
50 m
70 m
100 m
200 m
1000 m
2000 m
100 km
AD
Verona
Padua
Trieste
Venice
Fig. 3A; 11PO
Adige River
Po River
Parma
Bologna
Fig. 3B
Zadar
Krka River
Sarajevo
Arno River
Florence
Ancona
Split
Neretva River
Siena
Perugia
Fig. 8, A1
Dubrovnik
Pescara
Fig. 3C; 10GA
Rome
Sangro River
Tiber River
Gargano
Fig. 7TB
Ofanto River
10 m
30 m
50 m
70 m
100 m
200 m
1000 m
100 km

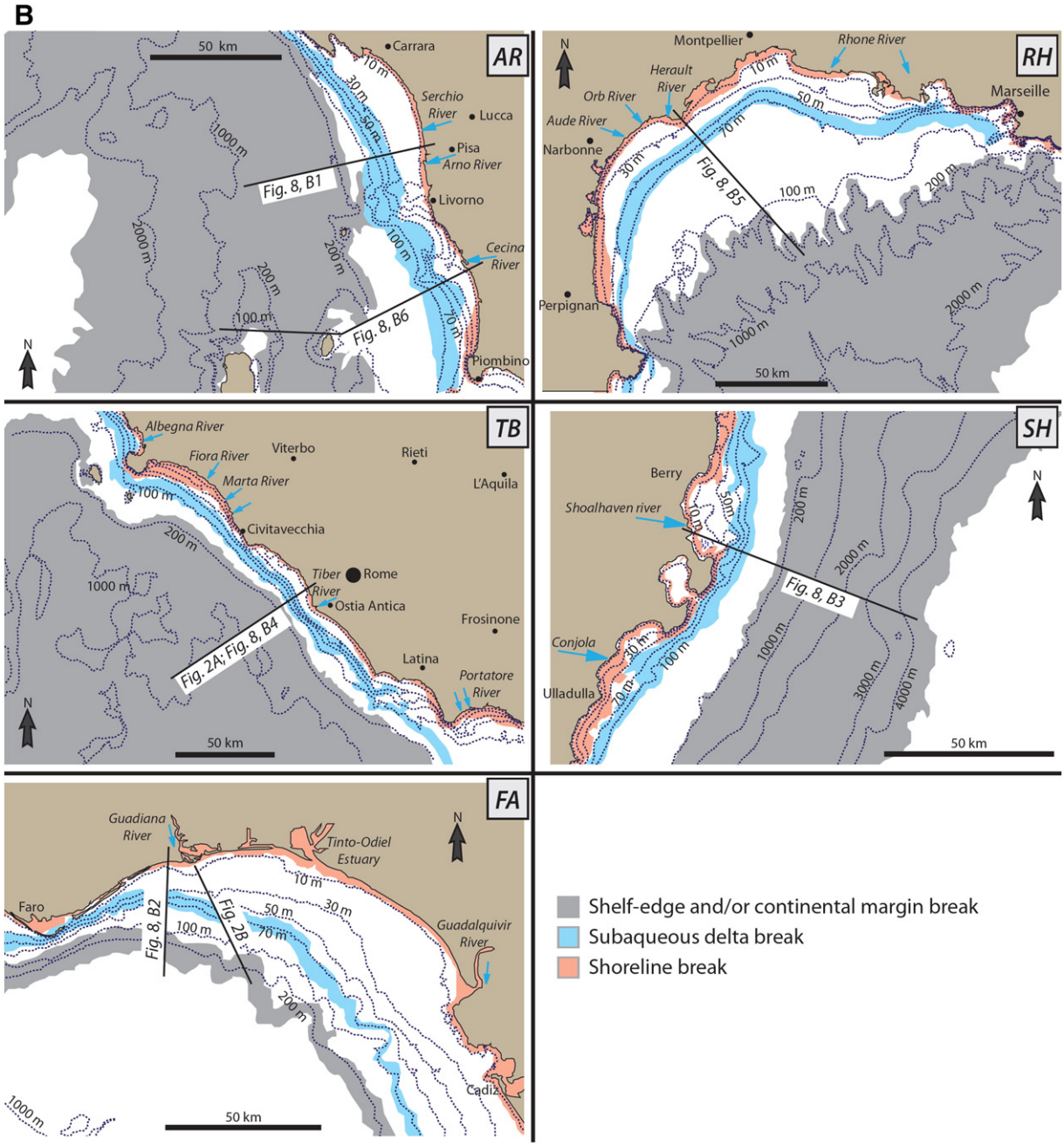

Fig. 7. Maps showing plan-view features of present-day macro-scale shelfal settings where delta-scale compound clinoforms and/or subaqueous clinoforms are actively prograding. Maps and contours are taken from the Global Multi-Resolution Topography dataset of Ryan et al. (2009). Steeper subaqueous areas on the inner-to-mid-shelf (with respect to the surrounding low-gradient shelf) are highlighted by grey shading. The majority of these areas of steeper shelf gradient correspond to the foresets of actively growing clinoforms, whereas in other cases they may correspond to steep erosional surfaces. (A) Cross-sectional profiles shown in Figs. 3, 14 and 16 are located. (HH) Northern Yellow Sea shelf (North-east China and Korea), including the mouth of the Yellow River; (YG) Southern Yellow Sea shelf (eastern China), including the mouth of the Yangtze River; (GB) Indian Ocean shelf off the mouth of the Ganges–Brahmaputra River system (eastern India and Bangladesh) (AM) Western Southern Atlantic Ocean shelf, off the Amazon River mouth (north-eastern Brazil); (FLY) shelf off the southern coasts of Papua New Guinea, including off the Fly River mouth; (ON) Western Southern Atlantic Ocean shelf, off the Orinoco River mouth (eastern Venezuela); (AT & MI) Northern Gulf of Mexico shelf, off the mouth of the Mississippi and Atchafalaya rivers (southern Louisiana, U.S.); (AD) Adriatic Sea shelf, Italy, including the cross-sectional profiles of Po-, Adriatic- and Gargano-type clinoforms in Fig. 3 and the Adriatic Shelf bathymetric profile in Fig. 10. (B) Cross-sectional profiles shown in Figs. 2, 14 and 16 are located. (AR) Tuscany coastlines (Tyrrhenian Sea, north-western Italy), including the profiles off the mouths of Cecina and Arno rivers; (RH) Languedoc shelf (southern France, Western Mediterranean) off the Rhone River mouth; (TB) Tyrrhenian Sea Shelf off the Tiber River mouth (central-western Italy, Western Mediterranean); (SH) shelf off the Shoalhaven River mouth (south-eastern Australia coast); (FA) Eastern North Atlantic Ocean shelf off the coasts of southern Spain and Portugal (Faro-Guadiana). (C) Cross-sectional profiles shown in Figs. 14 and 15 are located. (MN) Manawatu coast (New Zealand); (PJ & BB) South-eastern Australia shelf, including Port Jackson and Bate Bay profiles; (MB) shelf off Monterey Bay, near the Salinas River mouth (California, U.S.A.); (OC) shelf off Oceanside, near the Sand Diego river mouth (California, U.S.A.); (AL) Western Mediterranean Shelf off the Cabo de Gata promontory (Almeria, southern Spain); (AS) Atlantic ocean off the western coastlines of Ascension Island.

physiographic features typical of delta-scale subaqueous and compound clinoforms, and occur in close proximity to previously documented examples. For example, the Arno-Cecina (Italy), Shoalhaven (south-eastern Australia) and San Diego (USA) deltas are situated respectively along-strike of the Tiber, Port Jackson–Bate Bay–Botany Bay and the Oceanside subaqueous and compound clinoforms (c.f. Mitchell et al., 2012), even though they may not represent a unique, continuous subaqueous system. In the case of the

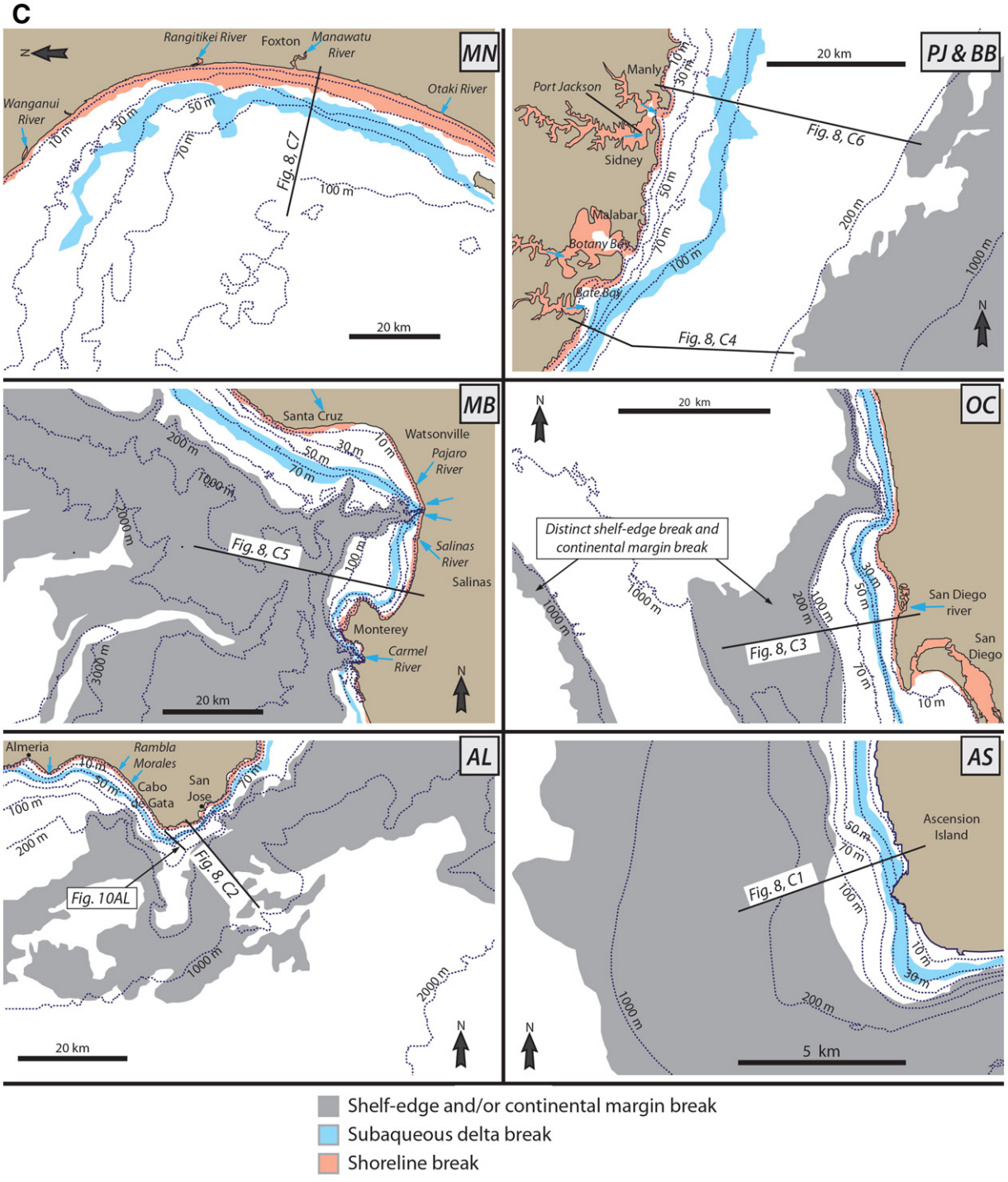

Fig. 7 (*continued*).

Rhone delta, a compound clinoform interpretation is also supported by Holocene sediment isopach and grain-size maps published by Gensous and Tesson (1997), Tesson et al. (2000) and Labaune et al. (2005).

Bathymetric contours and cross sections in Figs. 7–10 have been drawn using the Global Multi-Resolution Topography dataset of Ryan et al. (2009), and areas of relatively steep gradient on the inner-to-mid-shelf have been highlighted in the maps by grey shading. These steep areas form shoreline-parallel belts that generally correspond to the foresets of actively accreting clinoforms, although in some cases they may correspond to steep erosional surfaces (e.g., south-eastern Australia coastlines; Field and Roy, 1984). In most examples, it is possible to distinguish a subaerial delta clinoform at the shoreline, a subaqueous delta clinoform in the middle of the shelf, and a clinoform marking the shelf edge (shelf-prism or continental-margin clinoform). In most of the examples presented here, maps of Late Holocene sediment thickness support the interpretation of actively accreting clinoforms situated at the three present-day breaks in bathymetric gradient (e.g., Nittrouer et al., 1986; Gensous and Tesson, 1997; Michels et al., 1998; Cattaneo et al., 2003, 2007; Liu et al., 2004, 2007; Lobo et al., 2005; Yang and Liu, 2007; Le Dantec et al., 2010). Below, we summarise four representative and particularly well-documented examples of recent delta-

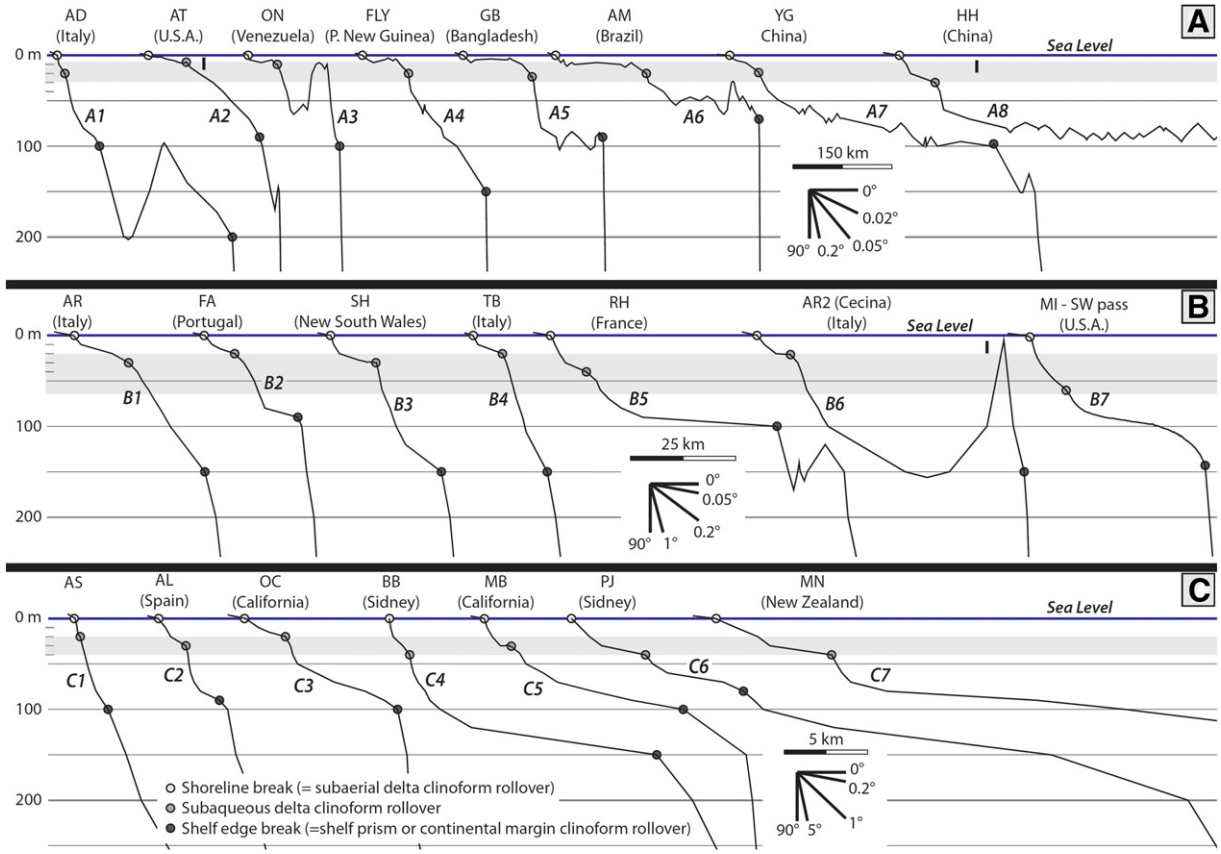

Fig. 8. Bathymetric profiles of typical present-day delta-scale subaqueous clinoforms and compound clinoforms, drawn by utilizing the Global Multi-Resolution Topography dataset of Ryan et al. (2009): (A) macro-scale system, characterised by a horizontal distance between shoreline and subaqueous delta rollover point of ≥10 km, and most commonly well in excess of 50 km (Fig. 7A); (B) meso-scale systems, with a horizontal distance between shoreline and subaqueous delta rollover point of ca. 7–10 km (Fig. 7B); and (C) micro-scale systems, characterised by a horizontal distance between shoreline and subaqueous delta rollover point of ≤7 km, and most often of only 1–2 km (Fig. 7C). The horizontal grey bars highlight the water depth ranges for subaqueous clinoform rollover points in macro-, meso- and micro-scale systems, respectively.

scale subaqueous clinoforms and compound clinoforms, before drawing general observations from comparisons between the associated maps and cross sections (Fig. 12).

3.1. Example 1: Po subaerial delta and Adriatic subaqueous delta clinoforms

Cattaneo et al. (2003, 2007) used high-resolution CHIRP sonar profiles and bathymetric data to constrain the architecture of Late Holocene muddy subaqueous clinoforms that are actively accreting on the western Adriatic shelf margin, offshore eastern Italy (Figs. 3, 7A–AD, 8A1, 10PO–GA). Biostratigraphic and chronostratigraphic data from cores were used to define a high-resolution chronology for the clinoform-bearing strata. The Adriatic subaqueous clinoform set is a laterally extensive (ca. 600 km), mud-rich belt that strikes parallel to the current Italian coastline, from the Po Delta in the north to the Gargano peninsula in the south. It is up to 35 m thick and clinoform foresets dip up to 0.5°. Adriatic shelf clinoforms started to form after the attainment of the Holocene sea-level highstand (6.5–5.5 ka), and are still prograding perpendicular to the north-to-south flowing Western Adriatic Coastal Current that drives shore-parallel advective sediment transport from the Po river and numerous other, smaller Adriatic rivers. The clinoform is compound in the north (Fig. 3B) and has a subaqueous clinoform topset-to-foreset rollover at a water depth of 8 m. In contrast, an isolated subaqueous clinoform is developed in the south (Fig. 3C) with a subaqueous clinoform topset-to-foreset rollover at a water depth of 30 m. Despite the absence of direct river supply in the southern portion of the clinoform set, the subaqueous delta accounts for up to 14% of the total volume (180 km^3) of the mud belt. Southward-flowing, bottom-hugging shelf currents play an important role in redistributing the sediment southwards and in limiting sedimentation in the bottomset region, by trapping most of the sediment on the inner shelf and forcing it along-shore rather than across-shelf. Lead isotope dates from several cores document a maximum sedimentation rate of up to 1.5 cm/yr in the clinoform foreset, and discrete episodes of active clinothem outbuilding separated by periods of condensed sedimentation. The onset of the most recent subaqueous clinothem-building phase is coeval with the initiation of major progradation of the subaerial Po Delta at the beginning of the Little Ice Age, about 500 years ago (Cattaneo et al., 2003; Correggiari et al., 2005).

3.2. Example 2: Yangtze subaqueous delta clinoforms

Since the Holocene relative sea-level highstand at 6–7 ka BP, the Yangtze (Changjiang) River has delivered ca. 1.7×10^{12} t of sediment to the coastline and submarine shelf, forming a broad tide-dominated subaerial delta (Hori et al., 2001) and an associated muddy subaqueous delta (Liu et al., 2006, 2007; Figs. 7A–YG, 8A7, 10YGs). Interlaminated sand–mud couplets and bidirectional ripple cross-laminations in the sediments of the subaerial delta indicate a strong tidal influence (Hori et al., 2001). The subaqueous delta forms a silt-to-clay-rich, sigmoidal clinothem oriented parallel to the coastline. This stretches along-shelf from the river mouth for 800 km, and extends across-shelf for up to nearly 100 km (Liu et al., 2006, 2007). Holocene subaqueous-delta clinoforms downlap onto a sub-horizontal, post-glacial, sandy transgressive layer (Fig. 7YG), and form a mud wedge encompassing a total volume of 4.5×10^{11} m^3; this accounts for approximately half the

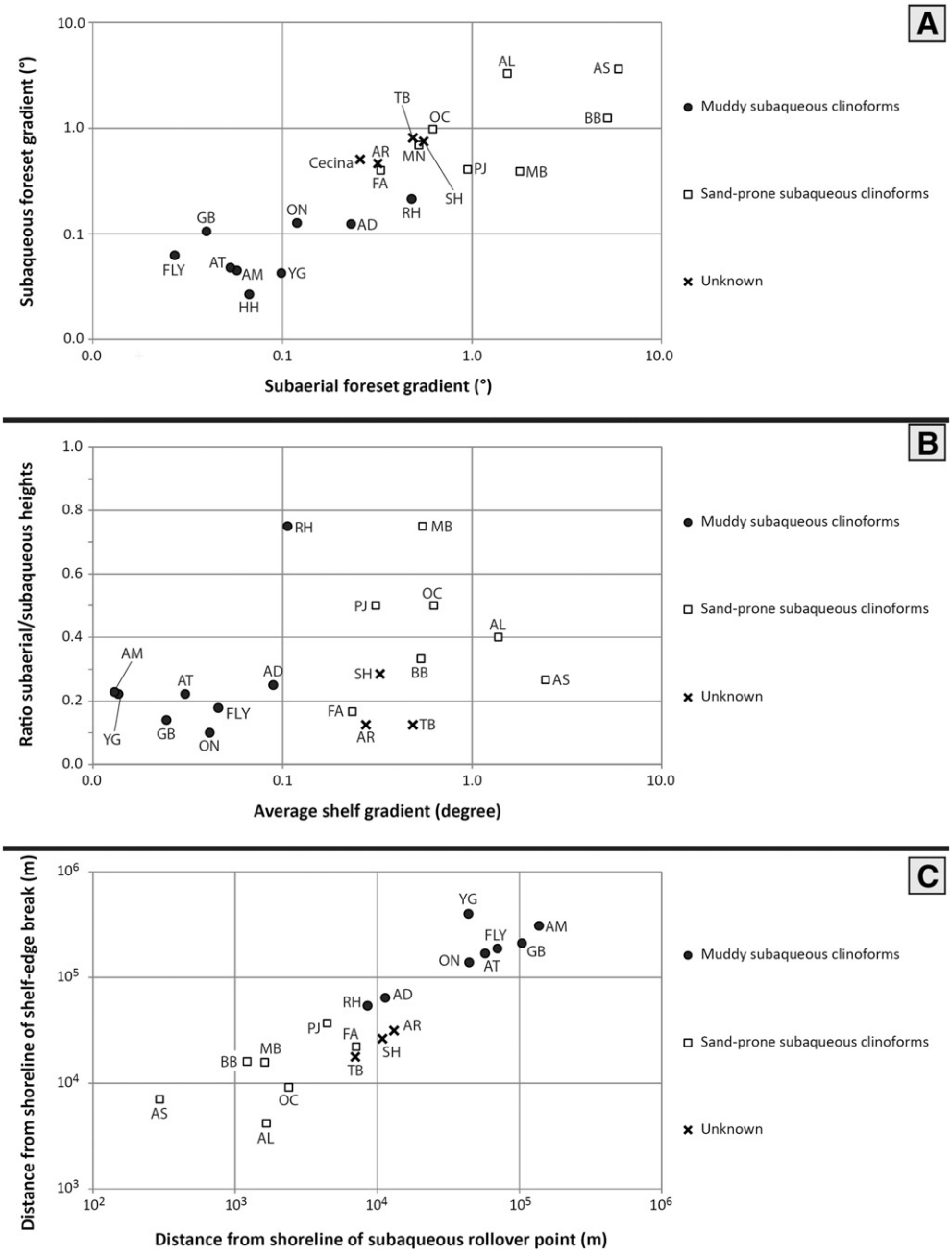

Fig. 9. Plots of morphological parameters of recent deltaic compound clinoforms and delta-scale subaqueous clinoforms (Figs. 11–14): (A) subaqueous clinoform foreset gradient versus subaerial clinoform foreset gradient; (B) ratio of subaerial to subaqueous clinoform heights versus average shelf gradient; and (C) distance from shoreline of shelf-edge break versus distance from shoreline of subaqueous rollover point. Abbreviations for clinoforms and clinoform sets are introduced in Tables 1 and 2.

current annual sediment discharge of the Yangtze (Liu et al., 2007). Subaqueous clinoform foresets are situated between the 20 and 30 m isobaths, corresponding to the main clinothem depocentre, which exhibits a maximum thickness of ca. 40 m. Bottomsets reach distances of up to 100 km offshore and terminate in water depths of 60–90 m (Liu et al., 2006, 2007). ^{14}C chronology indicates that average progradation rate of the subaerial delta since 5 ka BP was ca. 50 km/yr, but after 2 ka BP it abruptly increased to ca. 80 km/yr, possibly due to anthropogenic or climatic forcing; maximum sediment accumulation rate in the subaerial delta front has been ca. 3.5 m/kyr (Hori et al., 2001). ^{210}Pb data show that maximum sedimentation rates of 430 m/kyr occur in the portion of the subaqueous delta adjacent to the Yangtze subaqueous delta, and decrease both offshore and to the south (Liu et al., 2006, 2007). Mineralogical, geochemical and grain-size analyses suggest that subaqueous deposits have been fed by the alongshore Chinese Coastal Current, which has redistributed sediments sourced predominantly by the Yangtze River towards the south, with minor inputs from smaller local rivers (Liu et al., 2006). Interaction of strong tides, waves, upwelling and alongshore currents has created an oceanographic setting that has trapped most Yangtze-fed sediment on the inner shelf, forcing it to be transported alongshore rather than across-shelf. This formed a shelfal sediment wedge striking parallel to the shore and precluded sediment escape towards the deep-marine Okinawa Through (Liu et al., 2006).

3.3. Example 3: Ganges–Brahmaputra subaqueous delta clinoforms

The Ganges–Brahmaputra is the world's third largest river feeder in terms of sediment load (Kuehl et al., 1997). Kuehl et al. (1997), Michels

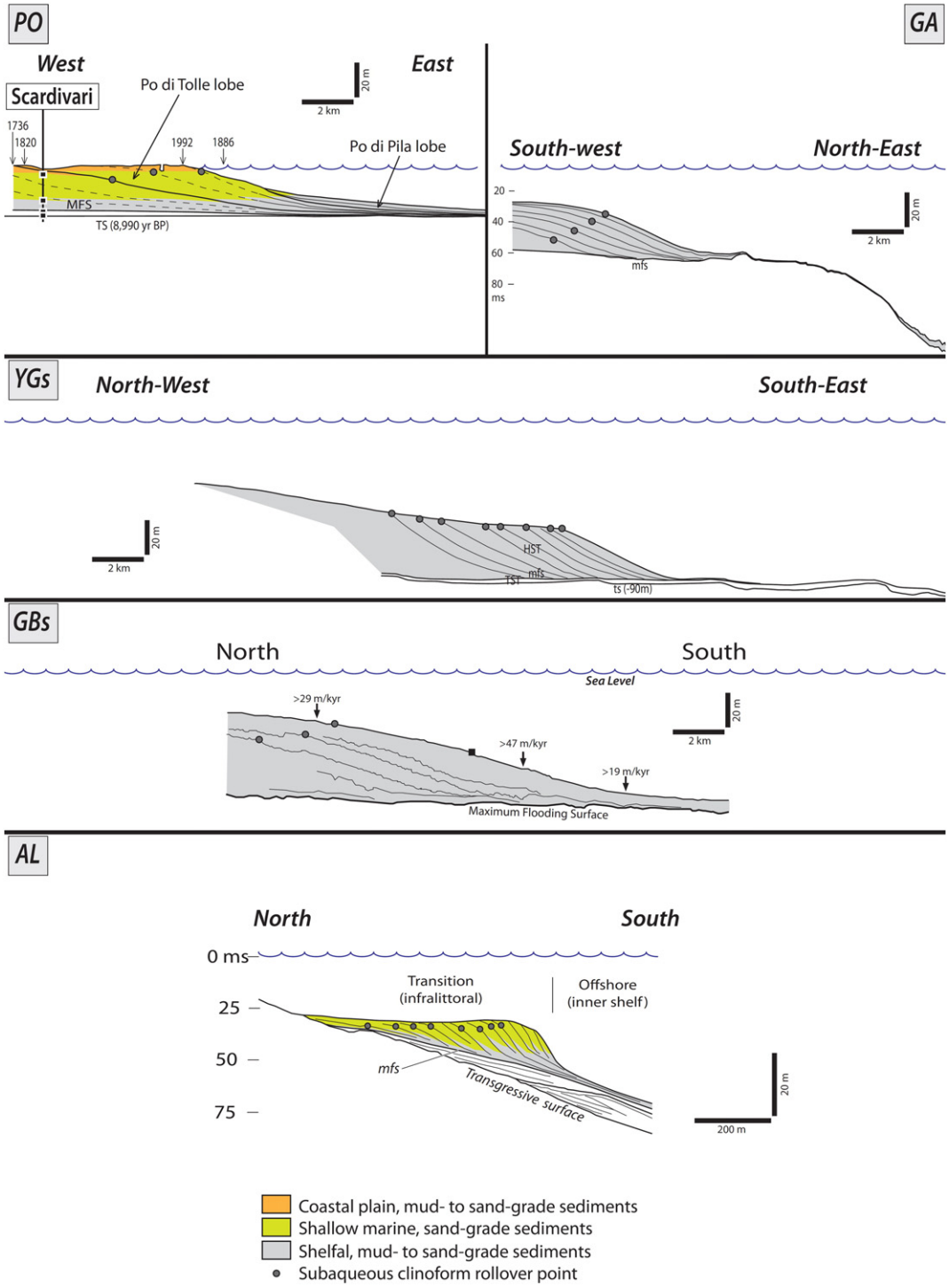

Fig. 10. Depositional-dip profiles across recent delta-scale subaqueous clinoforms: (PO) Po subaerial delta clinoform and linked (GA) Gargano subaqueous delta clinoform (after Correggiari et al. (2005); Cattaneo et al. (2003, 2007)); (YGs) subaqueous clinoform off the Yangtze River delta (after Liu et al. (2007)); (GBs) subaqueous clinoform off the Ganges–Brahmaputra River delta (after Palamenghi et al. (2011)); (AL) subaqueous clinoform off Cabo de Gata shoreline, southern Spain (after Hernández-Molina et al. (2000a)).

et al. (1998) and Palamenghi et al. (2011) utilized seismic reflection profiles and piston and gravity cores in order to study the Ganges–Brahmaputra sandy–silty subaqueous deltas, and estimated sediment accumulation rates using ^{210}Pb and ^{137}Cs gamma spectrometry. The sigmoidal clinoform formed by the subaqueous delta comprises a very gently-dipping topset and bottomset (0.02–0.04°), and a slightly steeper foreset (ca. 0.19°) (Figs. 7A–GB, 8A5, 10GB). The topset is located in <20 m water depth, whereas the bottomset is located in ca. 80 m water depth, where it overlies an Upper Pleistocene transgressive surface (Kuehl et al., 1997). Below this depth, no Holocene sediment is preserved (Michels et al., 1998). About 20% of the total sediment load of the Ganges–Brahamaputra river mouth is deposited on the foreset of the subaqueous clinoform, which is therefore characterised by higher sediment accumulation rates (ca. 50–100 m/kyr) than the bottomset (ca. 30 m/kyr). These interpretations are also supported by seismic-reflection profiles showing clinoform reflection surfaces progressively

Table 3
Parameters extracted from the Global Multi-Resolution Topography bathymetric dataset (Ryan et al., 2009), for present-day delta-scale compound clinoform systems (Figs. 7–10). The range refers to the 5- to 95-percentile of the statistical distribution.

	Muddy delta-scale subaqueous clinoforms	Sand-prone delta-scale subaqueous clinoforms
Water depth of rollover points of delta-scale subaqueous clinoforms (m)	6–59 m	21–57 m
Distance from shoreline to rollover point of delta-scale subaqueous clinoforms (m)	7500–126,000 m	610–7200 m
Distance from subaqueous rollover to shelf-edge-break (m)	15,000–308,000 m	3700–32,500 m
Distance from shoreline to shelf-edge break (m)	23,000–376,000 m	5000–32,500 m
Shelf average gradient (°)	0.01–0.38°	0.26–2.12°
Subaerial foreset gradient (°)	0.03–0.62°	0.40–5.67°
Subaqueous foreset gradient (°)	0.03–0.76°	0.39–3.49°
Ratio subaerial/subaqueous gradient (non-dimensional)	0.39–2.46	0.53–4.45
Ratio subaerial/subaqueous foreset heights (non-dimensional)	0.11–0.73	0.20–0.91

diverging from the topset to the foreset and converging again towards the bottomset (Kuehl et al., 1997). The clinoform foreset is formed by graded sandy–silty laminae interbedded with clay laminae. The coarsest-grained layers are presumably deposited by sediment-laden underflows generated during tropical storms, with up to 8 m thick mass flows created in the subaqueous delta front area by episodic earthquakes or storms (Michels et al., 1998). These last deposits are imaged in seismic reflection profiles as transparent units (Palamenghi et al., 2011). The subaqueous clinoform is actively prograding every year by ca. 12–17 m across the Bengal Shelf. Sediment becomes increasingly finer-grained offshore and westwards, which in combination with analyses of seabed palaeocurrent indicators, suggests that subaqueous clinoforms have been fed by westward-flowing cyclonic currents that transport sediment fed by the Ganges–Brahamaputra river mouth alongshore and offshore (Kuehl et al., 1997). A large canyon, known as 'Swatch of No Ground', deeply dissects the shelf and the subaqueous

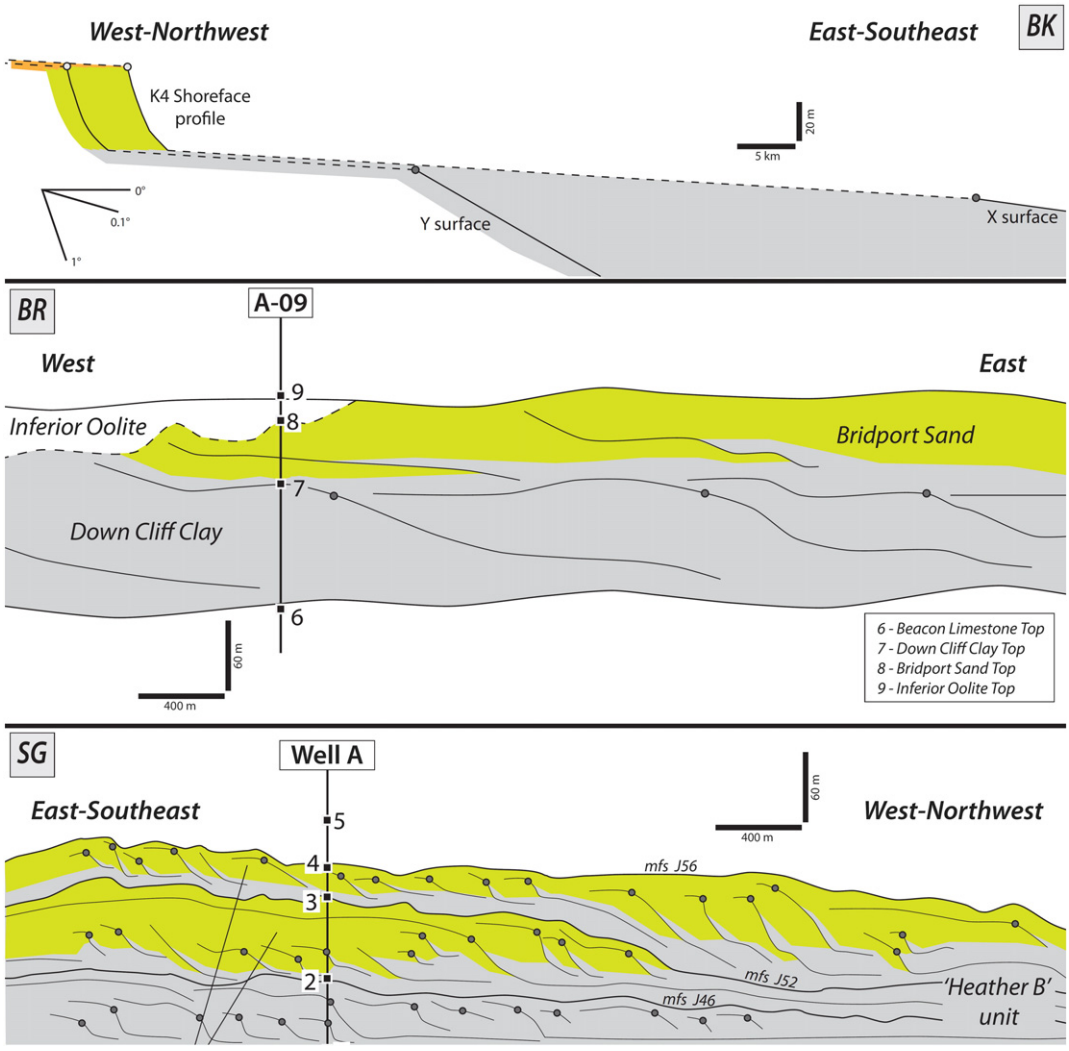

Fig. 11. Depositional-dip profiles across ancient delta-scale subaqueous clinoforms: (BK) Upper Cretaceous Blackhawk Formation subaerial delta clinoforms and linked Mancos Shale subaqueous delta clinoforms, Western Interior Basin, onshore USA (after Hampson (2010)); (BR) Lower Jurassic Bridport Sand Formation subaerial delta clinoforms and linked Down Cliff Clay subaqueous delta clinoforms, Wessex Basin, onshore UK (after Morris et al. (2006); Hampson et al. (in press)); (SG) Upper Jurassic Sognefjord Formation subaqueous delta clinoforms, North Sea Basin, offshore Norway (after Patruno et al. (2013b)); (MN) Upper Miocene calcareous grainstones, Menorcan platform (Spain), Mediterranean Basin (after Pomar et al. (2002)).

delta front (Fig. 7A–GB). This canyon captures most of the sediment load carried by the westward-flowing cyclonic currents, allowing shelf bypass of >35% of the fluviatile sediment load towards the deep-marine Bengal Fan. This oceanographic configuration has caused off-shelf sediment transport and turbidite deposition to the slope and basin-floor during the Holocene highstand, together with growth faults, slumping and high Holocene sedimentation rate (ca. 500 m/kyr) near the canyon head (Kuehl et al., 1986, 1997; Weber et al., 1997; Michels et al., 1998). Palamenghi et al (2011) suggest that sediment deposition towards the western part of the subaqueous delta has increased in the last few centuries, with subsequent higher sediment export to the deep-water fan through the 'Swatch of No Ground' canyon.

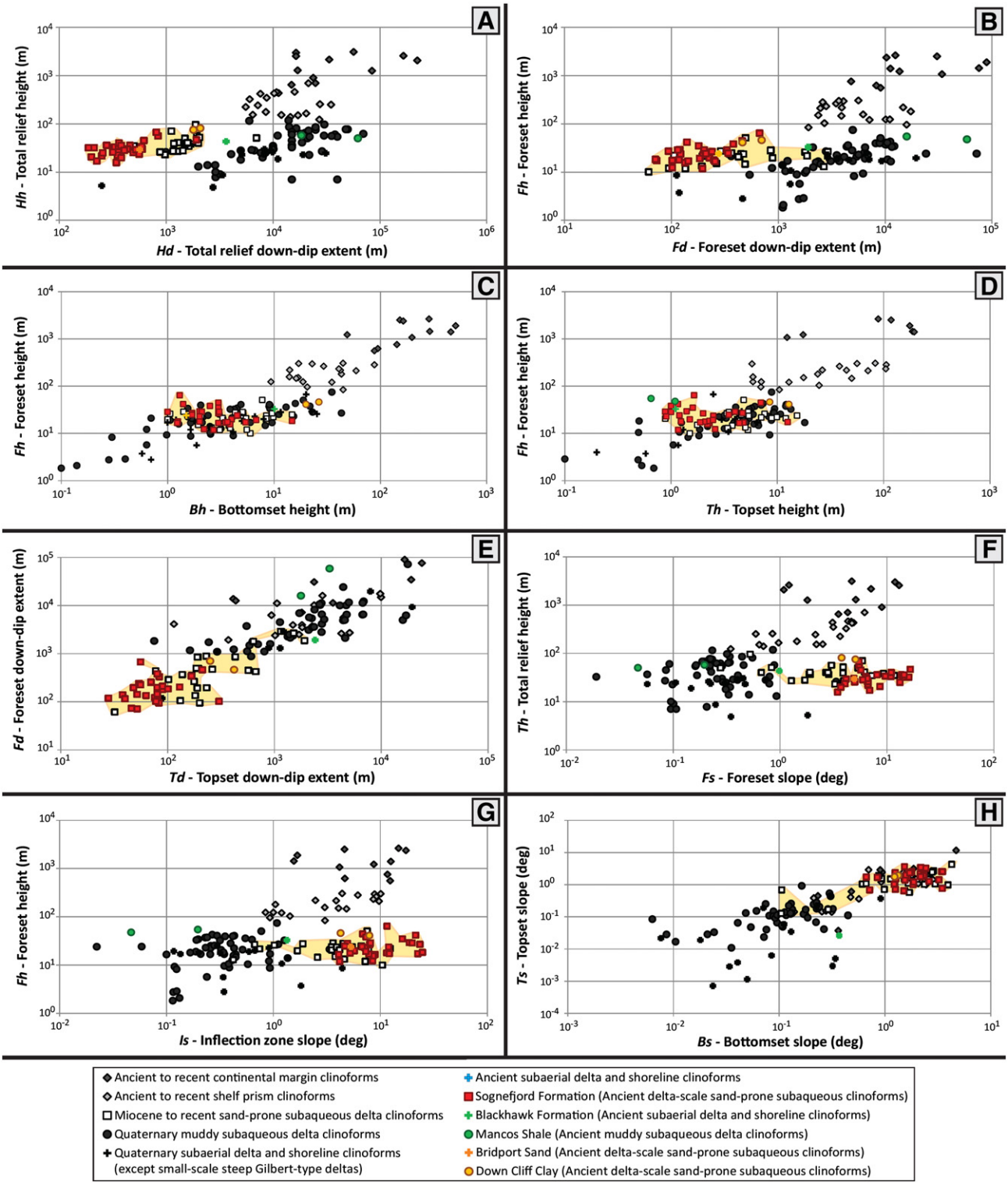

Fig. 12. Plots of clinoform morphological parameters. Different clinoform types tend to plot in different, but overlapping, fields. See Fig. 5 for units and clinoform nomenclature.

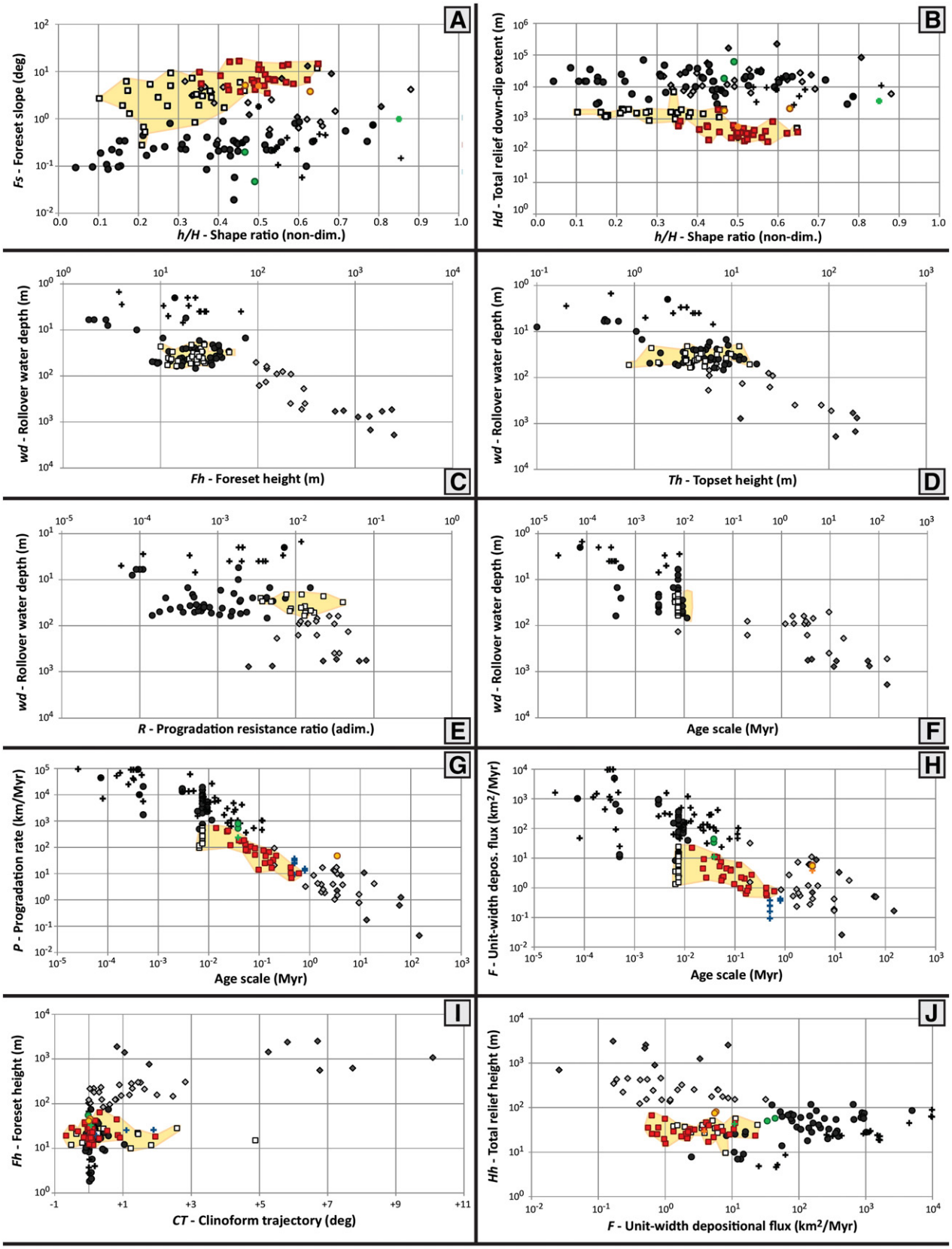

Fig. 13. Plots of clinoform morphological, architectural and chronostratigraphic parameters. Different clinoform types tend to plot in different, but overlapping, fields.

3.4. Example 4: Southern Iberia subaqueous clinoforms

Sand-prone subaqueous clinoforms dipping sub-parallel to the present-day seabed and striking parallel to the modern shoreline are situated south of the promontory of Capo de Gata (southern Spain, Mediterranean Iberia) and in the proximity of Faro (Portugal, Atlantic Iberia) (Fig. 7C–AL, 8C2, 10AL). These sandbodies have been described by Hernández-Molina et al. (2000a), Lobo et al. (2005) and Fernández-Salas et al. (2009) through the use of boomer seismic profiles. The clinoform wedge started to prograde during the Late Holocene sea-level highstand (from ca. 6.5 ka) and it downlaps older transgressive units. The seafloor over which this prograding wedge developed dips relatively steeply offshore (up to 0.50°) and the clinoform foresets within it become progressively steeper seawards. Mean grain sizes of medium-grained and fine-grained sands were described from surface grab samples located respectively 1 km seaward and 1 km landward of the clinoform topset-to-foreset rollover (Hernández-Molina et al., 2000a). The clinoform set is interpreted to have been generated by storm-related downwelling currents, with associated seawards sediment transport and deposition below fairweather wave base (Hernández-Molina et al., 2000a). The subaqueous clinoforms offshore southern Spain consist of a series on *en-échelon* bodies in plan-view (Fernández-Salas et al., 2009), suggesting that there was also a significant component of alongshore sediment transport. These subaqueous clinoforms are not apparently linked directly to riverine sediment input points. Instead, they onlap onto the underlying substrate and are associated with non-deltaic shorelines and strandplains (e.g., Fernández-Salas et al., 2009).

3.5. Comparison and general observations

Map views confirm that all of the identified delta-scale subaqueous clinoforms strike parallel to the adjacent coastline, particularly in systems dominated by waves and currents (Fig. 7A,B,C; Tables 1 and 2). On subaqueous shelves where tides are an important component of the overall hydrodynamic regime (e.g., Amazon and Orinoco systems), the plan-view geometry of delta-scale subaqueous clinoform bodies is less regular (Fig. 7AM, ON; Tables 1 and 2).

Cross-sections oriented parallel to depositional dip (Fig. 8) show overall subaqueous clinoform heights of 10–100 m, whilst the dip extent (1–100 km) and hence the gradients of the subaqueous clinoforms are extremely variable. Based on the amount of overall subaqueous clinoform progradation away from the shoreline, it is possible to distinguish three sizes of compound clinoform systems (Fig. 8): macro-scale (≥10 km, and often well in excess of 50 km), meso-scale (ca. 7–10) and micro-scale (≤7 km, and most commonly only 1–2 km). The water depth of the topset-to-foreset rollover point is relatively shallow in macro-scale, muddy subaqueous systems linked to major subaerial deltas (ca. 10–30 m depth; Fig. 8A), but relatively deep in meso- and micro-scale, sandier systems (ca. 20–60 m water depth; Fig. 8B–C). A likely explanation for this is that the position of the topset-to-foreset rollover point directly reflects the maximum entrainment depth of the upper 10-percentile wave-current traction field (cf., Pirmez et al., 1998; Hernández-Molina et al., 2000a; Cattaneo et al., 2003, 2007; Mitchell, 2012; Mitchell et al., 2012), and progressively stronger mean waves are required to transport increasingly coarser-grained sediments. In the transition from macro-scale, muddy deltaic systems towards meso- and micro-scale, sandier deltaic and shoreline systems, the associated subaqueous clinoforms and shelves become steeper and narrower (Fig. 8).

The average foreset slope gradients of both subaerial and subaqueous components of recent delta-scale compound clinoforms are ≤0.76° in muddy systems and ≥0.39° in sandy systems, with minimum values for muddy systems and maximum values for sandy systems of 0.03° and 6°, respectively (Fig. 9A). As shown in Fig. 9B, the height of the subaerial clinoform foreset is often greater than one fifth of the height of its subaqueous counterpart in sand-prone compound clinoforms. Values of this ratio in muddy compound clinoforms are generally smaller than 0.2 (Fig. 9B). The topset-to-foreset rollovers of sand-prone and muddy, delta-scale subaqueous clinoforms occur at distances from the present-day shoreline of 0.6–7.2 km and 7.5–125 km, respectively (Fig. 9C). Furthermore, mud-prone, subaqueous delta clinoforms are situated on gently-sloping (0.01–0.38°), wide (23–376 km) shelves, whereas sand-prone, subaqueous clinoforms are situated on steep (≥0.26°), narrow (5–32 km) shelves (Fig. 9B–C; Table 3).

Modern, delta-scale, sand-prone subaqueous clinoforms tend to occur on steep, wave-dominated, inner shelves where mean wave heights and periods are typically 1–2.5 m and 6–11 s respectively, with a maximum of 2–4.5 m and 8–13 s (Mitchell et al., 2012), and where a relatively high sediment supply is provided by longshore and/or storm-related downwelling currents (Hernández-Molina et al., 2000a; Xing and Davies, 2002). Numerical modelling suggests that strong seafloor agitation produced by the combined action of large waves and alongshore and downwelling bottom currents during the rising stage of storms result in net-seaward export of shoreface-derived sand (Mitchell, 2012; Mitchell et al., 2012). The availability of large volumes of reworked sand permits active accretion of sand-rich clinoforms below fairweather wave base by deposition along their foresets. In particular, upper-10 percentile waves are able to entrain sand-grade sediment at the topset-to-foreset rollover depth, and therefore clinoform rollover depth primarily reflects the upper-10 percentile wave base depth. Strong surface winds generate alongshore and seaward-directed (i.e., downwelling) advective bottom currents that may affect sites deeper than 60 m at distances of up to 15 km away from the shoreline. Currents and waves interact in a nonlinear pattern, and comparatively modest increases in current velocities result in much higher combined stresses at the seafloor (Mitchell, 2012; Mitchell et al., 2012). Furthermore, Friedrichs and Wright (2004) described how the hyperpycnal outflow of certain rivers may be modulated by wave action. This process may potentially aid bypass of riverine sediment across the inner shelf and the generation of delta-scale sand-prone subaqueous clinoforms seaward of the mouth of a river (e.g., Monterey Bay clinoforms, off the mouth of the River Salinas; Mitchell et al., 2012). This type of subaqueous clinoform is composed of sands that are more poorly-sorted than those derived from adjacent shorefaces (e.g., southern Iberia subaqueous clinoforms; Hernández-Molina et al., 2000a; Fernández-Salas et al., 2009).

4. Ancient delta-scale compound clinoforms

Compared to their modern equivalents, there are relatively few documented examples of ancient delta-scale subaqueous clinoforms. Each of these examples is summarised below, with the aid of cross sections showing the clinoforms and their associated stratigraphic architecture (Fig. 11).

4.1. Example 1: Blackhawk Formation subaerial delta and Mancos Shale subaqueous delta clinoforms

Hampson (2010) used large outcrop transects (ca. 200–300 km wide) and a large well dataset (ca. 2800 wells) to reconstruct the sedimentology and stratigraphic architecture of ca. 60,000 km^2 of the Santonian–Campanian, sub-tropical shelf of the Western Interior Seaway (Utah, USA) within a high-resolution (ca. 0.1 to 0.5 Myr) sequence stratigraphic framework. A wave-dominated delta with a compound clinoform morphology was interpreted for the Lower Campanian 'K4' shoreface-shelf tongue of the Blackhawk Formation and coeval Mancos Shale (Fig. 11BK). This deltaic shelf is characterised by a relatively high sediment accumulation rate (ca. 270 m/Myr) and by a concave-landward, net-regressive shoreline trajectory (>0.1°). The compound clinoform interpretation was suggested by Hampson (2010) because the 'X', 'Y' and 'Z' middle shelf gravity flow intervals of the Prairie

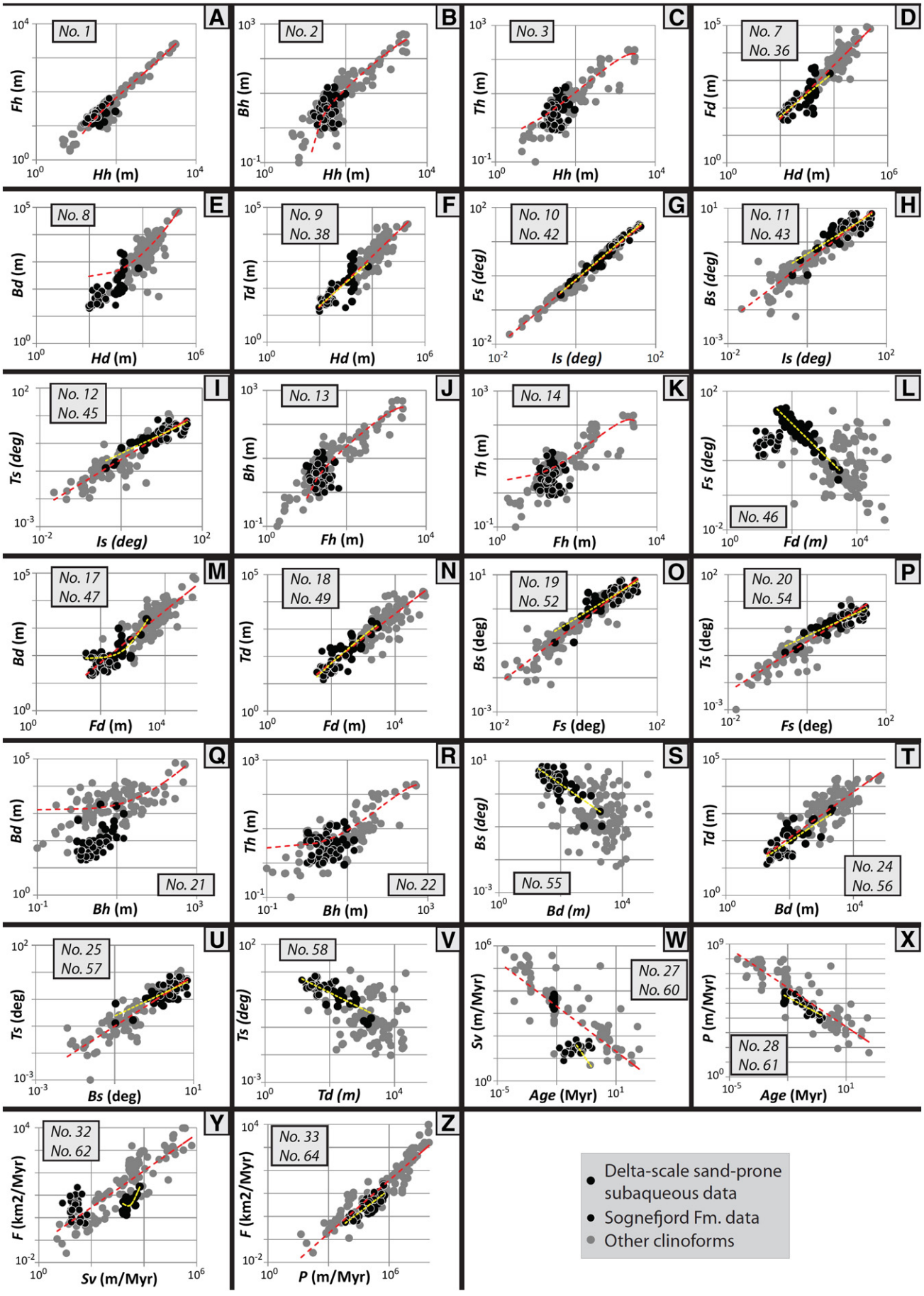
A
No. 1
Fh (m)
Hh (m)
B
No. 2
Bh (m)
Hh (m)
C
No. 3
Th (m)
Hh (m)
D
No. 7
No. 36
Fd (m)
Hd (m)
E
No. 8
Bd (m)
Hd (m)
F
No. 9
No. 38
Td (m)
Hd (m)
G
No. 10
No. 42
Fs (deg)
Is (deg)
H
No. 11
No. 43
Bs (deg)
Is (deg)
I
No. 12
No. 45
Ts (deg)
Is (deg)
J
No. 13
Bh (m)
Fh (m)
K
No. 14
Th (m)
Fh (m)
L
Fs (deg)
No. 46
Fd (m)
M
No. 17
No. 47
Bd (m)
Fd (m)
N
No. 18
No. 49
Td (m)
Fd (m)
O
No. 19
No. 52
Bs (deg)
Fs (deg)
P
No. 20
No. 54
Ts (deg)
Fs (deg)
Q
Bd (m)
No. 21
Bh (m)
R
Th (m)
No. 22
Bh (m)
S
Bs (deg)
No. 55
Bd (m)
T
Td (m)
No. 24
No. 56
Bd (m)
U
No. 25
No. 57
Ts (deg)
Bs (deg)
V
No. 58
Ts (deg)
Td (m)
W
No. 27
No. 60
Sv (m/Myr)
Age (Myr)
X
P (m/Myr)
No. 28
No. 61
Age (Myr)
Y
No. 32
No. 62
F (km2/Myr)
Sv (m/Myr)
Z
No. 33
No. 64
F (km2/Myr)
P (m/Myr)
Delta-scale sand-prone subaqueous data
Sognefjord Fm. data
Other clinoforms

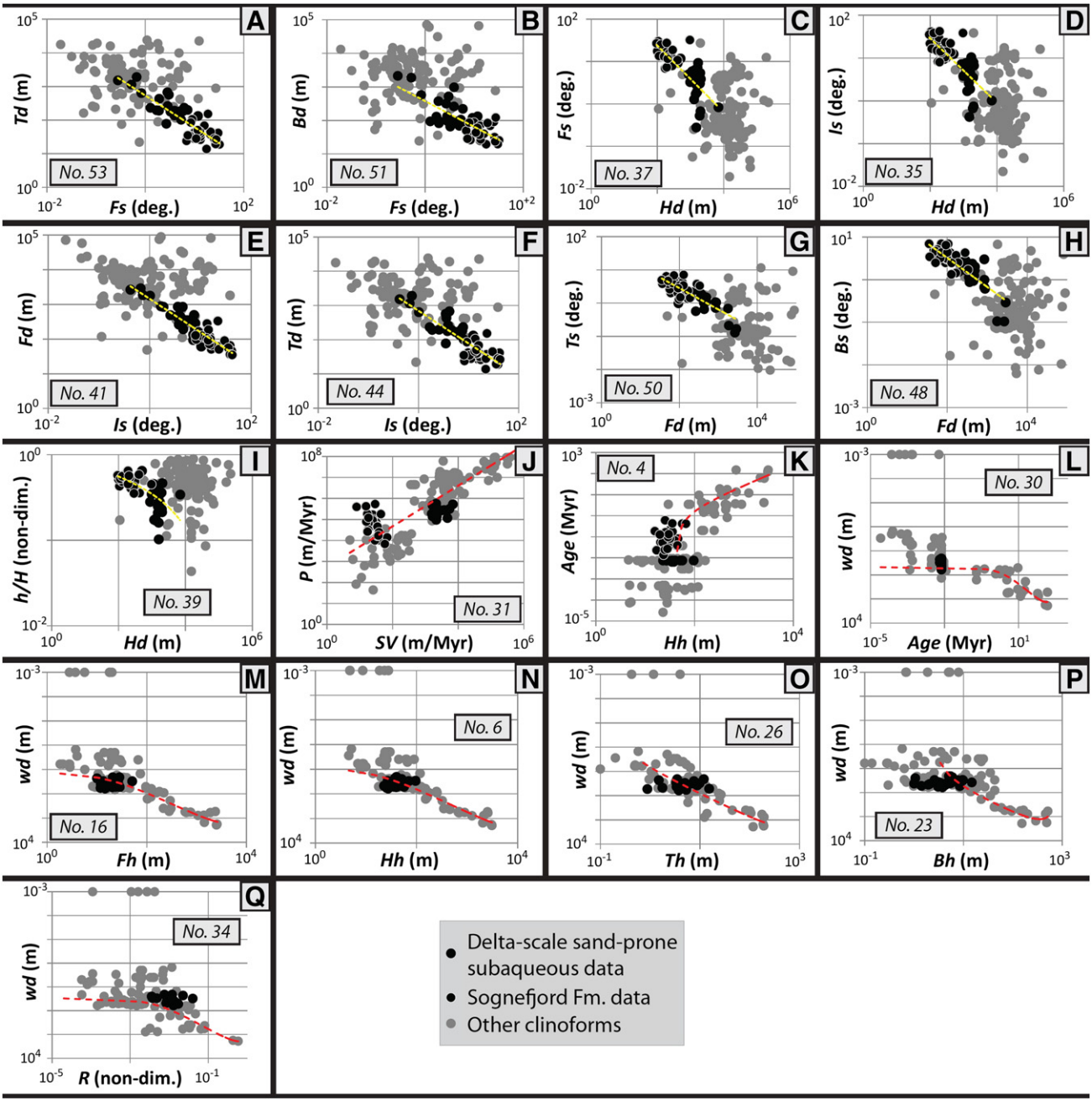

Fig. 15. Plots of parameter pairs showing moderate-to-strong ($R^2 > 0.5$) statistical correlations. Red and yellow best-fit lines correspond to correlations for all clinoforms and sand-prone subaqueous delta clinoforms, respectively. Equations for the best-fit lines are numbered in the grey boxes in each plot; these equations and values of the coefficient of determination (R^2) describing each best-fit line are given in Tables 5 and 7. See Fig. 5 for units and clinoform nomenclature.

Canyon Member (Mancos Shale) dip palaeoseaward of 0.1–0.2° relative to the underlying flooding surfaces, and correlate with the 'K4' shoreface-shelf 'subaerial delta' clinoform (Fig. 11BK). The wave-dominated shoreline clinoform is sandstone-prone, and is separated by a 2 to 22 km wide belt of nearshore, storm-reworked sandstones from a gently-dipping subaqueous clinoform on the middle shelf. The subaqueous clinoforms in this stratigraphic interval comprise a muddy topset and a foreset composed of gravity-flow siltstones and sandstones, and is part of a >250 km wide, offshore mudstone belt. Decompacted subaqueous clinoforms were inferred to have been low gradient (ca. 0.2–0.4°), and have a topset depth that implies a storm wave-base at ca. 50–80 m water depth. These geomorphological and facies characteristics are comparable to modern-day subaqueous deltas. Hampson (2010) noted that, in the case of the delta-scale compound clinoform system formed by the sandy 'K4' shoreline clinoforms and by the 'X' to 'Y' subaqueous clinoforms, shoreline progradation distance (9 km) was approximately three times smaller than the coeval subaqueous delta progradation (ca. 20–30 km), thus resulting in a progressive

Fig. 14. Plots of parameter pairs showing moderate-to-strong ($R^2 > 0.5$) statistical correlations. Red and yellow best-fit lines correspond to correlations for all clinoforms and sand-prone subaqueous delta clinoforms, respectively. Equations for the best-fit lines are numbered in the grey boxes in each plot; these equations and values of the coefficient of determination (R^2) describing each best-fit line are given in Tables 5 and 7. See Fig. 5 for units and clinoform nomenclature.

Table 4
Typical value ranges for the statistical parameters examined within the clinoform population shown in Tables 1 and 2. For each clinoform type, the value ranges refer to the 5- to 95-percentile of the parameter statistical distribution. In order to show chronostratigraphically-constrained rate values that can be readily compatible with the short-term (≤10 kyr) data obtained for muddy subaqueous clinoforms, both short-term (≤10 kyr) and longer term (>10 kyr) rates for the other delta-scale clinoforms are displayed in this table. (*) = The foreset gradient of sandy deltas is 0.1–2.7° if Gilbert-type deltas are not considered. However, if small-scale, steep, high-latitude Gilbert deltas are added to the dataset (i.e. Alta, Bella Coola, c.f. Table 2), the 5–95 percentile range of foreset gradients increases to 10°.

Feature			Continental-margin clinoforms	Shelf-prism clinoforms	Muddy subaqueous deltas (≤10 kyr)	Sand-prone subaqueous delta clinoforms		Muddy subaerial deltas and shoreline clinoforms		Sandy subaerial deltas and shoreline clinoforms	
						≤10 kyr	>10 kyr	≤10 kyr	>10 kyr	≤10 kyr	>10 kyr
			Values								
Total relief (H)	Height (m)	*Hh*	670–3050	140–460	9–103 m	25–68		8–84 m		5–29 m	
	Down-dip extent (m)	*Hd*	15,700–195,500	6100–33,900	2700–42,800 m	890–2040 m		2500–52,500 m		1750–24,000 m	
Inflection zone slope gradient (°)		*Is*	1.6–16.1°	0.9–9.8°	0.1–1.2°	0.7–10°	0.7–23°	0.2–1.5°		0.1–2.7°	
Foreset	Height (m)	*Fh*	1120–2570	97–300 m	3–46 m	12–45 m		6–58 m		4–26 m	
	Down-dip extent (m)	*Fd*	6540–82,300 m	2400–17,200 m	1000–11,800 m	73–2570 m		1200–18,300 m		116–12,800 m	
	Slope gradient (°)	*Fs*	1.1–12.5°	0.6–4.7°	0.1–0.9°	0.5–9°	0.5–16°	0.1–0.7°		0.1–2.7° (up to 10°)*	
Inner bottomset	Height (m)	*Bh*	69–487 m	14–59 m	0–27 m	1–11 m		4–25 m		1–7 m	
	Down-dip extent (m)	*Bd*	2800–66,300 m	401–7850 m	177–11,500 m	46–1813 m		2200–6200 m		295–7500 m	
	Slope gradient (°)	*Bs*	0.3–3.9°	0.2–2.5°	0–0.4°	0.1–3.9°		0–0.4°		0–0.6°	
Outer topset	Height (m)	*Th*	14–192 m	6–102 m	0.5–12 m	0.9–12 m				1–6 m	
	Down-dip extent (m)	*Td*	420–22,500 m	456–9940 m	260–12,740 m	37–1470 m		510–6410 m		150–16,000 m	
	Slope gradient (°)	*Ts*	0.2–9.0°	0–2.2°	0–0.4°	0.2–3.5°		0–0.2°		0–0.4°(*)	
Shape ratio (h/H; non-dim.)		*h/H*	0.38–0.76 (oblique)	0.33–0.69 (sigmoidal to oblique)	0.11–0.68 (mostly sigmoidal)	0.16–0.46 (sigmoidal)	0.16–0.60 (mostly sigmoidal)	0.38–0.88 (oblique)		0.48–0.81 (oblique)	
Net-to-gross (% sand + pebble)		*N-g*				36–89%		2–16%		10–58%	
Age scale (Myr)		Age	3.71 to 123.30	0.20 to 17.60	$5\cdot10^{-4}$ to 0.01	$6.5\cdot10^{-3}$ to $7.5\cdot10^{-3}$	0.01–0.43	$3\cdot10^{-4}$ to $7\cdot10^{-3}$	$1.2\cdot10^{-2}$ to $9\cdot10^{-2}$	$6\cdot10^{-5}$ to $5\cdot10^{-3}$	$9\cdot10^{-3}$ to 4
Vertical sediment accumulation rate (m/Myr)		Sv	7.7 to $2.6\cdot10^{2}$	$2.5\cdot10^{1}$ to $2\cdot10^{3}$	$4.6\cdot10^{2}$ to 10^{5}	$1.6\cdot10^{3}$ to $5.8\cdot10^{3}$	$1.6\cdot10^{1}$ to $5.6\cdot10^{3}$	$1.6\cdot10^{3}$ to $3.6\cdot10^{5}$	$2\cdot10^{3}$ to $9\cdot10^{3}$	$5\cdot10^{3}$ to $4\cdot10^{5}$	5 to 10^{4}
Clinoform progradation rate (km/Myr)		P	$8.2\cdot10^{-2}$ to 10^{1}	$8\cdot10^{-1}$ to $8\cdot10^{1}$	$7\cdot10^{2}$ to $2\cdot10^{4}$	$1.1–5\cdot10^{2}$ to $5.4\cdot10^{2}$	10^{1} to $5\cdot10^{2}$	$2\cdot10^{4}$ to $9\cdot10^{4}$	1 to 20	$4\cdot10^{3}$ to $8\cdot10^{4}$	1 to 30
Unit-width depositional flux (km^2/Myr)		F	$7\cdot10^{-2}$ to $7.1\cdot10^{0}$	$2\cdot10^{-1}$ to $1.1\cdot10^{1}$	$1.1\cdot10^{1}$ to $9.4\cdot10^{2}$	1.5 to $1.5\cdot10^{1}$	$6\cdot10^{-1}$ to $1.9\cdot10^{1}$	$4\cdot10^{2}$ to 10^{4}	$6\cdot10^{-1}$ to 10^{3}	$4\cdot10^{1}$ to $1.6\cdot10^{3}$	$1.4\cdot10^{-1}$ to $4.4\cdot10^{2}$
Progradation resistance ratio (non-dimensional)		R	$3\cdot10^{-3}$ to $4.3\cdot10^{-1}$	10^{-2} to $8\cdot10^{-2}$	10^{-4} to $7.3\cdot10^{-3}$	$3.7\cdot10^{-3}$ to $2.7\cdot10^{-2}$	$4\cdot10^{-5}$ to $3\cdot10^{-2}$	$7\cdot10^{-5}$ to $4\cdot10^{-3}$	$5\cdot10^{-4}$ to $4\cdot10^{-3}$	$4\cdot10^{-4}$ to $9\cdot10^{-3}$	$4.8\cdot10^{-4}$ to $6\cdot10^{-3}$
Clinoform trajectory (°)		CT	+0.9° to +49.4°	0° to +2.4°	0° to +0.5°	−0.4° to +3.5°		0° to +0.14°		0° to +0.08°	+0.05° to +1.7°
Water depth of rollover point (m)		Wd	550–1770 m	58–530 m	6–59 m	21–57 m		0–5 m		0–5 m	

lengthening of the subaqueous clinoform topset during this particular time interval.

4.2. Example 2: Bridport Sand Formation subaerial delta and Down Cliff Clay Member subaqueous delta clinoforms

The Lower Jurassic Bridport Sand Formation and coeval Down Cliff Clay Member were deposited in ca. 2 Myr in the Wessex Basin, southern UK, in a linked shoreface-to-shelf depositional system. The Bridport Sand Formation is dominated by bioturbated storm-event beds with calcite-cemented bioclastic lag horizons, which were deposited in an offshore transition to lower shoreface environment. These strata form 10–40 m thick, upward-shallowing units that overlie laterally-extensive, mudstone-rich horizons (Morris et al., 2006). The Down Cliff Clay Member comprises calcareous bioturbated mudstones that record deposition in an offshore transition to offshore environment (Morris et al., 2006). 2D and 3D seismic data calibrated with wells from the onshore Wytch Farm Field indicate that each upward-shallowing, shoreface-to-shelf unit of the Bridport Sand Formation corresponds to a steeply-dipping (2–3°), delta-scale, progradational clinoform set that downlaps onto the topset of a similar progradational clinoform set in the Down Cliff Clay Member (Morris et al., 2006; Hampson et al., in press; Fig. 11BR). Each clinoform set represents a duration of ca. 0.5 Myr, downlaps onto a basal maximum flooding surface and is likely arranged into a compound clinoform system (Hampson et al., in press). According to this interpretation, these systems comprise a subaerial delta clinoform composed by shoreface sediments (Bridport Sand Formation), grading seawards into an outer finer-grained, middle shelf clinoform (Down Cliff Clay unit) that displays a nearly linear plan-view geometry.

4.3. Example 3: Sognefjord Formation subaqueous delta clinoforms

The Upper Jurassic Sognefjord Formation forms a 100–300 m thick, coarse-grained, regressive–transgressive clastic wedge of ca. 6 Myr duration, developed on the eastern flank of the Northern North Sea rift system, offshore Norway (Vollset and Doré, 1984; Steel, 1993; Stewart et al., 1995; Fraser et al., 2002; Dreyer et al., 2005). Offshore shales of the Heather Formation occur above and below this sandstone-rich wedge and represent periods of tectonically-driven transgression (Steel, 1993; Ravnås et al., 2000; Fraser et al., 2002). The internal stratigraphic architecture of the Sognefjord Formation is dominated by the progradational-to-aggradational stacking of sandstone-prone clinoform sets, which are separated by basin-wide flooding surfaces (Patruno et al., 2015, in press; Fig. 11SG). Clinoform sets in the lower part of the Sognefjord Formation are linear in map view, strike parallel to the rift-margin fault (NNE–SSW), and are laterally extensive for at least 30 km along depositional strike (Dreyer et al., 2005; Patruno et al., 2015). Within each clinoform set, there is a progressive basinward increase in clinoform height (from 10–30 m to 60–70 m), foreset slope angle (from 1–6° to 16°) and along-strike length (from 1 km to 6 km), and a basinward decrease in clinoform dip extent (from 3000 m to 200 m) (Patruno et al., 2015). Clinoform foresets also exhibit distinct facies changes down depositional dip, becoming coarser-grained and more dominated by current-driven tractional structures in a basinward direction (Dreyer et al., 2005; Patruno, 2013; Patruno et al., 2015, in press).

The Sognefjord Formation was deposited by a deltaic system sourced from the Norwegian mainland that prograded westwards across a stable rift-margin platform for tens of kilometres, through incremental deposition of west-dipping clinothems (Stewart et al., 1995; Dreyer et al., 2005; Patruno et al., 2015, in press). The thicknesses of clinoform sets (10–60 m), clinoform foreset slope gradient (1°–14°) and inferred clinoform progradation rates (ca. 10–500 km/Myr) are compatible with those of modern coarse-grained deltas with small catchment areas (Patruno et al., 2015). Based on analysis of sedimentological facies in cores and stratigraphic relationships in 3D seismic reflection data from the Troll Field, Patruno et al. (2015) interpret that the clinoforms were deposited in a fully subaqueous delta. This interpretation is based on the following evidence: (a) absence of subaerial facies in cores; (b) presence of well-developed topsets in most the clinoforms observed; and (c) laterally-extensive, plan-view geometry orientated parallel to the shelf-edge break and to the alongshore currents that are inferred to have fed them.

4.4. Example 4: Calcarenite di Gravina subaqueous clinoforms

The progradational units in the lower member of the Pliocene–Pleistocene Calcarenite di Gravina unit are exposed in outcrops near the city of Matera (southern Italy), and comprise wave-dominated shoreline to offshore calcirudite and calcarenite facies (Pomar and Tropeano, 2001). These deposits form laterally extensive clinothems that strike parallel to the palaeo-shoreline and prograded seawards below wave base. High-angle (up to 35°) foresets are composed of offshore-transition sediments that downlap onto fine-grained offshore deposits. These sandbodies are interpreted by Pomar and Tropeano (2001) to represent avalanches of shoreface sand- to gravel-grade sediments, transported along shoreface-shelf depositional slopes by wind-driven storm waves and currents and subsequently emplaced in a subaqueous shelfal setting below wave base. Progradational clinoform sets correspond to upward-shallowing parasequences formed during relative sea-level stillstands or during falling relative sea-level, and are underlain by flooding surfaces and/or transgressive lag deposits. Evidence of subaerial exposure is absent in each offshore-transition-dominated delta-scale subaqueous clinothem, although a subaerial erosional surface may have formed above the beachface deposits of the coeval, thin, subaerial delta clinothems during forced regression. The overall parasequence stacking pattern is retrogradational, with clinoforms onlapping onto a Cretaceous limestone substrate, reflecting tectonically forced transgression (cf., Pomar and Tropeano, 2001).

4.5. Example 5: Calcareous Grainstone subaqueous clinoforms, Miocene, Menorca

Pomar et al. (2002) analysed the facies belts and depositional profile of the distally-steepened, Tortonian carbonate ramp outcropping along the sea cliffs of Menorca (Balearic Islands, Spain). Palaeoshoreline-detached, cross-bedded, coarse-grained grainstones were deposited below wave base on the Lower Tortonian carbonate ramp (Fig. 11MN). Fan deltas and beach deposits at the palaeoshoreline (subaerial delta) pass down-slope into 5 km-wide, gently-dipping topset strata in the inner–middle ramp, then into 12–20° foreset beds on the ramp slope and, eventually, into sub-horizontal bottomset strata in the outer ramp (subaqueous clinoform). The fan deltas and beaches at the palaeoshoreline contain continental conglomerates and red sandstones, structureless conglomerates, pebbly sandstones and beach face deposits. The subaqueous topset area is composed of bioturbated dolo-packstone; the subaqueous foreset strata contain dolo-grainstone/rudstone and, lower on the slope, are dominated by turbiditic and debris flow deposits and by sediment reworking by shore-parallel bottom currents. The bottomset basinal area contains mostly fine-grained dolo-packstone to dolo-wackestone, interbedded with distal turbidites and alongshore-transported grainstones at the toe of the slope. Coarse-grained carbonates are widespread on this ancient shallow-marine ramp, which are not subject to the usual decrease in grain-size with water depth along the ramp depositional profile (Fig. 11MN). Coarse-grained deposits occur: (1) on the beach/palaeoshoreline; (2) at 40–70 m water depth on the subaqueous topset, where medium-scale coarse-grained grainstone bedforms are oriented parallel to the palaeoshoreline; (3) on the subaqueous foreset area, as in-situ rhodoliths and small-scale subaqueous dunes migrating parallel to the slope; (4) at the transition between the subaqueous foreset and bottomset, as rudstone–grainstone slide/slump scar infills; and (5) at ca. 150 m of estimated water depth

at the toe of the bottomset, as coarse skeletal grainstone bedforms migrating parallel to the clinoform strike. Sediments in settings deeper than the inner ramp were continuously reworked by ubiquitous, westward-flowing, shore-parallel bottom currents, and by likely upwelling currents. Pomar et al. (2002) indicate that, without three-dimensional facies and bathymetric reconstructions, a similar succession may be interpreted as a shoal-rimmed carbonate shelf.

5. Dataset and methodology for quantitative comparative analysis of clinoforms

Quantitative comparative analysis of parameters directly measured from published cross-sections oriented parallel to clinoform dip was carried out for 47 clinoform systems belonging to continental margin, shelf prism, subaqueous delta, and subaerial delta categories (Table 1). All the parameters defined in Fig. 5 were systematically measured following a comparable methodology to that applied to the clinoforms listed in Table 1. Some quantitative data measured by previous authors and describing a further 44 recent subaerial delta and shelf-prism clinoform sets and 15 ancient subaerial delta clinoform sets was additionally taken from published compilations (Orton and Reading, 1993; Burgess and Hovius, 1998; Bristow and Pucillo, 2006; Howell et al., 2008; Olariu and Steel, 2009) and utilized in the analysis (Table 2). The resulting global dataset characterises modern and ancient clinoforms developed in various environmental and climatic settings (Fig. 6).

For each clinoform that has been directly measured from published seismic cross sections and maps (Table 1), the geometrical parameters described in Fig. 5 were systematically recorded. Furthermore, where possible, the water depth of the rollover point (*wd*) was measured, and if chronological data were available, average vertical sediment accumulation rate (*Sv*), clinoform progradation rate (*P*), cross-sectional net sediment flux (*F*) and progradation resistance ratio (*R*) were also estimated. The parameter 'duration' (*Age*) represents the time span over which these average chronostratigraphic measurements have been calculated, based on the available chronological data. Published quantitative data for additional clinoforms (Table 2) were used to get estimation of only a handful of available parameters: foreset slope gradient (*Fs*), bottomset slope gradient (*Bs*), topset slope gradient (*Ts*), water depth of the rollover point (*Wd*), average vertical sediment accumulation rate (*Sv*), clinoform progradation rate (*P*), cross-sectional net sediment flux (*F*), progradation resistance ratio (*R*), duration (*Age*), and clinoform trajectory as defined by successive positions of the upper rollover point (*CT*; only for ancient systems). Given the limitations imposed by seismic data resolution discussed earlier, parameters that describe bottomsets and topsets essentially refer to 'inner bottomsets' (between lower rollover point and clinoform toe point; Fig. 5) and 'outer topsets' (between clinoform head point and upper rollover point; Fig. 5).

6. Results of quantitative comparative analysis of clinoforms

Delta-scale, shelf-prism and continental-margin clinoform types are characterised by different geomorphological and stratigraphic parameters, and tend to occupy different fields of graphs were parameter pairs are plotted against each other (Figs. 12–15). For each clinoform type, ranges formed by the 5- to 95-percentile of the values of each geometric and chronostratigraphic parameter are summarised in Table 4. Relationships between these parameters are investigated in a series of cross-plots, which show best-fit lines generated by least-square regression methods for moderate or strong correlations (coefficient of determination, $R^2 = 0.5–0.8$ and 0.8–1.0, respectively) (Figs. 15–16; Tables 5 and 6). The equations describing best-fit lines between parameter pairs showing a moderate-to-strong correlation are shown in Tables 7 and 8. Best-fit lines have been plotted by utilizing either linear, power-law or second-degree polynomial functions. The function type that shows the best fit to the data (i.e., characterised by the highest R^2 value) has generally been selected for each parameter pair. The only exceptions are polynomial functions that give tightly curved best-fit lines with minima that are poorly constrained by data control, which are considered to be geologically unreasonable. In these cases, the second best-fit function type has been chosen (e.g., Fig. 15I–K).

Two types of relationships between parameters are observed. The first type comprises positive and negative correlations between parameters from the same dimensional domain (e.g., heights of the different portions of a clinoform) or from related dimensional domains (e.g., height versus down-dip extent of a certain clinoform portion). The second type comprises positive and negative correlations between parameters from different dimensional domains that were not derived from each other (e.g., slope gradient of a certain clinoform portion versus height of another clinoform portion; duration versus water depth of rollover points). This second type of relationship is perhaps more meaningful, because it highlights potential links between parameters that are not directly related. The presence of several strong correlations between these parameters is remarkable in its own right, as it indicates that all clinoforms, despite the differences in scales, palaeoenvironments and grain size, are subject to the same physical laws, which can be described quantitatively by our regression equations. These equations are potentially powerful tools that enable estimation of unknown parameters by utilizing other known parameters extracted from clinoforms. Furthermore, both modern and ancient clinoforms follow the same trends.

Despite a large lithological variability, subaerial delta-scale clinoforms are here treated as a unique group, since mud- and sand-dominated deltas are characterised by remarkably similar morphological and stratigraphic parameters (Table 4). Small-scale, coarser-grained Gilbert-type deltas represent the only exception. These systems are usually characteristic of high latitude zones with a narrow and steep hinterland, and often discharge water and sediment into freshwater lakes. Gilbert deltas form remarkably steeper and smaller clinoforms, and deserve to be treated as a separate group. Due to the absence of a statistically significant number of seismically imaged Gilbert deltas, however, this group is not represented in the statistical analyses of Figs. 13–16 and Tables 5 and 7.

6.1. Morphological parameters and correlation relationships

6.1.1. Clinoform heights

The examined dataset demonstrates that progressively larger scale clinoforms are deposited in increasingly deeper waters and over progressively larger time spans (Figs. 13F, 15K–L; Tables 4 and 8), as described by strong correlations between these parameters (Tables 7 and 8). Topset-to-foreset rollovers of subaerial delta clinoforms occur at <5 m water depth, whereas the corresponding rollovers in muddy and sandy delta-scale subaqueous clinoform are respectively at 6–59 m and 21–57 m. Topset-to-foreset rollovers of shelf-prism clinoforms (58–530 m) and continental-margin clinoforms (550–1770 m) occur at increasingly deeper water depths. Foreset height and total relief of delta-scale clinoforms are respectively <60 m and <100 m (Table 4). Shelf-prism clinoforms and continental margin clinoforms are characterised by foreset heights of 97–300 m and 590–2700 m, and total relief of 140–460 and 670–3050 m (Table 4; Fig. 12A–D).

6.1.2. Clinoform dips

The slope gradients of clinoform inflection zones range from 0.1–1.5° for muddy subaerial and subaqueous deltas, to 0.1–2.7° for sandy subaerial deltas, 0.9–9.8° for shelf-prism clinoforms and 0.9–16.2° for continental-margin clinoforms (Table 4; Fig. 12E–G). These slope angle values indicate that larger clinoforms are characterised by steeper foresets, independent of depositional environment. However, subaerial Gilbert deltas and delta-scale sand-prone subaqueous clinoforms are

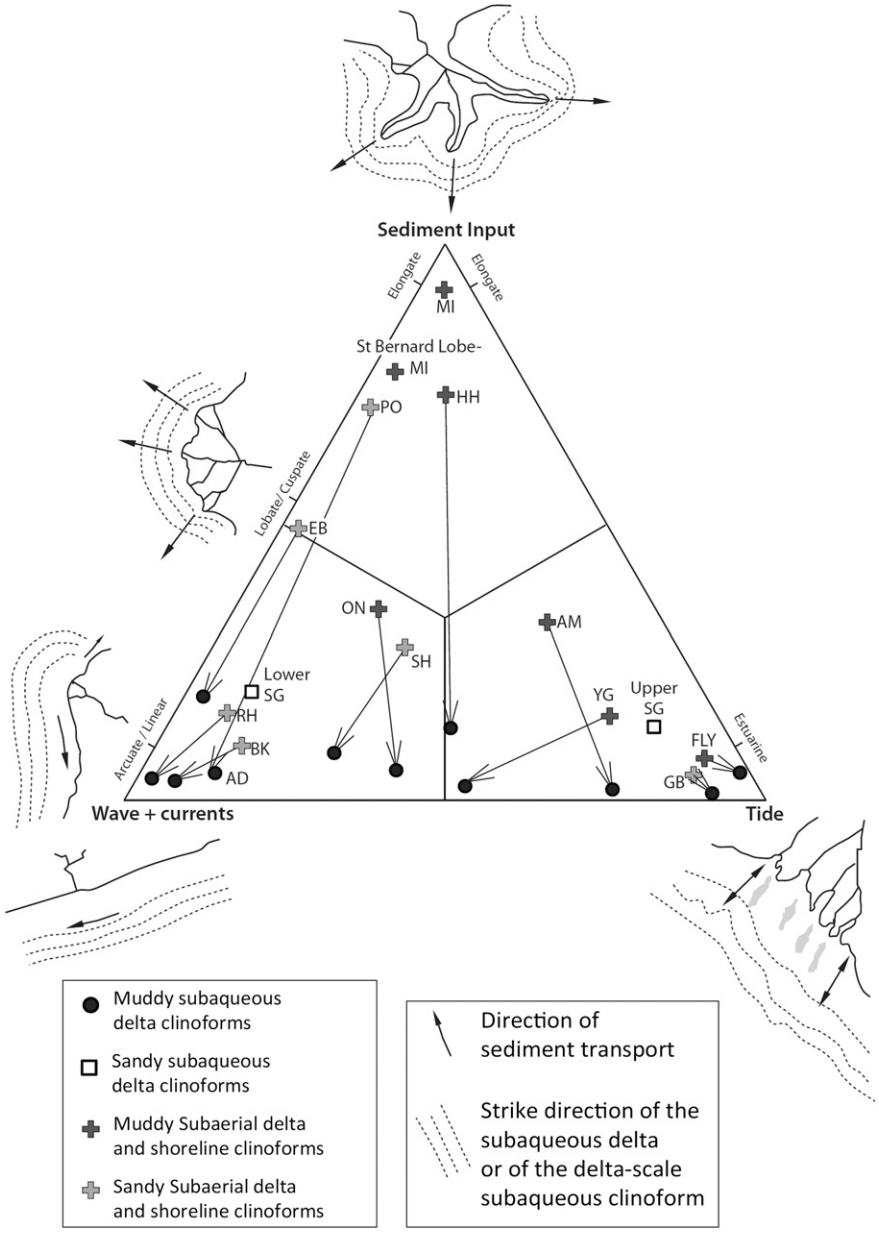

Fig. 16. Delta-scale compound clinoforms plotted on the tripartite classification scheme of Galloway (1975) for deltas. An arrow links each subaerial delta with its subaqueous delta counterpart. The positions of the subaerial delta clinoforms are derived from Orton and Reading (1993) and Galloway (1975). Approximate positions of the corresponding subaqueous delta clinoforms are inferred from the magnitude of waves and tides in the receiving basins for modern systems and from core-based facies analysis for ancient systems (supporting references listed in Tables 1 and 2). Qualitative changes in plan-view morphology of coeval subaerial and subaqueous delta clinoforms are also shown, and related to spatial changes in sedimentary processes.

typically characterised by inflection-point slope gradient values of 0.7–10°, up to a maximum of 23°, similar to those of the much larger shelf-prism clinoforms (Fig. 12E–G, Table 4). This contrasts strikingly with the maximum slope gradient values of typical sand-prone subaerial deltas (up to 2.7°; c.f. Table 4, Fig. 12E–F–G). We propose that these anomalously steep values for foreset slope are a diagnostic criterion for identifying delta-scale sand-prone subaqueous clinoforms. The heights of delta-scale sand-prone subaqueous clinoforms (12–45 m) are similar to those of other delta-scale clinoforms (c.f., Table 4), suggesting their greater slope gradient values are due to much smaller dip extents of their foresets (<2600 m, compared with values of <12,000 m for muddy subaqueous clinoforms and of <18,500 m for subaerial delta clinoforms; Table 4, Fig. 12A–B). Similar trends are observed for the inner bottomset and the outer topset areas of the clinoforms, which are characterised by heights of <28 m for all delta-scale clinoforms, but smaller dip extents for sand-prone subaqueous clinoforms (ca. 35–1820 m) than for other types of delta-scale clinoform (ca. 175–16,000 m) (Table 4; Fig. 12B–E). This gives rise to very low topset and bottomset slope gradients for both muddy subaqueous and subaerial delta clinoforms (generally <0.4°), and to much steeper slopes for recent sand-prone subaqueous delta clinoforms (up to 4°; c.f. Table 4; Fig. 12H). In particular, values of inner bottomset slope angle in sand-prone subaqueous delta clinoforms (0.1–3.9°) are greater than those in all the other clinoform types at every scale, except for continental margin clinoforms (0.3–3.9°, c.f. Table 4; Fig. 12H). These steep bottomset slope gradients are another diagnostic criterion of sand-prone subaqueous delta clinoforms.

6.1.3. Cross-sectional clinoform morphology

As shown in Fig. 13A–B and Table 4, the greatest values of shape ratio (h/H; c.f. Fig. 5) occur in subaerial delta clinoforms (0.38–0.88), with progressively lower values exhibited by continental-margin clinoforms

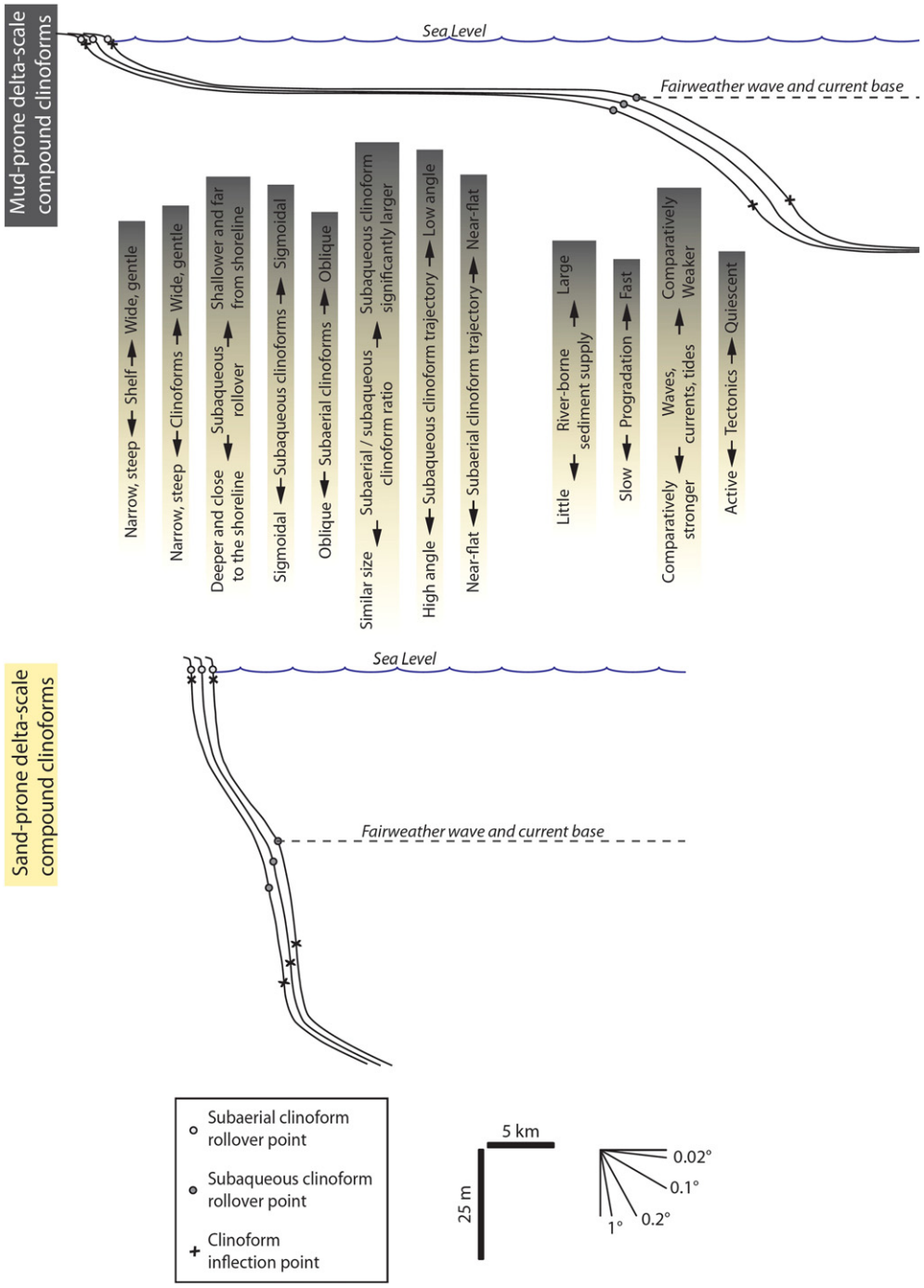

Fig. 17. Typical cross-sectional morphologies of mud- and sand-prone delta-scale compound clinoforms. The summarised differences between these two end-members are based on the analysis shown in Figs. 13–16 and Tables 2 and 8, and discussed in the text. Both types of compound clinoform are usually characterised by oblique subaerial delta clinoform morphologies and sigmoidal subaqueous clinoform morphologies. Intermediate systems between these two end members exist. In particular there are several examples of relatively sand-rich subaerial deltas associated with muddy subaqueous counterparts (e.g., Po, Ganges–Brahamaputra, c.f. Fig. 16). Muddy subaerial deltas associated with sandy subaqueous deltas have not been reported.

(0.38–0.76), shelf-prism clinoforms (0.33–0.69) and subaqueous delta clinoforms (0.11–0.68). Pirmez et al. (1998) proposed that oblique and sigmoidal clinoforms are characterised by values of shape ratio respectively higher and lower than 0.4. Although the ranges of shape ratio show overlap between the different types of clinoforms, the cross-sectional morphology of subaerial and subaqueous delta clinoforms can be used to an extent as a feature to distinguish them, with subaerial delta clinoforms being more oblique and subaqueous delta clinoforms being more sigmoidal, irrespective of grain size.

6.1.4. Parameter correlations

Moderate-to-strong positive correlations are observed for morphological parameters in three groups: (1) between the total vertical relief of clinoforms and the heights of their constituent foresets, bottomsets and topsets (Fig. 14A–C, J–K, R); (2) between the dip extents of clinoforms and their constituent foresets, bottomsets and topsets (Fig. 14D–F, M–N, T); and (3) between the slope gradients of clinoform inflection zones, foresets, bottomsets and topsets (Figs. 14G–I, 15O–P, U). Values of bottomset height and down-dip extent are weakly correlated (Fig. 14Q). Very strong correlations ($R^2 > 0.97$) are noted between

slope angles of foresets and inflection zones for all clinoforms (Fig. 14G), and between the total relief of all clinoforms and their foreset heights (Fig. 14A).

In the case of delta-scale sand-prone subaqueous clinoforms, strong negative correlations were observed between the dip extents and slope gradients of clinoforms, and between the same parameters for their constituent foresets, bottomsets, topsets and inflection zones (Figs. 14L,S,V, 15A–H). Furthermore, delta-scale sand-prone subaqueous clinoforms with narrower clinoform dip extents also show larger values of shape ratio (Fig. 15I). These correlations demonstrate the quantitative nature of the relationships between dip extents and slope gradients in delta-scale sand-prone subaqueous clinoforms, and reveal that narrower and steeper delta-scale subaqueous clinoforms are characterised by progressively more asymmetric, oblique geometries (Tables 7 and 8). Similar correlations do not occur in the dataset of all clinoform types, suggesting that they can be regarded as additional diagnostic criteria for recognition of delta-scale coarse-grained subaqueous clinoforms.

6.2. Chronostratigraphically-constrained parameters

6.2.1. Rates of progradation, vertical sedimentation, unit-width depositional flux

Clinothem outbuilding occurs over increasingly long time spans for delta-scale (usually, ca. 0.1–100 kyr), shelf-prism (0.2–17.6 Myr) and continental-margin clinoforms (3.7–123.3 Myr) (Table 4). This pattern is reflected in positive correlations between clinoform set duration and the water depth of rollover points, the height of clinoform foresets, and total clinoform relief (Figs. 13C–F, 15K–P). As a consequence, average vertical sedimentation rates, progradation rates and unit-width depositional flux of continental-margin clinoforms are respectively up to four, six and five orders of magnitude lower than the typical values for delta-scale clinoforms, with intermediate values for shelf-prism clinoforms (Table 4; Fig. 13G–H, J). In particular, in delta-scale clinoform sets deposited over time spans of less than 10 kyr, vertical sedimentation rates, progradation rates and unit-width depositional flux are greatest in subaerial deltas (respectively, 10^3–10^5 m/Myr, 10^3–10^5 km/Myr, 10^1–10^4 km^2/Myr), slightly lower in muddy subaqueous deltas (respectively, 10^2–10^5 m/Myr, 10^2–10^4 km/Myr, 11–950 km^2/Myr), and markedly lower in sand-prone subaqueous deltas (respectively, 1–6 $\times$ 10^3 m/Myr, 1–5 $\times$ 10^2 km/Myr, 1–15 km^2/Myr) (Table 4; Fig. 13G–H, J).

6.2.2. Clinoform trajectories and progradation resistance ratio

Clinoform trajectories generally tend to be relatively low angle in deltaic clinoform sets deposited during Milankovitch time scales ($\leq$0.5°), increasing for sandy subaerial deltas deposited over longer time scales (up to +1.7°), for shelf-prism clinoforms (0 to +2.4°) and becoming significantly higher for continental-margin clinoform sets (+0.9° to +49.0°) (Table 4; Fig. 13I). In concert with this trend, clinoform progradation resistance ratios increase from deltaic (10^{-4} to 7 $\times$ 10^{-3}) to shelf-prism (1–8 $\times$ 10^{-2}) and continental-margin clinoform sets (up to 4 $\times$ 10^{-1}) (Table 4; Fig. 13E). These trends reflect the dominance of short-term progradation and long-term aggradation in cycles of continental-shelf outbuilding (Bullimore et al., 2008; Helland-Hansen and Hampson, 2009). However, sand-prone subaqueous delta clinoform sets contain a larger spread of trajectories (from −0.4° to +3.5°), even in the short term (<10 kyr) (Table 4; Fig. 13I). Furthermore, the values of clinoform progradation resistance ratio ($\leq$3 $\times$ 10^{-2}) for sand-prone subaqueous delta clinoforms are up to two orders of magnitude higher than those typical of other delta-scale clinoforms, and are similar to those that characterise shelf-prism clinoform sets (Table 4; Fig. 13E). Low rates of progradation relative to aggradation are therefore characteristic of the outbuilding of sand-prone subaqueous deltas.

6.2.3. Parameter correlations

Moderate to strong negative power correlations exist between age duration and both vertical mean sedimentation rates ($R^2 > 0.57$) and horizontal mean progradation rates ($R^2 > 0.73$) for clinoform sets (Figs. 14W–X; 15J). Such trends were first documented by Sadler (1981), and indicate that the net rate of sediment accumulation recorded by a sedimentary unit has a systematic inverse relation to the average time duration of the unit, due to the occurrence of gaps in deposition of various frequencies and durations. Cross-sectional net-sediment flux, which directly depends on values of progradation rate and vertical mean sedimentation rate ($R^2 > 0.70$, Fig. 14Y–Z), shows only a modest negative correlation with clinoform set duration ($R^2 \approx 0.55$). This phenomenon was highlighted by Sadler and Jerolmack (in press), who argues that, for time intervals greater than 10^3 years, the product of aggradation and progradation rates (i.e., the cross-sectional sediment flux) is largely time scale-independent for siliciclastic passive margins.

In addition, the dataset comprising all the analysed clinoforms, regardless to their type, shows moderate-to-strong, positive correlations between water depths of topset-to-foreset rollover points and each of the following six parameters: total relief ($R^2 \approx 0.83$); foreset height ($R^2 \approx 0.77$); topset height ($R^2 \approx 0.81$); bottomset height ($R^2 \approx 0.74$); duration ($R^2 \approx 0.72$); progradation resistance ratio ($R^2 \approx 0.77$) (Fig. 15L–Q). The last two relationships are indirect consequences of the accumulation of hiatuses of different scales over increasingly longer time spans (Sadler, 1981). Each of these parameters can be therefore generally used as a palaeobathymetry proxy, according to the correlations given in Table 7 and 8. However, none of these relationships seem to be valid for statistical populations formed only by delta-scale, sand-prone subaqueous clinoforms (Fig. 15L–Q; Tables 5, 7 and 8). The data-points relating to this clinoform type generally follow the trend for the global clinoform dataset but, presumably due to the low spread of water depth values, do not form a clearly defined trend of their own (Fig. 15L–Q).

7. Discussion

In the preceding sections, examples of modern and ancient delta-scale subaqueous clinoforms have been summarised from the published literature, and their morphological and chronostratigraphic parameters have been quantitatively analysed in the context of other clinoform types. In this section, we return to the problems identified in the introduction to this article: (1) how can delta-scale subaqueous clinoforms be recognized in the stratigraphic record using seismic reflection, sedimentological and/or stratigraphical data?; (2) what kind of depositional processes and settings are implied by clinoform morphology, lithology and internal facies character?; and (3) what are the implications of recognizing this particular type of shallow-marine sediment body in ancient and modern environments for sequence stratigraphic models?

7.1. Diagnostic criteria for delta-scale subaqueous clinoforms

An interpretation of delta-scale subaqueous clinoform is likely whenever clinoforms encompassing heights of tens of metres are characterised by a relatively well-developed topset that lack evidences for subaerial exposure. In addition, the quantitative analysis presented herein indicates a series of diagnostic geomorphological, sedimentological and stratigraphic features for either muddy or sandy delta-scale subaqueous clinoforms (Figs. 13–16, Tables 3 and 8). Some of these quantitative characteristics can be recognized in high-resolution 3D seismic data, making it possible to propose a sandy or muddy delta-scale subaqueous clinoform interpretation even without detailed sedimentological data. All analysed delta-scale subaqueous clinoforms, irrespective of their dominant grain-size, share three common characteristics: (1) they have a shore-parallel, laterally extensive, near-linear, plan-view morphology (Fig. 16); (2) their stratigraphic architecture, geomorphology, sediment grain size and facies character

are dominated by basinal processes (waves, currents, tides) and tend to be more uniform than those of their subaerial delta counterparts (Fig. 16); and (3) their nearly symmetrical, usually sigmoidal cross-sectional geometry (shape ratio of 0.10–0.65) contrasts with the oblique cross-sectional geometries that characterise most subaerial deltas (Fig. 17).

Our analysis of recent clinoforms highlights three morphological differences that allow muddy and sandy delta-scale subaqueous clinoforms to be further differentiated (Figs. 16–17). Firstly, the dip extents of the topset, foreset and bottomset components of sand-prone delta-scale subaqueous clinoforms are ca. 1 order of magnitude smaller than in other delta-scale clinoforms (subaerial deltas and muddy subaqueous deltas) (Table 4; Figs. 12A–B; 13B; 14D–F, L–N; 15A–I). Secondly, steep topsets, foresets and bottomsets are diagnostic of sand-prone delta-scale subaqueous clinoforms, whereas markedly gentler gradients are typical of their mud-prone counterparts (Figs. 12F–H; 13A; 14G–I, L, O–P, S, U–V; 15A–H). A foreset gradient threshold between the two systems is observed at ca. 0.3–0.5° (Table 3; Fig. 9). Thirdly, delta-scale sand-prone subaqueous clinoforms show a moderate inverse correlation between the slope gradient and dip extents of their foresets, topsets and bottomsets slope gradients, which is not observed in other types of clinoforms (Fig. 15A–I).

Values of short term (≤10 kyr) progradation rates and depositional flux for sand-prone subaqueous clinoforms (respectively, 1–5 × 10^2 km/Myr and 1–15 km^2/Myr) are up to 3–4 orders of magnitude lower than in equivalent subaerial deltas, and average vertical sediment accumulation rate values (1–5 × 10^3 m/Myr) can be up to two orders of magnitude lower than in other delta-scale clinoforms (subaerial deltas and muddy subaqueous deltas) deposited over similar time spans (Fig. 14W–Y; Table 4). In addition, sand-prone systems are characterised by a larger spread of clinoform trajectory values (from −0.4° to +3.5°) than mud-prone delta-scale subaqueous clinoforms (0–0.5°), even in the Holocene (≤10 kyr duration). This is in marked contrast with the very low shoreline trajectory angles developed over similar timescales (<0.1°) (Figs. 14I, 18; Table 4).

7.2. Depositional processes and settings of delta-scale subaqueous clinoforms

7.2.1. Significance of plan-view clinoform morphology

Processes dispersing sediment away from river mouths range from fair-weather waves, storm waves and gravity flows, to hyperpycnal plumes, and tidal and oceanographic currents (e.g., Dreyer et al., 2005; Hampson, 2010). In the subaqueous portion of compound clinoforms, dispersal processes are dominated by persistent oceanographic currents, waves and tides that transport sediment alongshore. This shore-parallel marine transport belt, observed in many present-day mud-rich subaqueous deltas, causes a lateral deflection of sediment input beyond the river mouth, (e.g., Driscoll and Karner, 1999; Cattaneo et al., 2003, 2007; Liu et al., 2006; Mitchell et al., 2012; Fig. 16). As a consequence, delta-scale subaqueous clinoforms are predominantly controlled by basinal processes, and form laterally-extensive, near-linear, shore-parallel plan-view geometries (Figs. 7; 16).

Field and Roy (1984) and Hernández-Molina et al. (2000a) in their initial interpretations of 'infralittoral prograding wedges' state that delta-scale sand-prone subaqueous clinoforms are formed by the action of storm-generated downwelling currents transporting shoreline sands seawards from the surf zone, and are unconnected to subaerial delta input points. Furthermore, they indicate that these systems onlap on underlying discontinuities and do not form compound clinoform systems (c.f., coarse-grained variant of 'Gargano-type' clinoforms; Fig. 3C; see also Fernández-Salas et al. (2009)). The uniform sediment texture that is generally associated with delta-scale subaqueous clinoforms, which often causes their internal architecture to be poorly imaged on seismic data (Mitchell et al., 2012), is consistent with this origin, since shoreface sands are normally well sorted by wave action in the surf zone or during alongshore transport from river mouths. The modelling studies of Mitchell (2012) and Mitchell et al. (2012) suggest that the alongshore components of storm-generated bottom currents are usually much stronger and longer lasting than the offshore-directed component, resulting in near-bed stresses above the sediment transport thresholds even in the absence of combined wave action. This potentially gives rise to sedimentation patterns dominated by intermittent, current-driven alongshore sediment transport belts (Mitchell et al., 2012), which resemble the sedimentation style of typical mud-rich subaqueous deltas (e.g., Driscoll and Karner, 1999; Cattaneo et al., 2003, 2007; Liu et al., 2006; Mitchell et al., 2012).

7.2.2. Significance of cross-sectional clinoform morphology

Previous analysis of seismic reflection profiles has identified two types of clinoform morphology and related them to different environmental variables (e.g. Sangree and Widmier, 1977; Pirmez et al., 1998; Driscoll and Karner, 1999; Adams and Schlager, 2000). Oblique clinoforms exhibit asymmetrical morphologies which can be described by an exponential function for elevation (i.e. abrupt break in slope from topset-to-foreset, typically with toplap seismic terminations, and gradual break in slope from foreset-to-bottomset), have narrow topsets and steep foresets, and are associated with low angle, regressive clinoform trajectories that lack aggradation. In contrast, sigmoidal clinoforms exhibit symmetrical morphologies (i.e. gradual breaks in slope from topset-to-foreset and from foreset-to-bottomset), have broad topsets and gently dipping foresets, and are associated with regressive, aggradational clinoform trajectories. The 'shape ratio' values presented in our study indicates that both sandy and muddy delta-scale subaqueous clinoforms tend to show the most highly symmetrical, sigmoidal cross-sectional geometries, whereas subaerial delta clinoforms are oblique (Table 4; Figs. 13A–B, Fig. 17).

It is worth stressing that the distinction between oblique and sigmoidal geometries, particularly for clinoforms buried at depths >1000 m, will often be a matter of seismic resolution. Apparent stratal terminations are imaged where topsets becomes too thin to resolve, giving rise to apparent oblique geometries. More generally, all points of 'stratal termination' associated with clinoforms in seismic cross sections partly reflect imperfect resolution of progressive stratal pinchouts occurring landward of the upper rollover point ('offlap' or 'toplap') and basinward of the lower rollover point ('downlap'). In particular, seismic examples of shallowly buried clinoforms suggest that: (1) the downlap point often occurs between the lower rollover point and clinoform toe point (e.g., Fig. 10); (2) the toplap point occurs in close proximity to the upper rollover point in oblique clinoforms with narrow topsets (e.g., Fig. 10AL); and (3) in strongly progradational clinoform successions, the offlap point occurs at the clinoform head point, although in reality it may lie landward of this point (e.g. Fig 10YGs).

Clinoform cross-sectional geometries are controlled by a complex spatial and temporal interplay between mean grain size, clinoform height, sediment dispersal processes and water column energy distribution, clinoform trajectory type and basin physiography (Kenter, 1990; Orton and Reading, 1993; Pirmez et al., 1998; Driscoll and Karner, 1999; Adams and Schlager, 2000; Cattaneo et al., 2003, 2007; Swenson et al., 2005). In particular, oblique clinoform profiles, characterised by steep equilibrium slopes, are favoured by coarse-grained sediments, high clinoform relief, low trajectory angles, close proximity to the shoreline, and predominance of river-driven over basinal processes (Pirmez et al., 1998). All these conditions tend to favour sediment transport by diffusion, which in turns, would generate a depositional profile approximated by an exponential function for elevation.

The opposite conditions favour development of sigmoidal clinoforms and gentler slope gradients (Fig. 17). When one or more of the controlling parameters vary through space or time, clinoform cross-sectional profiles change accordingly. For example, Pirmez et al. (1998) point out that when sigmoidal clinoforms prograde across a sloping basin floor towards greater water depths, their cross-sectional profile tends to

become more oblique even if the base level does not change (height-induced changes, see also Fig. 10AL). However the clinoforms change from oblique to sigmoidal geometries if the rate of sediment supply cannot keep pace with the rate of water depth rise (shoreline trajectory-induced changes; e.g., Mortimer et al., 2005). Due to the changes in shoreline trajectory implicit in a typical sinusoidal relative sea level cycle, clinoforms are predicted to evolve through time from oblique to sigmoidal in lowstand system tracts, and from sigmoidal to oblique in highstand system tracts (e.g., Mitchum et al., 1977; Vail et al., 1977; Mitchum and Van Wagoner, 1991).

The typical sigmoidal profile of most shelf-prism clinoforms is due to the predominance of basinal processes, their fine grain-size and generally high-angle trajectories. Despite the similarities in palaeoenvironmental and depositional conditions with the shelf-prism clinoforms, continental-margin scale clinoforms are characteristically oblique because of their very high clinoform relief (Table 4). In contrast, although their relief is not high, subaerial-delta clinoforms are oblique because they are predominantly associated with river-driven sediment dispersal processes, low-angle clinoform trajectories, shallow water and rapid progradation (low progradation resistance ratio) (Table 4; Fig. 13A–B). Delta-scale subaqueous clinoforms tend to be sigmoidal due to the effects of strong wave, current and tidal processes and of higher-angle clinoform trajectories than in subaerial deltas (Table 4; Fig. 13A–B; Fig. 17). The anomalously steep gradients typical of delta-scale sand-prone subaqueous clinoforms are more similar to the slope angles of continental-margin clinoforms than to those of other delta-scale clinoform types (Table 4; Fig. 12F–H), and are probably the result of the higher friction experienced in subaqueous environments below fairweather wave base, combined with the availability of well-sorted, coarse-grained sediment.

7.2.3. Significance of chronostratigraphically-constrained parameters for clinoform sets

Delta-scale sand-prone subaqueous clinoforms are characterised by a larger spread of clinoform trajectory values (from $-0.4°$ to $+3.5°$) than mud-prone subaqueous systems (0–0.5°) and, above all, shoreline systems deposited during similar time-spans (<0.1°) (Figs. 13I, 17; Table 4). This characteristic, coupled with progradation resistance ratio values that in sand-prone subaqueous systems are up to two orders of magnitude higher ($\leq 3 \times 10^{-2}$) than in those typical of other delta-scale clinoform types deposited during similar time spans (Fig. 13E; Table 4), shows that lower progradation relative to aggradation is characteristic of delta-scale sand-prone subaqueous clinoform sets (Fig. 17). Similar steep clinoform trajectory angles are displayed by larger-scale clinoforms, deposited in longer time spans (e.g., shelf-prism and continental-margin clinoform; cf. Fig. 13I, Table 4), reflecting the dominance of short-term progradation and long-term aggradation in cycles of continental-shelf outbuilding (Bullimore et al., 2008; Helland-Hansen and Hampson, 2009).

Slow progradation and the very low values of unit-width depositional flux typical of delta-scale sand-prone subaqueous clinoform systems may reflect the distance of many sand-prone subaqueous clinoform foreset from direct river sediment input points (Figs. 7, 17) and/or the sporadic nature of sediment supply and depositional episodes by basinal processes in these settings (c.f., Mitchell, 2012; Mitchell et al., 2012). Higher sediment supply and progradation rate values in muddy subaqueous deltas are attributed to the association of these clinoform types with large feeder rivers and subaerial deltas (Figs. 7, 17). Subaerial deltas may prograde seawards very rapidly (e.g. the Po Delta has prograded at a rate of 45 km/kyr in the last 360 years, partly due to anthropogenic forcing), but at the same time may be subject to topset subaerial truncation and also to frontal erosion and retreat in between rapid episodes of progradation (e.g., Po di Tolle lobe of the Po Delta) (Correggiari et al., 2005; Friedrichs and Scully, 2007).

7.2.4. Depositional settings of delta-scale compound clinoforms

Muddy subaerial deltas are commonly formed by large river systems draining vast, gentle cratonic areas, whereas short river systems draining a steep, mountainous hinterland, usually in tectonically active areas favour development of sandy subaerial deltas (Orton and Reading, 1993; Bhattacharya, 2006). Sandy subaqueous delta-scale clinoforms are either associated with sand-prone subaerial deltas and shorelines (e.g., offshore River Salinas, California), or to a lack of direct deltaic sediment input point (e.g., southern Spain; c.f. Fernández-Salas et al., 2009). Muddy subaqueous deltas, conversely, may be linked directly to either silty large-scale subaerial deltas (e.g., Yangtze, Amazon) or to subaerial deltas dominated by fine-grained sands (e.g., Po, Ganges–Brahamaputra) (Fig. 16). Exceptions where subaqueous deltas are apparently not directly associated with any subaerial deltas situated directly up-dip have been also documented (i.e., Gargano, Cattaneo et al., 2003, 2007), and are associated with shore-parallel currents feeding the subaqueous clinoforms. Muddy subaerial deltas associated with sandy subaqueous counterparts have not been reported as yet. Such a system is unlikely: how could a muddy coastline provide sand to be transported further offshore?

Holocene delta-scale sand-prone compound clinoforms form in different oceanographic and depositional settings than muddy compound clinoforms (Table 3; Figs. 7–10; Figs. 16–17): (1) in sandy systems, the water depth of the rollover point of the subaqueous clinoform (ca. 20–60 m) tends to be ca. 10–30 m deeper than in muddy subaqueous deltas (c.f. also Mitchell et al. (2012)); (2) delta-scale muddy and sandy subaqueous clinoforms are characterised by relatively wide and narrow subaqueous topsets, respectively, with a threshold value between the two systems of ca. 9 km of distance between the subaqueous rollover point and the shoreline break; (3) delta-scale sand-prone subaqueous clinoforms are hosted by steep ($\geq 0.26°$) and narrow (<35 km) shelves, whereas muddy systems are found on broad and gently sloping shelves, with critical cut-off values between the two systems of ca. 30–70 km distance from the shoreline to the shelf-edge break and 0.2–0.5° average shelf-gradients; and (4) muddy and sandy compound clinoforms respectively contain a larger and smaller subaqueous clinoform relative to the associated subaerial clinoform, with a threshold value between the two systems for the ratio of subaerial foreset to subaqueous foreset height of ca. 0.2.

The amount of river-derived sediment delivered to the subaqueous clinoform relative to that retained in the subaerial clinoform is proportional to the predominance of basinal processes over fluvial processes (Swenson et al., 2005). As a consequence, the degree of relative growth and development of subaerial and subaqueous clinoforms tends to be inversely related to each other, with a negative correlation between width of coastal plain and the width of the shelfal mudstone belt (c.f., Swenson et al., 2005; Hampson, 2010). In some cases, compound clinoform systems are characterised by large subaqueous clinoforms with a clearly sigmoidal geometry (shape ratio <0.4) and a broad, well-developed subaqueous topset (e.g., muddy delta systems fed by large rivers and strongly influenced by waves or tides, such as the Amazon, Ganges–Brahmaputra, Fly, Yangtze River deltas). Other systems are characterised by much larger subaerial delta or shoreline clinoforms with an oblique to top-truncated geometry (shape ratio ≥ 0.4), and by a much reduced to absent subaqueous counterpart (e. g. sandy delta systems or muddy delta systems containing a strongly progradational subaerial delta, such as the Mississippi River delta) (cf., Figs. 16–17).

As a consequence of the relationship described above, the wide, low-gradient shelves that typically host mud-rich subaqueous deltas, together with the greater distance of these clinoforms from the shoreline, are interpreted to reflect the lower angle of repose of fine-grained sediments, and the high values of riverine sediment supply and subaqueous delta progradation rates that typify these systems. The deeper clinoform rollovers for sand-prone systems are attributed to the greater wave and current velocities needed to transport sand- rather than mud-grade

sediment. These greater velocities are mirrored by a deeper storm wave-base that, in turn, directly affects the depth of the delta-scale subaqueous rollover (e.g., Pirmez et al., 1998; Swenson et al., 2005; Mitchell et al., 2012).

Sand-prone delta-scale subaqueous clinoforms are particularly common in tectonically active settings, such as the periphery of rift basins (e.g., the Sognefjord Formation) or in the vicinity of compressional to transpressional plate boundaries (e.g., California Borderlands, southern Iberia) (Table 1 and 2; Figs. 6, 7, 17). These contexts are effective in: (1) delivering coarse-grained clastic sediment to the shelf via short, steep subaerial drainages; (2) favouring the formation of narrow, steep shelves; and (3) triggering or enhancing strong oceanographic circulation (e.g., Færseth and Ravnås, 1998; Gawthorpe and Leeder, 2000). Conversely, muddy subaqueous deltas are particularly common on broad, low-gradient shelves situated in passive margin or cratonic basins (Tables 1 and 2; Figs. 6, 7, 17). However, exceptions to these rules are also present, since the catchment lithology, the general oceanographic and climatic settings play a very important role as well. For instance, the muddy Adriatic clinoforms are situated in a foreland-type basin fronting evolving thrust-and-fold belts.

7.3. Implications for sequence stratigraphic models

It has been pointed out that positive correlations exist between water depths of topset-to-foreset rollover points and various geometric and stratigraphic parameters (total relief, foreset height, topset height, bottomset height, duration, progradation resistance ratio) (Fig. 15L–Q). This means that it is now possible to quantitatively infer palaeobathymetries of clinoform-bearing sedimentary successions once one or more of these parameters have been constrained. This has potentially important implications, as palaeobathymetry is a crucial constraint for established sequence stratigraphic and quantitative stratigraphic techniques (e.g., backstripping, Allen and Allen, 2005). This new technique to infer the palaeo-water depth at the rollover point, together with the geometric method proposed by Patruno et al. (in press) for estimating the palaeobathymetry at any point on a clinoform surface away from the rollover, has the potential to complement palaeontologically-constrained palaeobathymetry estimates or to replace them completely.

Furthermore, the recognition of delta-scale subaqueous clinoforms in the stratigraphic record has profound implications for the interpretation of ancient clinoform-bearing strata, because topset-to-foreset rollovers in delta-scale clinoforms are near-universally interpreted as palaeo-shorelines and are thus treated as robust indicators of relative sea-level position. Vertical stacking of delta-scale clinoform sets in seismic data is typically used as evidence for repeated regression and transgression of a palaeo-shoreline (i.e. a subaerial delta) (e.g., Helland-Hansen and Hampson, 2009).

An alternative interpretation of delta-scale compound clinoform geometries is that their subaerial and subaqueous clinoforms were shoreline clinoforms deposited at different times under different relative sea-level conditions (e.g. highstand and lowstand delta clinoforms). This alternative interpretation is particularly troublesome in the case of Quaternary compound clinoforms, because a major sea-level rise (up to 120 m) occurred following the last de-glaciation, at about 7–8 Ka, such that modern subaqueous delta clinoforms superficially resemble Pleistocene subaerial delta clinoforms developed during the last glacial sea-level lowstand. However, direct dating of several mud- and sand-prone subaqueous clinoforms clearly indicates that they were initiated and grew after the attainment of the Late Holocene sea-level highstand (e.g. sand-prone subaqueous clinoforms off south-eastern Australia, southern Iberia, and California; Field and Roy, 1984; Roy et al., 1994; Hernández-Molina et al., 2000a; Le Dantec et al., 2010; muddy subaqueous clinoforms of the Adriatic shelf and Yangtze River delta; Cattaneo et al., 2003, 2007; Liu et al., 2006). Seismically resolved lap-out relationships also indicate development and progradation of subaqueous delta clinoforms after the Late Holocene sea-level highstand (e.g. subaqueous clinoforms off the Manawatu coast, New Zealand and the Tiber River mouth, Italy; Amorosi and Milli, 2001; Dunbar and Barrett, 2005). Thus, recent examples demonstrate that delta-scale compound clinoforms and subaqueous clinoforms are a viable template for interpretation of ancient strata. The diagnostic criteria presented above provide a tool to differentiate subaerial and subaqueous delta-scale clinoforms using subsurface data (cores, wireline logs, seismic data, biostratigraphic and other chronostratigraphic data), and also to indicate whether delta-scale subaqueous clinoforms are sand-prone or mud-prone. Delta-scale subaqueous clinoform trajectories within clinoform sets are likely to directly reflect changes in wave base, which in turn are modulated by variations in both relative sea level and wave climate. The stacking of consecutive delta-scale subaqueous clinoform sets is likely to reflect relative sea-level and sediment supply history, in the same way as stacking of subaerial delta clinoform sets.

The very different time scales over which delta-, shelf-prism- and continental margin-scale clinoform systems prograde cause the formation of shelf-edge deltas in <0.15 Myr during relative sea-level stillstands. Nevertheless, shore-parallel marine sediment transport can result in significantly longer shelf-transit times, and may inhibit the establishment of shelf-edge deltas if river sediment input rates are outpaced by the shelf transport rates (Burgess and Hovius, 1998; Yoshida et al., 2007; Burgess and Steel, 2008; Helland-Hansen and Hampson, 2009; Olariu and Steel, 2009) or even encourage delta autoretreat (sensu Muto and Steel, 1992; Muto et al., 2007). In the case of delta-scale subaqueous clinoforms, ascending normal-regressive clinoform trajectories and sediment transport by powerful alongshore currents are likely to cause progressive decrease of across-shelf net-sediment fluxes and progradation rates as the subaqueous delta approaches the shelf-edge. Much of the sediment budget in delta-scale subaqueous clinoform systems is redistributed alongshore rather than across the shelf and towards the shelf break. This pattern is commonly observed in present-day subaqueous deltas, which form laterally extensive (up to 10^2–10^3 km), shore-parallel traps for river-fed sediments on the shelf, at the expense of sediment bypass across the shelf to the basin floor (e.g., in the Yangtze River delta, Liu et al., 2006). As a consequence, the presence of delta-scale subaqueous clinoform sets on an ancient shelf may suggest that sediment storage on the shelf was greater than sediment bypass across the shelf, except where canyons are observed to extend across the shelf to the palaeoseaward limit of the subaqueous delta. Such canyons constitute efficient conduits for the transfer of sediment to the basin floor (e.g., Milliman et al., 1984; Nittrouer et al., 1986; Posamentier et al., 1991; Johnson and Baldwin, 1996; Covault et al., 2007), as observed in the present day Ganges–Brahamaputra subaqueous delta (Kuehl et al., 1997; Michels et al., 1998).

8. Conclusions

Delta-scale subaqueous clinoforms are common features of Holocene-to-modern shelves, but ancient examples are rarely interpreted. This study analyses a large dataset of modern and ancient clinoforms, characterised by heights of tens, hundreds and thousands of metres (i.e., respectively, 'delta-scale', 'shelf-prism-scale' and 'continental-margin-scale'). Diagnostic criteria are identified that allow different clinoform types and their dominant grain-sizes to be interpreted in seismic reflection, sedimentological and/or stratigraphic data. Our quantitative approach demonstrates that all clinoforms, despite remarkable differences in size, age and palaeoenvironments, are subject to similar physical laws. These are exemplified by regression equations, extracted from cross-plots of architectural and/or stratigraphic parameters.

The examined dataset demonstrates that progressively larger scale clinoforms are deposited in increasingly deeper waters, over progressively larger time spans. Delta-scale, shelf-prism-scale and

continental-margin-scale clinoforms are respectively deposited at rollover water depths of 0–60 m, 58–530 m, 550–1770 m, and over time spans of 0.1–100 kyr, 0.2–17.6 Myr, 3.7–123.3 Myr. Accordingly, vertical sedimentation rates, progradation rates and depositional fluxes of continental-margin clinoforms are up to 4–6 orders of magnitude lower than typical delta-scale clinoform values. For all clinoform types, strong statistical correlations exist between: (1) the water depths of rollover points, (2) foreset, topset and bottomset heights, (3) durations, and (4) progradation resistance ratio. It is therefore now possible to quantitatively infer paleobathymetries of clinoform-bearing sedimentary successions once one of these parameters has been constrained.

Both muddy and sandy delta-scale subaqueous clinoforms share four characteristics. Firstly, they are formed during relative sea-level stillstands, For example, all recent subaqueous clinoforms started prograding after the attainment of the Late Holocene highstand (c. 6–7 ka). Secondly, their stratigraphic architecture, geomorphology and facies character are dominated by basinal waves, currents and tides, and tend to be more uniform than those of subaerial deltas. Thirdly, their plan-view morphology is shore-parallel, laterally extensive (up to 10^2–10^3 km) and near-linear, with the sediment budget primarily redistributed alongshore and a low chance of shelf bypass. Lastly, their nearly symmetrical, sigmoidal cross-sectional geometry is similar to that of shelf-prism clinoforms and contrasts with the oblique profiles of most subaerial deltas. Sigmoidal morphologies are due to the predominance of fine-grained lithologies, influence of basinal processes, relatively slow progradation and high-angle trajectories. The opposite conditions generate typical oblique profiles in subaerial deltas.

Despite the similarities, differences in morphology and sedimentary dynamics allow muddy and sandy delta-scale subaqueous clinoforms to be differentiated. In particular, delta-scale sand-prone subaqueous clinoforms have diagnostically steep foresets (0.7–10°, and up to 23°) and topsets/bottomsets (0.4–5°). Similarly steep foreset gradients were observed in muddy shelf-prism- and continental-margin-scale clinoforms (respectively, 0.9–9.8° and 0.9–16.2°). Progressively gentler foreset gradients are shown by sand-prone subaerial deltas (0.1–2.7°) (except Gilbert deltas), and by mud-prone subaqueous and subaerial deltas (0.03–1.50°). A foreset gradient threshold between recent mud- and sand-prone delta-scale clinoforms is observed at ca. 0.3–0.5°. These relationships reveal that larger and/or coarser-grained clinoforms are characterised by steeper foresets, independent of depositional environment. Delta-scale sand-prone subaqueous clinoforms have foreset dip extents (<2.6 km) that are approximately 10 times smaller than those of other delta-scale clinoforms. The quantitative nature of the relationships between dip extents and slope gradients is demonstrated by inverse correlations between these parameters, which are not observed in other clinoform types. Holocene delta-scale (foreset height <50 m), sand-prone subaqueous clinoforms occur on steep (≥0.26°) and narrow (5–32 km) shelves, at typical distances of 0.6–7.2 km from the shoreline break. These characteristics contrast with mud-prone subaqueous deltas, which form clinoforms on gently-sloping (0.01–0.38°), wide (23–376 km) shelves, at usual distances of 7.5–125 km from the shoreline. Cut-off values between the two systems were identified: (a) c. 9 km distance from the shoreline to the delta-scale subaqueous rollover; (b) c. 30–70 km shelf width; (c) 0.2–0.5° average shelf-gradients. In sandy delta-scale systems, the water depth of the subaqueous clinoform rollover point (≈20–60 m) is ca. 10–30 m deeper than in muddy subaqueous deltas, and the height of the subaerial clinoform is greater than about one fifth of the associated subaqueous clinoform.

Due to the sporadic nature of depositional episodes and the typical lack of direct connections with river mouths, Holocene delta-scale sand-prone subaqueous clinoform deposits have progradation rates (1–5 × 10^2 km/Myr) and unit-width depositional flux (1–15 km^2/Myr) that are up to 3–4 and 2–3 orders of magnitude lower, respectively, than in age-equivalent subaerial deltas and muddy subaqueous deltas (typically associated with large feeder rivers). Even in the Holocene, lower progradation/aggradation ratios are reflected in a larger spread of progradational clinoform trajectory values (from −0.4° to +3.5° relative to horizontal) than the very low angles displayed by age-equivalent muddy subaqueous deltas (<0.5°) and by progradational subaerial-deltas (<0.1°). Due to the well-known dominance of short-term progradation and long-term aggradation in most sedimentary successions, clinoform trajectories are increasingly steep for sandy subaerial deltas deposited over longer (10^5–10^6 yr) timescales (up to +1.7°), shelf-prism clinoforms (0 to +2.4°) and continental-margin clinoform sets (+0.9° to +49.0°).

Our analysis indicates that delta-scale compound clinoforms and subaqueous clinoforms are a viable template for interpretation of ancient strata. These clinoform types can be diagnosed using geomorphological, sedimentological and stratigraphic features that are readily applicable to subsurface data (cores, wireline logs, seismic data, biostratigraphic and other chronostratigraphic data). The capacity to recognise different clinoform types based on seismic geomorphological parameters is particularly important, since seismic data is the pre-eminent tool for analysis of many ancient sedimentary basins. Robust recognition of different clinoform types is significant, because they denote different palaeo-environmental conditions and require different sequence stratigraphic interpretations. For example, the presence of delta-scale subaqueous clinoform sets suggests predominant alongshore sediment transport and correspondingly little sediment bypass to the basin floor. Furthermore, sand-prone delta-scale subaqueous clinoforms tend to be associated with active tectonic settings, whereas muddy delta-scale subaqueous clinoforms are usually associated with tectonic quiescence.

Acknowledgements

We thank Clara Rodriguez Rondon for her valuable suggestions and observations, Dr. Nicholas Holgate for his comments on a previous draft of this manuscript, and Prof. Philip Allen and Dr. Fabio Trincardi for their insightful discussions and observations. We are grateful to Prof. William Helland-Hansen, Prof. Andrew Miall and an anonymous reviewer for their editing and reviewing a previous version of this manuscript. This work has benefited from their valuable expertise and ideas. We also acknowledge the Troll Field partners, Statoil ASA, Petoro AS, A/S Norske Shell, Total E&P Norge AS and ConocoPhillips Skandinavia AS, for their permission to publish the Sognefjord Formation data. Thanks also to Schlumberger Limited for the provision of Petrel seismic and well interpretation software via an academic software donation.

References

Adams, E.W., Schlager, W., 2000. Basic types of submarine slope curvature. J. Sediment. Res. 70, 814–828.
Alexander, C.R., DeMaster, D.J., Nittrouer, C.A., 1991. Sediment accumulation in a modern epicontinental-shelf setting: the Yellow Sea. Mar. Geol. 998, 51–72.
Allen, P.H., Allen, J.R., 2005. Chapter 9 — Subsidence and thermal history. Basin Analysis, Principles and Applications Second ed. Blackwell Publishing, pp. 349–395.
Amorosi, A., Milli, S., 2001. Late Quaternary depositional architecture of Po and Tevere river deltas (Italy) and worldwide comparison with deltaic successions. Sediment. Geol. 144, 357–375.
Asquith, D.O., 1970. Depositional topography and major marine environments, Late Cretaceous, Wyoming. AAPG Bull. 54, 1184–1224.
Barrell, J., 1912. Criteria for the recognition of ancient delta deposits. Geol. Soc. Am. Bull. 23, 377–446.
Bates, C.C., 1953. Rational theory of delta formation. Am. Assoc. Pet. Geol. Bull. 37, 2119–2162.
Bhattacharya, J.P., 2006. Deltas. In: Walker, R.G., Posamentier, H. (Eds.), Facies Models Revisited. SEPM (Society for Sedimentary Geology) Special Publications, Tulsa (Oklahoma) 84, pp. 237–292.
Bornhold, B.D., Yang, Z.-S., Keller, G.H., Prior, D.B., Wiseman, W.J., Wright, L.D., 1986. The sedimentary framework of the modern Huanghe (Yellow River) Delta. Geo-Mar. Lett. 6, 77–83.

Appendix A. Quantitative correlation between clinoform parameters

Table 5
Strength of correlation between each possible pair of statistical parameters within the global clinoform dataset. Weak-to-strong positive correlations ($R^2 > 0.1$) are shown by light grey boxes, and weak-to-strong negative correlations by dark grey boxes. Moderate-to-strong correlations ($R^2 > 0.5$) are indicated by numbers, each corresponding to an equation in Tables 6 and 7 and Fig. 9–10.

Features			*Hh*	*Hd*	*Is*	*Fh*	*Fd*	*Fs*	*Bh*	*Bd*	*Bs*	*Th*	*Td*	*Ts*	*h/H*	Age	Sv	P	F	R	CT	Wd
Total relief (H)	Height (m)	*Hh*	–			1			2			3				4				5		6
	Down-dip extent (m)	*Hd*		–			7			8			9									
Inflection zone slope (°)		*Is*			–			10			11			12								
Foreset	Height (m)	*Fh*	1			–			13			14								15		16
	Down-dip extent (m)	*Fd*		7			–			17			18									
	Slope (°)	*Fs*			10			–			19			20								
Inner bottomset	Height (m)	*Bh*	2			13			–	21		22										23
	Down-dip extent (m)	*Bd*		8			17		21	–			24									
	Slope (°)	*Bs*			11			19			–			25								
Outer topset	Height (m)	*Th*	3			14			22			–										26
	Down-dip extent (m)	*Td*		9			18			24			–									
	Slope (°)	*Ts*			12			20			25			–								
Shape ratio (h/H; non-dim.)		*h/H*													–							
Age scale (Myr)		Age	4													–	27	28		29		30
Vertical sediment accumulation rate (m/Myr)		Sv														27	–	31	32			
Clinoform progradation rate (m/Myr)		P														28	31	–	33			
Unit-width depositional flux (km^2/Myr)		F															32	33	–			
Progradation resistance ratio (non-dimensional)		R	5			15										29				–		34
Clinoform trajectory (°)		CT																			–	
Water depth of rollover point (m)		Wd	6			16			23			26				30				34		–

Table 6
Strength of correlation between each possible pair of statistical parameters within the dataset of sand-prone subaqueous delta clinoforms. Weak-to-strong positive correlations ($R^2 > 0.1$) are shown by light grey boxes, and weak-to-strong negative correlations by dark grey boxes. Moderate-to-strong correlations ($R^2 > 0.5$) correlations are indicated by numbers, each corresponding to an equation in Tables 6 and 7 and Figs. 9–10. Parameter pairs characterised by absence of correlation whereas in the global dataset (Table 5) a correlation exist (and vice versa) are highlighted by an asterisk (*). A double asterisk (**) marks parameter pairs showing an opposite correlation type than in the global dataset (cf. Table 5).

Features			Hh	Hd	Is	Fh	Fd	Fs	Bh	Bd	Bs	Th	Td	Ts	h/H	Age	Sv	P	F	R	CT	Wd
Total relief (H)	Height (m)	Hh	–		**			**			*			*	*	*	**	*	*		*	**
	Down-dip extent (m)	Hd		–	35	*	36	37					38		39	**	40 *	*			*	*
Inflection zone slope (°)		Is	**	35	–		41 *	42	*		43	*	44	45	*				*	*		*
Foreset	Height (m)	Fh		*		–		*	*	*		*		*	*		*			*	*	*
	Down-dip extent (m)	Fd		36	41 *		–	46	*	47	48		49	50	*	**	*	*			*	*
	Slope (°)	Fs	**	37	42	*	46	–		51	52	*	53	54	*				*	*	*	*
Inner bottomset	Height (m)	Bh			*	*	*		–			*			*	*		*			*	*
	Down-dip extent (m)	Bd				*	47	51		–	55		56		*	**		*			*	*
	Slope (°)	Bs	*		43		48	52		55	–			57	*					*		*
Outer topset	Height (m)	Th			*	*		*	*			–		*	*	**	*	*			*	*
	Down-dip extent (m)	Td		38	44		49	53		56			–	58	*	*	59	*	*			*
	Slope (°)	Ts	*		45	*	50	54			57	*	58	–						*	*	*
Shape ratio (h/H; non-dim.)		h/H	*	39	*	*	*	*	*	*	*	*	*		–	*	*	*	*	*		
Age scale (Myr)		Age	*	**	**		**		*	**		**	*		*	–	60	61			*	
Vertical sediment accumulation rate (m/Myr)		Sv	**	40 *	*	*	*					*	59		*	60	–		62	63 *	*	**
Clinoform progradation rate (m/Myr)		P	*	*			*		*	*		*	*		*	61		–	64		*	*
Unit-width depositional flux (km^2/Myr)		F	*		*			*					*		*		62	64	–	*		*
Progradation resistance ratio (non-dimensional)		R			*	*		*			*			*	*		63 *		*	–	*	
Clinoform trajectory (°)		CT	*	*		*	*	*	*	*		*		*		*	*	*		*	–	*
Water depth of rollover point (m)		Wd	**	*	*	*	*	*	*	*	*	*	*	*			**	*	*		*	–

Table 7
Equations describing best-fit lines between parameter pairs showing a moderate-to-strong correlation ($R^2 > 0.5$). Graphical representations of data point distributions and best-fit lines are shown in Fig. 14.

Correlations	All clinoforms			Sand-prone subaqueous delta clinoforms		
	No.	Type	Regression equation	No.	Type	Regression equation
Total relief height (*Hh*)–foreset height (*Fh*)	1	Positive polynomial	$Fh = [4 \cdot 10^{-5}(Hh)^2 + 0.71\,(Hh) - 4.33]$ ($R^2 = 0.98$)	–	Positive weak correlation ($R^2 \leq 0.40$)	
Total relief height (*Hh*)–bottomset height (*Bh*)	2	Positive polynomial	$Bh = [-10^{-5}(Hh)^2 + 0.16(Hh) - 2.10]$ ($R^2 = 0.80$)	–	Positive, weak correlation ($R^2 \leq 0.30$)	
Total relief height (*Hh*)–topset height (*Fh*)	3	Positive polynomial	$Th = [-2 \cdot 10^{-5}(Hh)^2 + 0.11(Hh) + 0.47]$ ($R^2 = 0.7551$)	–	No correlations at all ($R^2 \leq 0.12$)	
Total relief down-dip extent (*Hd*)–foreset down-dip extent (*Fd*)	7	Positive power	$Fd = [0.4789(Hd)^{0.9696}]$ ($R^2 = 0.8834$)	36	Positive power	$Fd = [1.2386(Hd)^{0.8049}$ ($R^2 = 0.62$)
Total relief down-dip extent (*Hd*)–bottomset down-dip extent (*Bd*)	8	Positive polynomial	$Bd = [8 \cdot 10^{-7}(Hd)^2 + 1.72(Hd) + 275.94]$ ($R^2 = 0.91$)	–	Positive, weak correlation ($R^2 \leq 0.50$)	
Total relief down-dip extent (*Hd*)–topset down-dip extent (*Td*)	9	Positive power	$Td = [0.271(Hd)^{0.94}]$ ($R^2 = 0.94$)	38	Positive power	$Td = [0.43(Hd)^{0.86}]$ ($R^2 = 0.63$)
Inflection zone slope (*Is*)–foreset slope (*Fs*)	10	Positive power	$Fs = [0.74\,(Is)^{0.98}]$ ($R^2 = 0.98$)	42	Positive power	$Fs = [0.77(Is)^{1.005}]$ ($R^2 = 0.97$)
Inflection zone slope (*Is*)–bottomset slope (*Bs*)	11	Positive power	$Bs = [0.27\,(Is)^{0.89}$ ($R^2 = 0.86$)	43	Positive power	$Bs = [0.45(Is)^{0.73}]$ ($R^2 = 0.695$)
Inflection zone slope (*Is*)–topset slope (*Ts*)	12	Positive power	$Ts = [0.265(Is)^{0.88}]$ ($R^2 = 0.84$)	45	Positive power	$Ts = [0.43\,(Is)^{0.69}]$ ($R^2 = 0.72$)
Foreset height (*Fh*)–bottomset height (*Bh*)	13	Positive power	$Bh = [0.19\,(Fh)^{0.96}]$ ($R^2 = 0.75$)	–	No correlations at all ($R^2 \leq 0.1$)	
Foreset height (*Fh*)–topset height (*Th*)	14	Positive polynomial	$Th = [-3 \cdot 10^{-5}(Fh)^2 + 0.135(Fh) + 2.23]$ ($R^2 = 0.68$)	–	No correlations at all ($R^2 \leq 0.1$)	
Foreset down-dip extent (*Fd*)–foreset slope (*Fs*)	–	Negative, weak correlation ($R^2 \leq 0.38$) (relationship breaks down at *Fd* >2000 *m*)		46	Negative power	$Fs = [794.68(Fd)^{-0.92}]$ ($R^2 = 0.89$)
Foreset down-dip extent (*Fd*)–bottomset down-dip extent (*Bd*)	17	Positive power	$Bd = [0.71\,(Fd)^{0.94}]$ ($R^2 = 0.83$)	47	Positive polynomial	$Bd = [0.0002(Fd)^2 + 0.04(Fd) + 77.48]$ ($R^2 = 0.84$)
Foreset down-dip extent (*Fd*)–topset down-dip extent (*Td*)	18	Positive power	$Td = [0.9062(Fd)^{0.90}]$ ($R^2 = 0.82$)	49	Positive polynomial	$Td = [-2 \cdot 10^{-5}(Fd)^2 + 0.58(Fd) - 2.17]$ ($R^2 = 0.745$)
Foreset slope (*Fs*)–bottomset slope (*Bs*)	19	Positive power	$Bs = [0.3594(Fs)^{0.88}]$ ($R^2 = 0.875$)	52	Positive power	$Bs = [0.5559(Fs)^{0.71}]$ ($R^2 = 0.70$)
Foreset slope (*Fs*)–topset slope (*Ts*)	20	Positive power	$Ts = [0.3237(Fs)^{0.92}]$ ($R^2 = 0.85$)	54	Positive power	$Ts = [0.528(Fs)^{0.68}]$ ($R^2 = 0.72$)
Bottomset height (*Bh*)–bottomset down-dip extent (*Bd*)	21	Positive polynomial	$Bd = [0.0548(Bh)^2 + 74.57\,(Bh) + 1358.4]$ ($R^2 = 0.62$)	–	Positive, weak correlation ($R^2 \leq 0.33$)	
Bottomset height (*Bh*)–topset height (*Th*)	22	Positive polynomial	$Th = [-5.15 \cdot 10^{-4}(Bh)^2 + 6.217\,(Bh) + 2.6869]$ ($R^2 = 0.78$)	–	No correlations at all ($R^2 \leq 0.1$)	
Bottomset down-dip extent (*Bd*)–bottomset slope (*Bs*)	–	Negative, weak correlation ($R^2 \leq 0.33$)		55	Negative power	$Bs = [40.265(Bd)^{-0.654}]$ ($R^2 = 0.61$)
Bottomset down-dip extent (*Bd*)–topset down-dip extent (*Td*)	24	Positive power	$Td = [2.7414(Bd)^{0.84}]$ ($R^2 = 0.7458$)	56	Positive polynomial	$Td = [0.0001(Bd)^2 + 0.40(Bd) + 78.35]$ ($R^2 = 0.76$)
Bottomset slope (*Bs*)–topset slope (*Ts*)	25	Positive power	$Ts = [0.8655(Bs)^{0.94}]$ ($R^2 = 0.805$)	57	Positive power	$Ts = [1.1555(Bs)^{0.6864}]$ ($R^2 = 0.55$)
Topset down-dip extent (*Td*)–topset slope (*Ts*)	–	Negative, weak correlation ($R^2 \leq 0.39$)		58	Negative power	$Ts = [25.949(Td)^{-0.58}]$ ($R^2 = 0.63$)
Age scale (*Age*)–vertical sedimentation rate (*Sv*)	27	Negative power	$Sv = [95.827(Age)^{-0.669}]$ ($R^2 = 0.57$)	60	Negative power	$Sv = [2.1202(Age)^{-1.27}]$ ($R^2 = 0.63$)
Age scale (*Age*)–progradation rate (*P*)	28	Negative power	$P = [19\,(Age)^{-0.88}]$ ($R^2 = 0.73$)	61	Negative power	$P = [9930.6(Age)^{-0.70}]$ ($R^2 = 0.73$)
Vertical sedimentation rate (*Sv*)–sediment fluxes (*F*)	32	Positive power	$F = [0.067(Sv)^{0.82}]$ ($R^2 = 0.72$)	62	Positive polynomial	$F = [10^{-6}(Sv)^2 - 0.0051\,(Sv) + 9.68]$ ($R^2 = 0.83$)
Vertical sedimentation rate (*Sv*)–progradation resistance ratio (*R*)	–	Maximum point at $Sv \approx 200$ *m/Myr*; $R \approx 0.6$		63	Positive power	$R = [3 \cdot 10^{-5}(Sv)^{0.745}]$ ($R^2 = 0.74$)
Progradation rate (*R*)–sediment fluxes (*F*)	33	Positive power	$F = [8.95^{*}10^{-4}(R)^{0.77}]$ ($R^2 = 0.87$)	64	Positive power	$F = [0.0013(R)^{0.67}]$ ($R^2 = 0.71$)

Table 8
Equations describing best-fit lines between parameter pairs showing a moderate-to-strong correlation ($R^2 > 0.5$). Graphical representations of data point distribution and best-fit lines are shown in Fig. 15.

Correlations	All clinoforms			Sand-prone subaqueous delta clinoforms		
	No.	Type	Regression equation	No.	Type	Regression equation
Total relief height (*Hh*)–age scale (*Age*)	4	Positive linear*	$Age = [0.03(Hh) - 1.363]$ $(R^2 = 0.57)$	–	No correlation at all ($R^2 \leq 0.10$)	
Total relief height (*Hh*)–progradation resistance ratio (*R*)	5	Positive polynomial	$P = [5 \cdot 10^{-8}(Hh)^2 - 4 \cdot 10^{-5}(Hh) + 0.011]$ $(R^2 = 0.60)$	–	Positive, weak correlation ($R^2 \leq 0.17$)	
Total relief height (*Hh*)–water depth of rollover (*Wd*)	6	Positive linear	$Wd = [0.48(Hh) + 16.33]$ $(R^2 = 0.83)$	–	Negative, weak correlation ($R^2 \leq 0.12$)	
Total relief down-dip extent (*Hd*)–inflection zone slope (*Is*)	–	Negative, weak correlation ($R^2 \leq 0.34$) (relationship breaks down at $Hd > 5000$ *m*)		35	Negative power	$Is = [935.31(Hd)^{-0.754}]$ $(R^2 = 0.60)$
Total relief down-dip extent (*Hd*)–foreset slope (*Fs*)	–	Negative, weak correlation ($R^2 \leq 0.3751$) (relationship breaks down at $Hd > 5000$ *m*)		37	Negative power	$Fs = [876.14(Hd)^{-0.784}]$ $(R^2 = 0.63)$
Total relief down-dip extent (*Hd*)–shape ratio (*h/H*)	–	No correlation at all ($R^2 \leq 0.1$)		39	Negative logarithmic*	$h/H = -0.09 \ln(Hd) + 0.97]$ $(R^2 = 0.50)$
Total relief down-dip extent (*Hd*)–vertical sedimentation rate (*Sv*)	–	Positive?, weak correlation ($R^2 \leq 0.18$)		40	Positive power	$Sv = [0.0021(Hd)^{1.8334}]$ $(R^2 = 0.79)$
Inflection zone slope (*Is*)–topset down-dip extent (*Td*)	–	Negative, weak correlation ($R^2 \leq 0.38$) (relationship breaks down at $1° < Is < 10°$)		44	Negative power	$Td = [701.11(Is)^{-0.955}]$ $(R^2 = 0.73)$
Inflection zone slope (*Is*)–foreset down-dip extent (*Fd*)	–	Negative, weak correlation ($R^2 \leq 0.34$) (relationship breaks down at $1° < Is < 20°$)		41	Negative power	$Fd = [1460.5(Is)^{-0.961}]$ $(R^2 = 0.84)$
Foreset height (*Fh*)–progradation resistance ratio (*P*)	15	Positive polynomial	$P = [7 \cdot 10^{-8}(Fh)^2 - 4 \cdot 10^{-5}(Fh) + 0.0096]$ $(R^2 = 0.60)$	–	No correlation at all ($R^2 \leq 0.1$)	
Foreset height (*Fh*)–water depth of rollover (*Wd*)	16	Positive polynomial	$Wd = [-1.08 \cdot 10^{-4}(Fh)^2 + 0.819(Fh) + 13.101]$ $(R^2 = 0.81)$	–	No correlation at all ($R^2 \leq 0.1$)	
Foreset down-dip extent (*Fd*)–bottomset slope (*Bs*)	–	Negative, weak correlation ($R^2 \leq 0.38$) (relationship breaks down at $Fd > 2000$ *m*)		48	Negative exponential	$Bs = [3.50e^{-0.001Fd}]$ $(R^2 = 0.70)$
Foreset down-dip extent (*Fd*)–topset slope (*Ts*)	–	Negative, weak correlation ($R^2 \leq 0.33$) (relationship breaks down at $Fd > 2000$ *m*)		50	Negative power	$Ts = [54.52(Fd)^{-0.642}]$ $(R^2 = 0.68)$
Foreset slope (*Fs*)–bottomset down-dip extent (*Bd*)	–	Negative, weak correlation ($R^2 \leq 0.28$)		51	Negative power	$Bd = [377.49(Fs)^{-0.77}]$ $(R^2 = 0.57)$
Foreset slope (*Fs*)–topset down-dip extent (*Td*)	–	Negative, weak correlation ($R^2 \leq 0.40$)		53	Negative power	$Td = [539.34(Fs)^{-0.94}]$ $(R^2 = 0.74)$
Bottomset height (*Bh*)–water depth of rollover (*Wd*)	23	Positive polynomial	$Wd = [-0.011(Bh)^2 + 7.36(Bh) - 19.11]$ $(R^2 = 0.75)$	–	No correlation at all ($R^2 \leq 0.1$)	
Topset height (*Th*)–water depth of rollover (*Wd*)	26	Positive polynomial	$Wd = [-0.0094(Th)^2 + 8.29(Th) - 1.52]$ $(R^2 = 0.70)$	–	No correlation at all ($R^2 \leq 0.1$)	
Topset down-dip extent (*Td*)–vertical sedimentation rate (*Sv*)	–	Positive, weak correlation ($R^2 \leq 0.22$)		59	Positive power	$Sv = [0.096(Td)^{1.679}]$ $(R^2 = 0.69)$
Age scale (*Age*)–progradation resistance ratio (*R*)	29	Positive polynomial	$R = [3 \cdot 10^{-5}(Age)^2 - 0.0009(Age) + 0.0095]$ $(R^2 = 0.88)$	–	Minimum point at $Age \approx 0.01$ *Myr*; $R \approx 5 \cdot 10^{-4}$	
Age scale (*Age*)–water depth of rollover (*Wd*)	30	Positive polynomial	$Wd = [-0.073(Age)^2 + 19.49(Age) + 48.14]$ $(R^2 = 0.72)$	–	Positive, weak correlation ($R^2 \leq 0.11$)	
Vertical sedimentation rate (*Sv*)–progradation rate (*P*)	31	Positive power*	$P = [521.81(Age)^{0.964}]$ $(R^2 = 0.68)$	–	Positive, weak correlation ($R^2 \leq 0.26$)	
Progradation resistance ratio (*R*)–Water depth of rollover (*Wd*)	34	Positive polynomial	$Wd = [-4785(R)^2 + 6050.3(R) + 30.23]$ $(R^2 = 0.77)$	–	Positive, weak correlation ($R^2 \leq 0.19$)	

Bristow, C.S., Pucillo, K., 2006. Quantifying rates of coastal progradation from sediment volume using GPR and OSL: the Holocene fill of Guichen Bay, south-east South Australia. Sedimentology 53, 769–788.

Bullimore, S., Henriksen, S., Liestøl, F., Helland-Hansen, W., 2005. Clinoform stacking patterns, shelf-edge trajectories and facies associations in the Tertiary coastal deltas, offshore Norway. Implications for the prediction of lithology in prograding systems. Nor. J. Geol. 85, 169–187.

Bullimore, S.A., Helland-Hansen, W., Henriksen, S., Steel, R.J., 2008. Shoreline trajectory and its impact on coastal depositional environments: an example from the Upper Cretaceous Mesaverde Group, NW Colorado. In: Hampson, G.J., Steel, R.J., Burgess, P.M., Dalrymple, R.W. (Eds.), Recent Advances in Models of Siliciclastic Shallow-Marine Stratigraphy. SEPM Special Publication 90, pp. 209–236.

Burgess, P.M., Hovius, N., 1998. Rates of delta progradation during highstands; consequences for timing of deposition in deep-marine systems. J. Geol. Soc. 155, 217–222.

Burgess, P.M., Steel, R.J., 2008. Stratigraphic forward modelling of delta auto-retreat and shelf width: implications for controls on shelf width and timing of formation of shelf-edge deltas. In: Hampson, G.J., Steel, R.J., Burgess, P.M., Dalrymple, R.W. (Eds.), Recent Advances in Models of Siliciclastic Shallow-Marine Stratigraphy. SEPM Special Publication 90, pp. 35–45.

Carvajal, C., Steel, R.S., 2006. Thick turbidite successions from supply-dominated shelves during sea-level highstand. Geology 34, 665–668.

Cattaneo, A., Correggiari, A., Langone, L., Trincardi, F., 2003. The late-Holocene Gargano subaqueous delta, Adriatic shelf: sediment pathways and supply fluctuations. Mar. Geol. 193, 61–91.

Cattaneo, A., Trincardi, F., Langone, L., Asioli, A., Puig, P., 2004. Clinoform generation on Mediterranean margins. Oceanography 17 (4), 104–117.

Cattaneo, A., Trincardi, F., Asioli, A., Correggiari, A., 2007. The western Adriatic shelf clinoform: energy-limited bottomset. Cont. Shelf Res. 27, 506–525.

Chin, J.L., Clifton, H.E., Mullins, H.T., 1988. Seismic stratigraphy and late Quaternary shelf history, south-central Monterey Bay, California. Mar. Geol. 81, 137–157.

Correggiari, A., Cattaneo, A., Trincardi, F., 2005. The modern Po Delta system: lobe switching and asymmetric prodelta growth. Mar. Geol. 222–223, 49–74.

Covault, J.A., Normark, W.R., Romans, B.W., Graham, S.A., 2007. Highstand fans in the California borderland: the overlooked deep-water depositional systems. Geology 35, 783–786.

Dreyer, T., Whitaker, M., Dexter, J., Flesche, H., Larsen, E., 2005. From spit system to tide dominated delta: integrated reservoir model of the upper Jurassic Sognefjord Formation on the Troll West Field. In: Doré, A.G., Vining, B. (Eds.), Petroleum Geology of North-West Europe and Global Perspectives, Proceedings of the 6th Petroleum Geology Conference. Geological Society of London, London, pp. 1–26.

Driscoll, N.W., Karner, G.D., 1999. Three-dimensional quantitative modelling of clinoform development. Mar. Geol. 154, 383–398.

Dunbar, G.B., Barrett, P.J., 2005. Estimating palaeobathymetry of wave-graded continental shelves from sediment texture. Sedimentology 52, 253–269.

Færseth, R.B., Ravnås, R., 1998. Evolution of the Oseberg Fault-Block in the context of the northern North Sea structural framework. Mar. Pet. Geol. 15, 467–490.

Fernández-Salas, L.M., Dabrio, C.J., Goy, J.L., Díaz Del Río, V., Zazo, C., Lobo, F.J., Sanz, J.L., Lario, J., 2009. Land-sea correlation between Late Holocene coastal and infralittoral deposits in the SE Iberian Peninsula (Western Mediterranean). Geomorphology 104, 4–11.

Field, M.E., Roy, P.S., 1984. Offshore transport and sand-body formation: evidence from a steep, high-energy shoreface, southeastern Australia. J. Sediment. Petrol. 54, 1292–1302.

Fraser, S.I., Robinson, A.M., Johnson, H.D., Underhill, J.R., Kadolski, D.G.A., Connell, R., Johannessen, P., Ravnås, R., 2002. Upper Jurassic. In: Evans, D., Graham, C., Armour, A., Bathurst, P. (Eds.), The Millennium Atlas: Petroleum Geology of the Central and Northern North Sea. Geological Society of London, London, pp. 157–189.

Friedrichs, C.T., Scully, M.E., 2007. Modeling deposition by wave-supported gravity flows on the Po River prodelta: from seasonal floods to prograding clinoforms. Cont. Shelf Res. 27, 322–337.

Friedrichs, C.T., Wright, L.D., 2004. Gravity-driven sediment transport on the continental shelf: implications for equilibrium profiles near river mouths. Coast. Eng. 51, 795–811.

Galloway, W.E., 1975. Process framework for describing the morphologic and stratigraphic evolution of deltaic depositional systems. In: Broussard, M.L. (Ed.), Deltas: Models for Exploration. Houston Geological Society, Houston, pp. 87–98.

Gawthorpe, R.L., Leeder, M.R., 2000. Tectono-sedimentary evolution of active extensional basins. Basin Res. 12, 195–218.

Gensous, B., Tesson, M., 1997. Les dépôts postglaciaires de la plate-forme rhodanienne. organisation stratigraphique et conditions de mise en place. C. R. Acad. Sci. II 325, 695–701.

Gilbert, G.K., 1885. The topographic feature of lake shores. U.S. Geological Survey, Annual Report 5, pp. 104–108.

Hampson, G.J., 2010. Sediment dispersal and quantitative stratigraphic architecture across an ancient shelf. Sedimentology 57, 96–141.

Hampson, G.J., Morris, J.E., Johnson, H.D., 2015. Impact of time-stratigraphic relationships on hydrocarbon reservoir distribution and performance, Bridport Sand Formation, Wessex Basin, UK. Geol. Soc. Lond. Spec. Publ. (in review).

Hampson, G.J., Storms, J.E.A., 2003. Geomorphological and sequence stratigraphic variability in wave-dominated, shoreface-shelf parasequences. Sedimentology 50, 667–701.

Hampson, G.J., Morris, J.E., Johnson, H.D., 2015. Synthesis of time-stratigraphic relationships and their impact on hydrocarbon reservoir distribution and performance, Bridport Sand Formation, Wessex Basin, UK. In: Smith, D.G., Bailey, R.J., Burgess, P.M., Fraser, A.J. (Eds.), Strata and Time Probing the Gaps in our Understanding. Geological Society of London, Special Publications, London vol. 404. http://dx.doi.org/10.1144/SP404.2 (in press).

Helland-Hansen, W., Gjelberg, H., 2012. Towards a hierarchical classification of clinoforms. AAPG Annual Convention and Exhibition, April 22–25, 2012, Long Beach, California, U.S., Search and Discovery article #90142 (http://www.searchanddiscovery.com/abstracts/html/2012/90142ace/abstracts/hell.htm).
Helland-Hansen, W., Hampson, G.J., 2009. Trajectory analysis: concepts and applications. Basin Res. 21, 454–483.
Helland-Hansen, W., Steel, R.J., Sømme, T., 2012. Shelf genesis revisited. J. Sediment. Res. 82, 133–145.
Henriksen, S., Hampson, G.J., Helland-Hansen, W., Johannessen, E.P., Steel, R.J., 2009. Shelf edge and shoreline trajectories, a dynamic approach to stratigraphic analysis. Basin Res. 21, 445–453.
Hernández-Molina, F.J., Fernández-Salas, L.M., Lobo, F., Somoza, L., Díaz-del-Río, V., Alveirinho Dias, J.M., 2000a. The infralittoral prograding wedge. A new large-scale progradational sedimentary body in shallow marine environments. Geo-Mar. Lett. 20, 109–117.
Hernández-Molina, F.J., Somoza, L., Lobo, F., 2000b. Seismic stratigraphy of the Gulf of Cadiz Continental Shelf: a model for Late Quaternary very high-resolution sequence stratigraphy and response to sea-level fall. In: Hunt, D., Gawthorpe, R.L. (Eds.), Sedimentary Responses to Forced Regression. Special Publication 172. Geological Society of London, London, pp. 329–362 (London).
Hori, K., Saito, Y., Zhao, Q., Cheng, X., Wang, P., Sato, Y., Li, C., 2001. Sedimentary facies and Holocene progradation rates of the Changjiang (Yangtze) delta, China. Geomorphology 41, 233–248.
Howell, J.A., Skorstad, A., MacDonald, A.C., Fordham, A., Flint, S.S., Fjellvoll, B., Manzocchi, T., 2008. Sedimentological parameterization of shallow-marine reservoirs. Pet. Geosci. 14, 17–34.
Jackson, W.E., 1964. Depositional topography and cyclic deposition in west-central Texas. Bull. Am. Assoc. Pet. Geol. 48 (3), 317–328.
Johannessen, E.P., Steel, R.J., 2005. Shelf-margin clinoforms and prediction of deepwater sands. Basin Res. 15, 521–550.
Johnson, H.D., Baldwin, C.T., 1996. Shallow clastic seas. In: Reading, H.G. (Ed.), Sedimentary Environments: Processes, Facies and Stratigraphy. Blackwell Science, Oxford, pp. 232–280.
Jol, H.M., Lawton, D.C., Smith, D.G., 2002. Ground penetrating radar: 2-D and 3-D subsurface imaging of a coastal barrier spit, Long Beach, WA, USA. Geomorphology 53, 165–181.
Kenter, J.A.M., 1990. Carbonate platform flanks: slope angle and sediment fabric. Sedimentology 37, 777–794.
Kenyon, P.M., Turcotte, D.L., 1985. Morphology of a delta by bulk sediment transport. Geol. Soc. Am. Bull. 96, 1457–1465.
Kuehl, S.A., Nittrouer, C.A., DeMaster, D.J., 1986. Nature of sediment accumulation on the Amazon continental shelf. Cont. Shelf Res. 6, 209–225.
Kuehl, S.A., Levy, B.M., Moore, W.S., Allison, M.A., 1997. Subaqueous delta of the Ganges–Brahmaputra river system. Mar. Geol. 144, 81–96.
Kuehl, S.A., Allison, M.A., Goodbred, S.L., Kudrass, H., 2005. The Ganges–Brahmaputra Delta. In: Giosan, L., Bhattacharya, J.P. (Eds.), River Deltas: Concepts, Models and Examples. SEPM Special Publication 83, pp. 413–434.
Labaune, C., Jouet, G., Berné, S., Gensous, B., Tesson, M., Delpeint, A., 2005. Seismic stratigraphy of the deglacial deposits of the Rhône prodelta and of the adjacent shelf. Mar. Geol. 222–223, 299–311.
Le Dantec, N., Hogarth, L.J., Driscoll, N.W., Babcock, J.M., Barnhardt, W.A., Schwab, W.C., 2010. Tectonic controls on nearshore sediment accumulation and submarine canyon morphology offshore La Jolla, Southern California. Mar. Geol. 268, 115–128.
Liu, J.P., Milliman, J.D., Gao, S., Cheng, P., 2004. Holocene development of the Yellow River's subaqueous delta, North Yellow Sea. Mar. Geol. 209, 45–67.
Liu, J.P., Li, A.C., Xu, K.H., Velozzi, D.M., Yang, Z.S., Milliman, J.D., DeMaster, D.J., 2006. Sedimentary features of the Yangtze River-derived along-shelf clinoform deposit in the East China Sea. Cont. Shelf Res. 26, 2141–2156.
Liu, J.P., Xu, K.H., Li, A.C., Milliman, J.D., Velozzi, D.M., Xiao, S.B., Yang, Z.S., 2007. Flux and fate of Yangtze River sediment delivered to the East China Sea. Geomorphology 85, 208–224.
Lobo, F.J., Fernández-Salas, L.M., Hernández-Molina, F.J., González, R., Dias, J.M.A., Díaz Del Río, G., Somoza, L., 2005. Holocene highstand deposits in the Gulf of Cadiz, SW Iberian Peninsula: a high-resolution record of hierarchical environmental changes. Mar. Geol. 219, 109–131.
Løseth, T.M., Steel, R.J., Crabaugh, J.P., Schellpeper, M., 2006. Interplay between shoreline migration paths, architecture and pinchout distance for siliciclastic shoreline tongues: evidence from the rock record. Sedimentology 53, 735–767.
Methling, D., Jaschinski, W., Narcisi, B., Stemberg, R.W., Cacchione, D.A., Paulson, B., Kineke, G.C., Drake, D.E., 1996. Observations of sediment transport on the subaqueous Amazon delta. Cont. Shelf Res. 16, 697–715.
Michels, K.H., Kudrass, H.R., Hübscher, C., Suckow, A., Wiedicke, M., 1998. The submarine delta of the Ganges–Brahmaputra: cyclone-dominated sedimentation patterns. Mar. Geol. 149, 133–154.
Milliman, J.D., Quraishee, G.S., Beg, M.A.A., 1984. Sediment discharge from the Indus River to the ocean, past, present and future. In: Haq, B.U., Milliman, J.D. (Eds.), Marine Geology and Oceanography of the Arabian Sea and Coastal Pakistan. Van Norstrand Rheinhold Co., New York, pp. 65–70.
Mitchell, N.C., 2012. Modelling the rollovers of sandy clinoforms from the gravity effect on wave-agitated sand. J. Sediment. Res. 82, 464–468.
Mitchell, N.C., Masselink, G., Huthnance, J.M., Fernández-Salas, L.M., Lobo, F.J., 2012. Depths of modern coastal sand clinoforms. J. Sediment. Res. 82, 469–481.
Mitchum, R.M., Van Wagoner, J.C., 1991. High frequency sequences and their stacking patterns: sequence-stratigraphic evidence of high-frequency eustatic cycles. Sediment. Geol. 70, 131–160.
Mitchum, R.M., Vail, P.R., Thompson, S., 1977. Seismic stratigraphy and global changes in sea level, part 2: the depositional sequence as the basic unit for stratigraphic analysis. In: Payton, C.E. (Ed.), Seismic Stratigraphy: Applications to Hydrocarbon Exploration. AAPG Memoir 26, Tulsa, Oklahoma, pp. 53–62.
Morris, J.E., Hampson, G.J., Johnson, H.D., 2006. A sequence stratigraphic model for an intensely bioturbated shallow-marine sandstone: the Bridport Sand Formation, Wessex Basin, UK. Sedimentology 53, 1229–1263.
Mortimer, E., Gupta, S., Cowie, P., 2005. Clinoform nucleation and growth in coarse-grained deltas, Loreto basin, Baja California Sur, Mexico: a response to episodic accelerations in fault displacement. Basin Res. 17, 337–359.
Mullins, H.T., Gardulski, A.F., Hine, A.C., Melillo, A.J., Wise Jr., S.W., Applegate, J., 1988. Three-dimensional framework of the carbonate ramp slope of central west Florida: a sequential seismic stratigraphic perspective. Geol. Soc. Am. Bull. 100, 514–533.
Muto, T., Steel, R.J., 1992. Retreat of the front in a prograding delta. Geology 20, 967–970.
Muto, T., Steel, R.J., Swenson, J.B., 2007. Autostratigraphy: a framework norm for genetic stratigraphy. J. Sediment. Res. 77, 2–12.
Neill, C.F., Allison, M.A., 2005. Subaqueous deltaic formation on the Atchafalaya Shelf, Louisiana. Mar. Geol. 214, 411–430.
Nittrouer, C.A., Wright, L.D., 1994. Transport of particles across continental shelves. Rev. Geophys. 32, 85–113.
Nittrouer, C.A., Kuehl, S.A., DeMaster, D.J., Kowsmann, R.O., 1986. The deltaic nature of Amazon shelf sedimentation. GSA Bull. 97, 444–458.
Nittrouer, C.A., Kuehl, S.A., Figueiredo, A.G., Allison, M.A., Sommerfield, C.K., Rine, J.M., Faria, E.C., Silveira, O.M., 1996. The geological record preserved by Amazon shelf sedimentation. Cont. Shelf Res. 16, 817–841.
Olariu, C., Steel, R.J., 2009. Influence of point- source sediment- supply on modern shelf-break morphology: implications for interpretation of ancient shelf margins. Basin Res. 21, 484–501.
Orton, G.J., Reading, H.G., 1993. Variability of deltaic processes in terms of sediment supply, with particular emphasis on grain size. Sedimentology 40, 475–512.
Palamenghi, L., Schwenk, T., Spiess, V., Kudrass, H.R., 2011. Seismostratigraphic analysis with centennial to decadal time resolution of the sediment sink in the Ganges–Brahmaputra subaqueous delta. Cont. Shelf Res. 31, 712–739.
Patruno, S., 2013. Geological characterization of sand-prone subaqueous delta systems: a case study of the Upper Jurassic Sognefjord Formation (Troll Field, Northern North Sea, offshore Norway) and global examples. Ph.D. Thesis, Imperial College London 470 pp.
Patruno, S., Hampson, G.J., Jackson, C.A-L., Whipp, P., 2013a. Geomorphology, Facies Character and Stratigraphic architecture of an ancient sand-prone subaqueous delta: Upper Jurassic Sognefjord Formation, Troll Field, Offshore Norway. Extended abstract 1554161. AAPG Annual Convention and Exhibition, May 19–22, 2013, Pittsburgh, Pennsylvania, U.S., Search and Discovery article #20193, posted online June 17, 2013 (http://www.searchanddiscovery.com/documents/2013/20193patruno/ndx_patruno.pdf).
Patruno, S., Jackson, C.A-L., Hampson, G.J., Whipp, P., 2013b. Quantitative stratigraphic architecture, depositional history and progradation rates of an ancient sand-prone subaqueous delta (Sognefjord Formation, Troll Field, Norwegian North Sea). Extended Abstract 1554156, AAPG Annual Convention and Exhibition, May 19–22, 2013, Pittsburgh, Pennsylvania, U.S., Search and Discovery Article #20193, Posted online September 23, 2013 (http://www.searchanddiscovery.com/pdfz/documents/2013/20209patruno/ndx_patruno.pdf.html).
Patruno, S., Hampson, G.J., Jackson, C.A-L., Dreyer, T., 2015. Clinoform geometry, geomorphology, facies character and stratigraphic architecture of a sand-rich subaqueous delta: Jurassic Sognefjord Formation, offshore Norway. Sedimentology 62 (1), 350–388. http://dx.doi.org/10.1111/sed.12153.
Patruno, S., Hampson, G.J., Jackson, C.A-L., Whipp, P., 2015. Quantitative progradation dynamics and stratigraphic architecture of ancient shallow-marine clinoform sets: a new method and its application to the upper Jurassic Sognefjord Formation, Troll Field, offshore Norway. Basin Res. http://dx.doi.org/10.1111/bre.12081 (in press).
Pirmez, C., Pratson, L.F., Steckler, M.S., 1998. Clinoform development by advection–diffusion of suspended sediment: modeling and comparison to natural systems. J. Geophys. Res. 103, 24,141–24,157.
Pomar, L., Tropeano, M., 2001. The Calcarenite di Gravina Formation in Matera (southern Italy): new insights for coarse-grained, large-scale, cross-bedded bodies encased in offshore deposits. AAPG Bull. 85, 661–689.
Pomar, L., Obrador, A., Westphal, H., 2002. Sub-wave base cross-bedded grainstones on a distally steepened carbonate ramp, Upper Miocene, Menorca, Spain. Sedimentology 49, 139–169.
Porębski, S.J., Steel, R.J., 2003. Shelf-margin deltas: their stratigraphic significance and relation to deepwater sands. Earth-Sci. Rev. 62, 283–326.
Posamentier, H.W., Erskin, R.D., Mitchum Jr., R.M., 1991. Models for submarine fan deposition within a sequence stratigraphic framework. In: Weimer, P., Link, M.H. (Eds.), Seismic Facies and Sedimentary Processes of Submarine Fans and Turbidite Systems. Springer-Verlag, NewYork, pp. 127–136.
Pratson, L.F., Ryan, W.B.F., Mountain, G.S., Twichell, D.C., 1994. Submarine canyon initiation by downslope eroding sediment flows: evidence in Late Cenozoic strata on the New Jersey continental slope. Geol. Soc. Am. Bull. 106, 395–412.
Ravnås, R., Nøttvedt, A., Steel, R.J., Windelstad, J., Ravnås, R., Nøttvedt, A., Steel, R.J., Windelstad, J., 2000. Syn-rift sedimentary architectures in the Northern North Sea. In: Nøttvedt, A. (Ed.), Dynamics of the Norwegian Margin. Special Publications 167. Geological Society of London, London, pp. 133–177.
Rich, J.L., 1951. Three critical environments of deposition and criteria for recognition of rocks deposited in each of them. GSA Bull. 62, 1–20.
Roy, P.S., Cowell, P.J., Ferland, M.A., Thom, B.G., 1994. Wave-dominated coasts. In: Carter, R.W.G., Woodroffe, C.D. (Eds.), Coastal Evolution; Late QuaternaryShoreline Morphodynamics. Cambridge University Press, New York, pp. 121–186.
Ryan, W.B.F., Carbotte, S.M., Coplan, J.O., O'Hara, S., Melonian, A., Arko, R., Weissel, R.A., Ferrini, V., Goodwillie, A., Nitsche, F., Bonczkowski, J., Zemsky, R., 2009. Global

multi-resolution topography synthesis. Geochem. Geophys. Geosyst. 10 (3), 1–9. http://dx.doi.org/10.1029/2008GC002332 (Q03014).
Sadler, P.M., 1981. Sedimentation rates and the completeness of stratigraphic sections. J. Geol. 89, 569–584.
Sadler, P.M., Jerolmack, J., 2015. Scaling laws for aggradation, denudation and progradation rates: the case for timescale invariance at sediment sources and sinks. In: Smith, D.G., Bailey, R.J., Burgess, P.M., Fraser, A.J. (Eds.), Strata and Time probing the gaps in our understanding. Special Publications vol. 404. Geological Society of London, London. http://dx.doi.org/10.1144/SP404.7 (in press, London).
Sangree, J.B., Widmier, J.M., 1977. Seismic stratigraphy and global changes in sea level; 9, Seismic interpretation of depositional facies. In: Payton, C.E. (Ed.), Seismic Stratigraphy: Applications to Hydrocarbon Exploration. American Association of Petroleum Geologists, Tulsa, Oklahoma, pp. 165–184.
Schlee, J.S., Dillon, W.P., Grow, J.A., 1979. Structure of the continental slope off the eastern United States. In: Doyle, L.J., Pilkey, O.H. (Eds.), Geology of Continental Slopes. Society of Economic Paleontologists and Mineralogists, Special Publication 27, pp. 95–117.
Shepard, F.P., 1959. The Earth Beneath the Sea. Johns Hopkins Press, Baltimore, MD 275 pp.
Southard, J.B., Stanley, D.J., 1976. Shelf-break processes and sedimentation. In: Stanley, D.J., Swift, D.J.P. (Eds.), Marine Sediment Transport and Environmental Management. Wiley-Interscience, New York, pp. 351–377.
Steckler, M.S., Mountain, G.S., Miller, K.G., Christie-Blick, N., 1999. Reconstruction of Tertiary progradation and clinoform development on the New Jersey passive margin by 2-D backstripping. Mar. Geol. 154, 399–420.
Steel, R.J., 1993. Triassic–Jurassic megasequence stratigraphy in the Northern North Sea. Rift to post-rift evolution. In: Parker, J.R. (Ed.), Petroleum Geology of North-West Europe. Geological Society of London, pp. 299–315 London.
Steel, R.J., Olsen, T., 2002. Clinoforms, clinoform trajectory and deepwater sands. In: Armentrout, J.M., Rosen, N.C. (Eds.), Sequence Stratigraphic Models for Exploration and Production: Evolving Methodology, Emerging Models and Application Histories. Publication, GCS-SEPM Special, pp. 367–381.
Stewart, D.J., Schwander, M., Bolle, L., 1995. Jurassic depositional systems of the Horda Platform, Norwegian North Sea: practical consequences of applying sequence stratigraphic models. In: Steel, R.J., Felt, V.L., Johannessen, E.P., Mathieu, C. (Eds.), Sequence Stratigraphy on the Northwest European Margin. Norwegian Petroleum Society Special Publication 5. Elsevier, pp. 291–323.
Suter, J.R., Berryhill, H.L., 1985. Late Quaternary shelf margin deltas, northwest Gulf of Mexico. AAPG Bull. 69, 77–91.
Swenson, J.B., Paola, C., Pratson, L., Voller, V.R., Murray, A.B., 2005. Fluvial and marine controls on combined subaerial and subaqueous delta progradation: morphodynamic modeling of compound-clinoform development. J. Geophys. Res. 110, 1–16.
Ta, T.K.O., Nguyen, V.L., Tateishi, M., Kobayashi, I., Tanabe, S., Saito, Y., 2002. Holocene delta evolution and sediment discharge of the Mekong River, southern Vietnam. Quat. Sci. Rev. 21, 1807–1819.
Tesson, M., Posamentier, H.W., Gensous, B., 2000. Stratigraphic organization of Late Pleistocene deposits of the western part of the Golfe du Lion Shelf (Languedoc Shelf), western Mediterranean Sea, using high-resolution seismic and core data. AAPG Bull. 84 (1), 119–150.
Thorne, J., 1995. On the scale independent shape of prograding stratigraphic units. In: Barton, C.B., La Point, P.R. (Eds.), Fractals in Petroleum Geology and Earth processes. Plenum Press, New York, pp. 97–112.
Vail, P.R., Mitchum Jr., R.M., Todd, R.G., Widmeir, J.R., Thompsons III, S., Sangree, J.R., Bubb, J.N., Hatlid, W.G., 1977. Sequence stratigraphy and global changes in sea level. In: Payton, C.E. (Ed.), Seismic Stratigraphy, Applications to Hydrocarbon Exploration. American Association of Petroleum Geology Memoirs 26, pp. 49–205.
Vanney, J.R., Stanley, D.J., 1983. Shelfbreak physiography: an overview. In: Stanley, D.J., Moore, G.T. (Eds.), The Shelf Break: Critical Interface on Continental Margins. SEPM Special Publication 33, pp. 1–24.
Vollset, J., Doré, A.G., 1984. A revised Triassic and Jurassic lithostratigraphy nomenclature for the Norwegian North Sea, northern area. Norw. Petrol. Direct. Bull. 3, 1–53.
Walsh, J.P., Nittrouer, C.A., Palinkas, C.M., Ogston, A.S., Sternberg, R.W., Brunskill, G.J., 2004. Clinoform mechanics in the Gulf of Papua, New Guinea. Cont. Shelf Res. 24, 2487–2510.
Warne, A.G., Meade, R.H., White, W.A., Guevara, E.H., Gibeaut, J., Smyth, R.C., Aslan, A., Tremblay, T., 2002. Regional controls on geomorphology, hydrology and ecosystem integrity in the Orinoco Delta, Venezuela. Geomorphology 44, 273–307.
Wear, C.M., Stanley, D.J., Boula, J.E., 1974. Shelf break physiography between Wilmington and Norfolk canyons. Mar. Technol. Soc. J. 8, 37–48.
Weber, M.E., Wiedicke, M.H., Kudrass, H.R., Hubsher, C., Erlenkueser, H., 1997. Active growth of the Bengal Fan during sea-level rise and highstand. Geology 25, 315–318.
Xing, J., Davies, A.M., 2002. Influence of wind direction, wind waves, and density stratification upon sediment transport in shelf edge regions: the Iberian shelf. J. Geophys. Res. 107 (C8), 16.1–16.24.
Yang, Z.S., Liu, J.P., 2007. A unique Yellow River-derived distal subaqueous delta in the Yellow Sea. Mar. Geol. 240, 169–176.
Yoshida, S., Steel, R.J., Dalrymple, R.W., 2007. Changes in depositional processes: an ingredient in a new generation of sequence stratigraphic models. J. Sediment. Res. 77, 447–460.